MAGNETOM Flash

MAGNETOM Free. Platform Special Issue

magnetomworld.siemens-healthineers.com

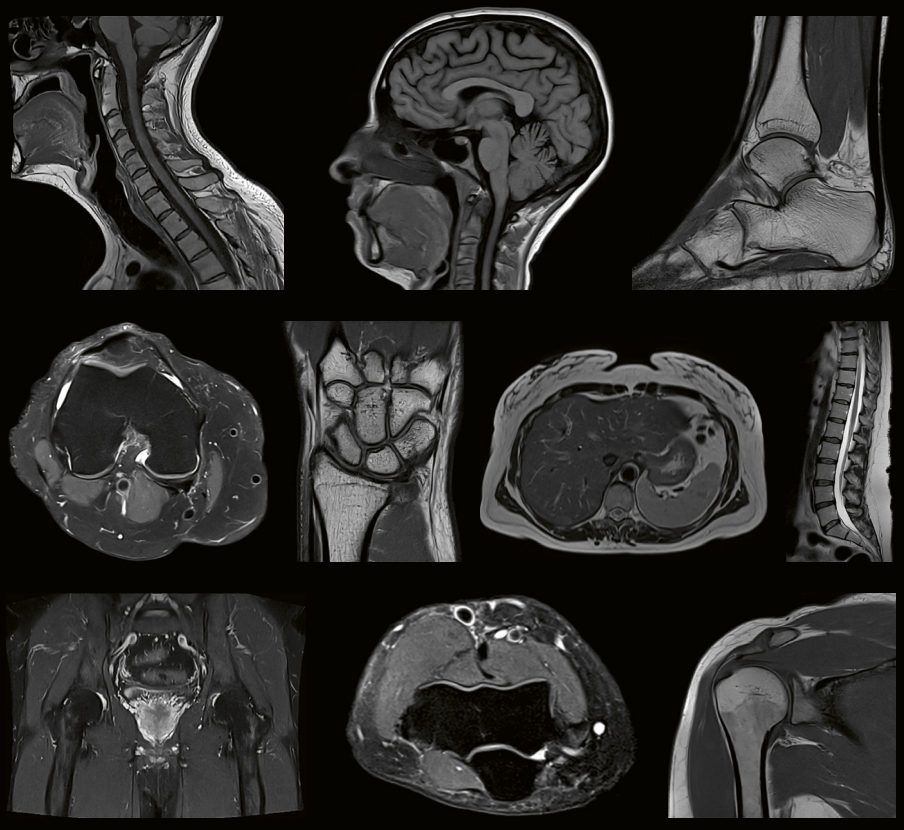

SIEMENS Healthineers

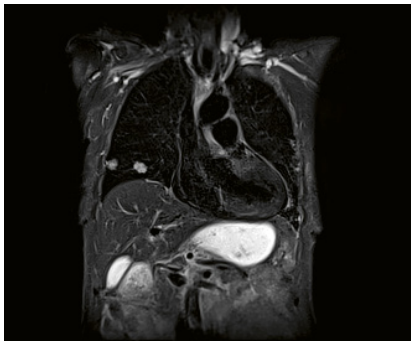
4aaaa0484

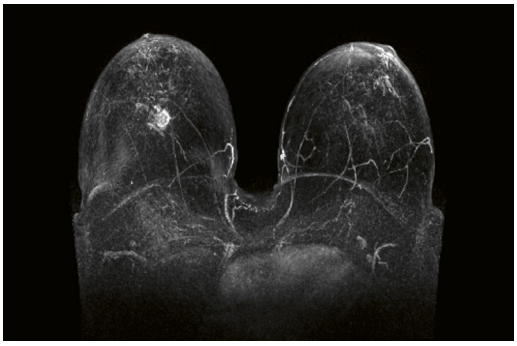
7aaaa0296

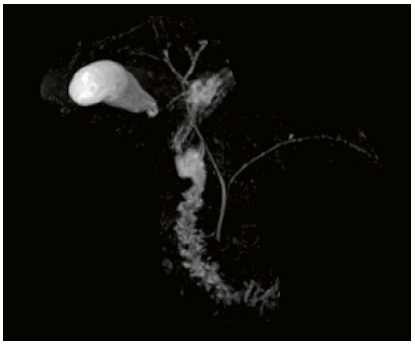
4aaaa0465

Image Gallery

Abdominal Imaging

Musculoskeletal Imaging

Fetal Imaging

Cardiovascular Imaging

Interventional MRI

Siemens Healthineers internal image IDs cover page:
7aaaa0694, 7aaaa0447, 7aaaa0369,
7aaaa0421, 7aaaa0404, 7aaaa0535, 7aaaa0532,
7aaaa0692, 7aaaa0425, 7aaaa0702

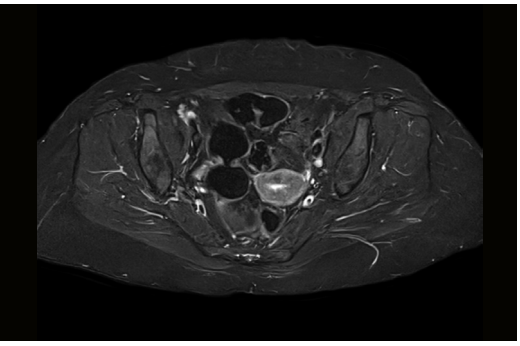

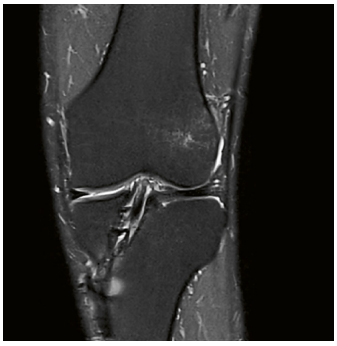

4aaaa0494

Spotlight

Technology

Meet Siemens Healthineers

[1]The MRI restrictions (if any) of the metal implant must be considered prior to patient undergoing MRI exam. MR imaging of patients with metallic implants brings specific risks. However, certain implants are approved by the governing regulatory bodies to be MR conditionally safe. For such implants, the previously mentioned warning may not be applicable. Please contact the implant manufacturer for the specific conditional information. The conditions for MR safety are the responsibility of the implant manufacturer, not of Siemens Healthineers.

[2]MR scanning has not been established as safe for imaging fetuses and infants less than two years of age. The responsible physician must evaluate the benefits of the MR examination compared to those of other imaging procedures.

[3]Images are acquired with a custom sequence that is not available as product. Availability of the custom sequence cannot be guaranteed.

MAGNETOM Free.Max. The Power of Deep Resolve

Image acquisition with Magnetic Resonance Imaging has conventionally required delicate and application-dependent balancing of image resolution and acquisition time for a given signal-to-noise ratio (SNR) scenario. Whereas we conventionally leveraged higher field strength to acquire high-resolution images at a reasonable acquisition time, the evolution of coil- and software technology has equipped us with innovative and powerful tools to achieve this general objective.

The introduction of Deep Resolve[2], our AI powered image reconstruction technology, is changing the game in MRI. This is especially the case at lower field with the constraints once imposed by conventional image reconstruction due to limited SNR. Deep Resolve employs a deep neural network in an iterative process to reduce noise that is introduced by an accelerated acquisition. The network is trained with tens of thousands of data pairs representing accelerated and non-accelerated acquisitions. Based on this training, the network within Deep Resolve is able to precisely detect noise that originates from the accelerated acquisition and is able to remove it. The originally acquired raw data is incorporated throughout the entire reconstruction process, until the output of the final reconstructed image. This ensures robust results and that all the potentially clinically relevant information is preserved. On the other hand, the architecture of the networks within Deep Resolve do not have a generative component and can therefore not introduce new features that are not represented in the acquired raw data.

With these inherent characteristics, Deep Resolve offers a unique value and an unmatched performance, enabling reduced acquisition time while preserving the integrity of the underlying signal and the clinical information.

Today, we can revisit image acquisition at lower field strength with confidence, leveraging its inherent benefits for imaging new cohorts of patients, adding new procedures into MRI workflow, and making this valuable imaging modality more ubiquitous and accessible to patients across our globe.

T1 TSE, PAT 4, 2 steps,
Deep Resolve, 2 x 19 slices,
0,5 x 0,5 x 3 mm^3,
FOV 2 x 348 mm,
TA 2 x 1:43 min

T2 TSE, PAT 4, 2 steps,
Deep Resolve, 2 x 19 slices,
0,5 x 0,5 x 3 mm^3,
FOV 2 x 348 mm,
TA 2 x 1:28 min

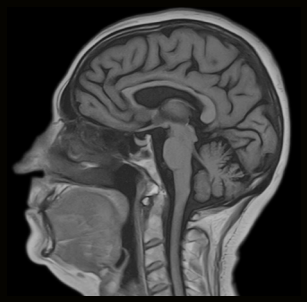

T1 TSE Dark Fluid, PAT 4,
Deep Resolve, 22 slices,
0,5 x 0,4 x 5 mm³,
FOV 230 mm, TA 2:14 min

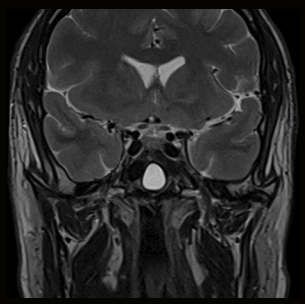

T2 TSE, PAT 4,
Deep Resolve, 12 slices,
0,4 x 0,4 x 2,2 mm³,
FOV 150 mm, TA 1:20 min

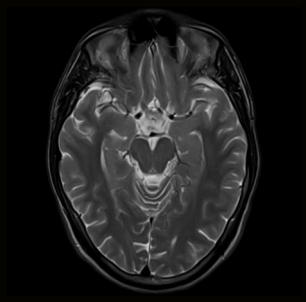

T2 TSE, PAT 4,
Deep Resolve, 28 slices,
0,4 x 0,4 x 5 mm³,
FOV 230 mm, TA 1:08 min

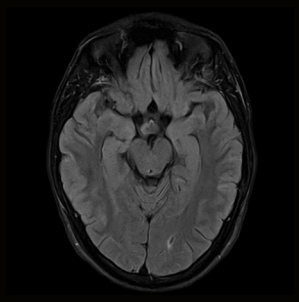

T2 TSE Dark Fluid, PAT 4,
Deep Resolve, 28 slices,
0,5 x 0,4 x 5 mm³,
FOV 230 mm, TA 2:08 min

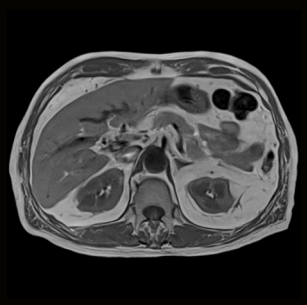

T1 TSE, PAT 4,
Deep Resolve, 40 slices,
0,8 x 0,8 x 5 mm³,
FOV 420 mm, TA 4 x 6 s

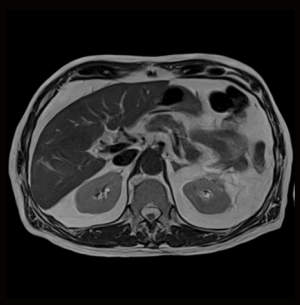

T2 TSE, PAT 4,
Deep Resolve, 40 slices,
0,8 x 0,8 x 5 mm³,
FOV 420 mm, TA 3 x 6 s

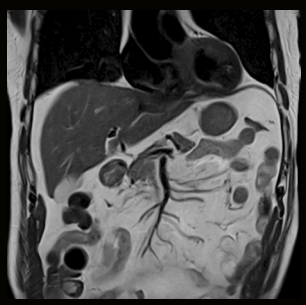

T2 TSE, PAT 4,
Deep Resolve, 40 slices,
0,8 x 0,8 x 5 mm³,
FOV 350 mm, TA 4 x 8 s

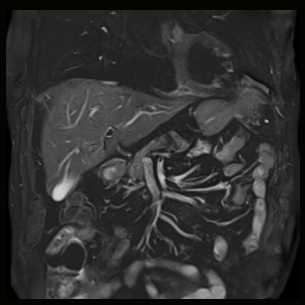

T2 TSE SPAIR, PAT 4,
Deep Resolve, 40 slices,
1,0 x 0,8 x 5 mm³,
FOV 350 mm, TA 5 x 10 s

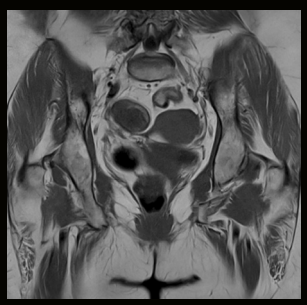

T1 TSE, PAT 4,
Deep Resolve, 30 slices,
0,5 x 0,5 x 5 mm³,
FOV 420 mm, TA 3 x 30 s

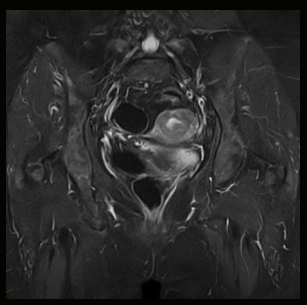

T2 TSE STIR, PAT 4,
Deep Resolve, 30 slices,
0,6 x 0,5 x 5 mm³,
FOV 420 mm, TA 1:50 min

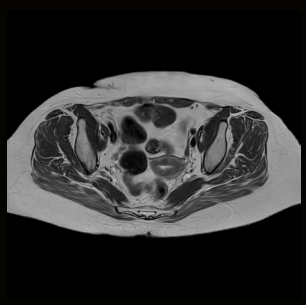

T2 TSE, PAT 4,
Deep Resolve, 40 slices,
0,4 x 0,4 x 5 mm³,
FOV 420 mm, TA 1:44 min

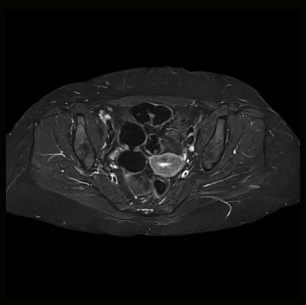

T2 TSE SPAIR, PAT 4,
Deep Resolve, 40 slices,
0,6 x 0,5 x 5 mm³,
FOV 420 mm, TA 2:44 min

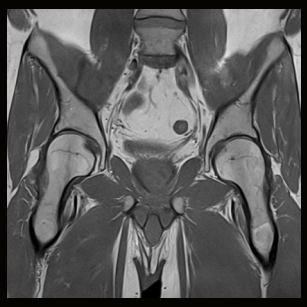

T1 TSE, PAT 4,
Deep Resolve, 50 slices,
0,6 x 0,6 x 4 mm³,
FOV 360 mm, TA 1:54 min

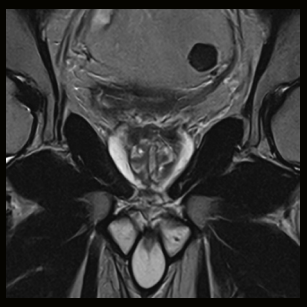

T2 TSE, PAT 4,
Deep Resolve, 28 slices,
0,5 x 0,5 x 3,5 mm³,
FOV 200 mm, TA 2:09 min

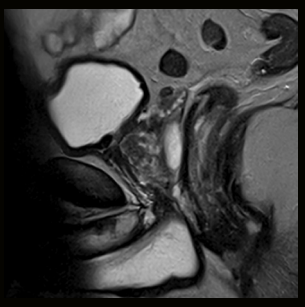

T2 TSE, PAT 4,
Deep Resolve, 28 slices,
0,4 x 0,4 x 5 mm³,
FOV 230 mm, TA 1:08 min

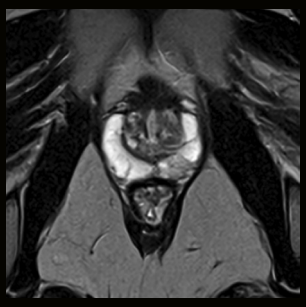

T2 TSE, PAT 4,
Deep Resolve, 30 slices,
0,5 x 0,5 x 3,5 mm³,
FOV 200 mm, TA 2:15 min

T1 TSE, PAT 2,
Deep Resolve, 15 slices,
0,5 x 0,5 x 3 mm³,
FOV 225 mm, TA 2:36 min

T1 TSE, PAT 2,
Deep Resolve, 15 slices,
0,5 x 0,5 x 3 mm³,
FOV 225 mm, TA 1:56 min

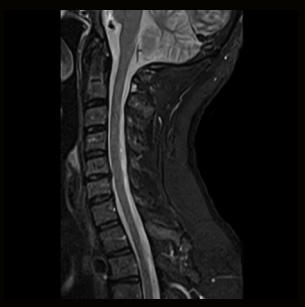

T2 TSE STIR, PAT 2,
Deep Resolve, 15 slices,
0,7 x 0,6 x 3 mm³,
FOV 225 mm, TA 3:24 min

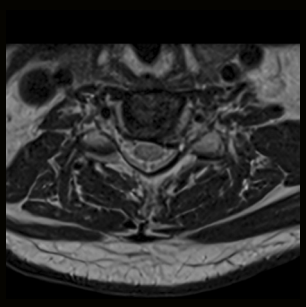

T2 TSE, PAT 2,
Deep Resolve, 30 slices,
0,5 x 0,5 x 3 mm³,
FOV 160 mm, TA 2:36 min

T1 TSE, PAT 2,
Deep Resolve, 15 slices,
0,6 x 0,5 x 4 mm³,
FOV 360 mm, TA 3:26 min

T1 TSE, PAT 2,
Deep Resolve, 15 slices,
0,6 x 0,5 x 4 mm³,
FOV 360 mm, TA 2:56 min

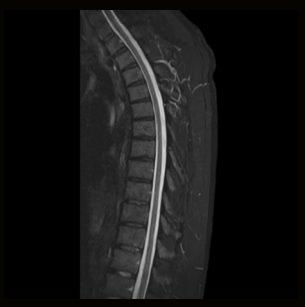

T2 TSE STIR, PAT 2,
Deep Resolve, 15 slices,
0,8 x 0,6 x 4 mm³,
FOV 360 mm, TA 3:07 min

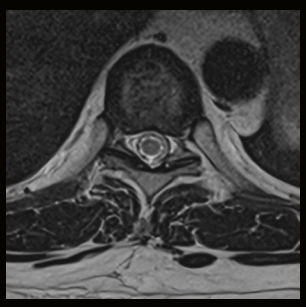

T2 TSE, PAT 2,
Deep Resolve, 30 slices,
0,5 x 0,5 x 4 mm³,
FOV 160 mm, TA 2:22 min

T1 TSE, PAT 4,
Deep Resolve, 19 slices,
0,6 x 0,5 x 3 mm³,
FOV 300 mm, TA 2:20 min

T2 TSE, PAT 4,
Deep Resolve, 19 slices,
0,6 x 0,5 x 3 mm³,
FOV 300 mm, TA 2:04 min

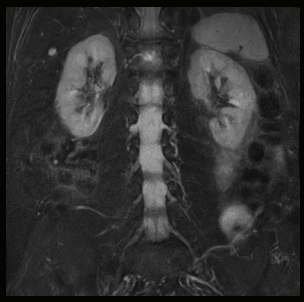

T2 TSE STIR, thin MIP, PAT 4,
Deep Resolve, 19 slices,
0,6 x 0,5 x 4 mm³,
FOV 300 mm, TA 1:45 min

T2 TSE, PAT 3,
Deep Resolve, 32 slices,
0,5 x 0,5 x 3 mm³,
FOV 160 mm, TA 2:18 min

T1 TSE, PAT 4,
Deep Resolve, 28 slices,
0,3 x 0,3 x 3 mm³,
FOV 160 mm, TA 1:33 min

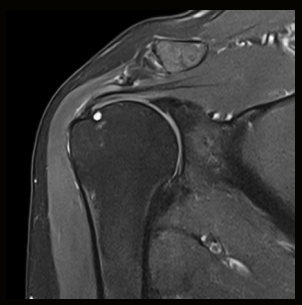

PD TSE FatSat, PAT 4,
Deep Resolve, 28 slices,
0,5 x 0,4 x 3 mm³,
FOV 160 mm, TA 1:20 min

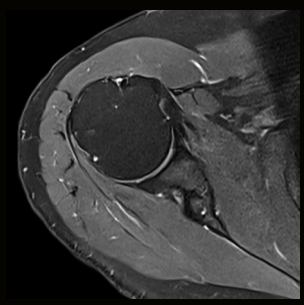

PD TSE FatSat, PAT 4,
Deep Resolve, 28 slices,
0,5 x 0,4 x 3 mm³,
FOV 160 mm, TA 1:24 min

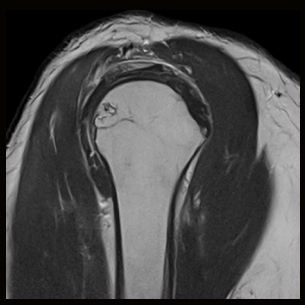

T2 TSE, PAT 4,
Deep Resolve, 30 slices,
0,4 x 0,3 x 3 mm³,
FOV 160 mm, TA 1:06 min

T1 TSE, PAT 4,
Deep Resolve, 20 slices,
0,3 x 0,3 x 3 mm³,
FOV 130 mm, TA 53 s

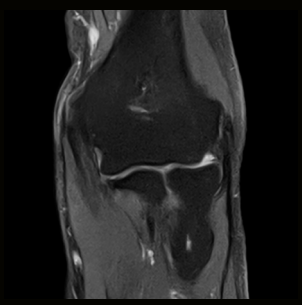

PD TSE FatSat, PAT 4,
Deep Resolve, 20 slices,
0,3 x 0,3 x 3 mm³,
FOV 130 mm, TA 1:34 min

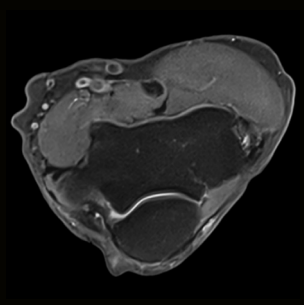

PD TSE FatSat, PAT 4,
Deep Resolve, 24 slices,
0,3 x 0,3 x 3 mm³,
FOV 130 mm, TA 2:04 min

T2 TSE, PAT 4,
Deep Resolve, 22 slices,
0,3 x 0,3 x 3 mm³,
FOV 130 mm, TA 52 s

T1 TSE, PAT 4,
Deep Resolve, 20 slices,
0,3 x 0,3 x 2 mm³,
FOV 240 mm, TA 1:59 min

PD TSE FatSat, PAT 4,
Deep Resolve, 20 slices,
0,4 x 0,4 x 2 mm³,
FOV 240 mm, TA 2:04 min

PD TSE FatSat, PAT 4,
Deep Resolve, 30 slices,
0,4 x 0,4 x 3 mm³,
FOV 150 mm, TA 1:28 min

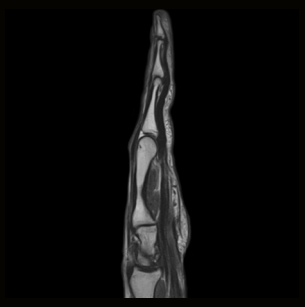

T2 TSE, PAT 4,
Deep Resolve, 21 slices,
0,3 x 0,3 x 2 mm³,
FOV 240 mm, TA 1:11 min

T1 TSE, PAT 4,
Deep Resolve, 24 slices,
0,4 x 0,4 x 3 mm³,
FOV 200 mm, TA 1:21 min

PD TSE FatSat, PAT 4,
Deep Resolve, 24 slices,
0,5 x 0,4 x 3 mm³,
FOV 200 mm, TA 1:36 min

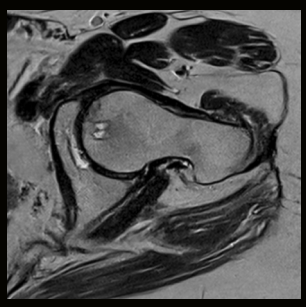

T2 TSE, PAT 4,
Deep Resolve, 28 slices,
0,4 x 0,4 x 3 mm³,
FOV 200 mm, TA 1:20 min

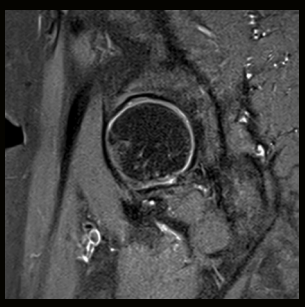

PD TSE FatSat, PAT 4,
Deep Resolve, 30 slices,
0,5 x 0,4 x 3 mm³,
FOV 200 mm, TA 1:51 min

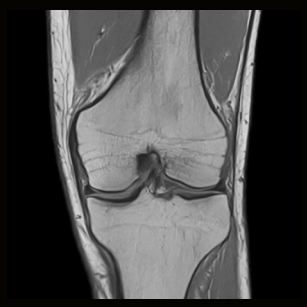

T1 TSE, PAT 4,
Deep Resolve, 30 slices,
0,4 x 0,4 x 3 mm³,
FOV 170 mm, TA 1:31 min

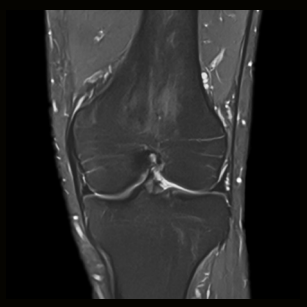

PD TSE FatSat, PAT 4,
Deep Resolve, 30 slices,
0,4 x 0,4 x 3 mm³,
FOV 170 mm, TA 1:16 min

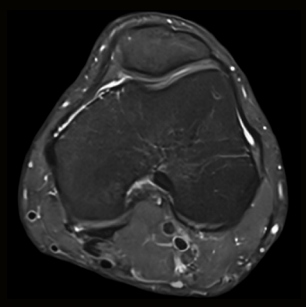

PD TSE FatSat, PAT 4,
Deep Resolve, 36 slices,
0,4 x 0,4 x 3 mm³,
FOV 170 mm, TA 1:33 min

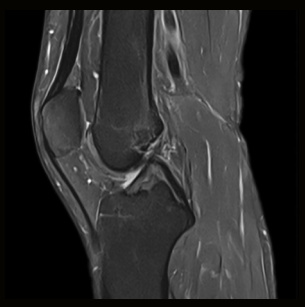

PD TSE FatSat, PAT 4,
Deep Resolve, 28 slices,
0,5 x 0,4 x 3 mm³,
FOV 170 mm, TA 1:05 min

T1 TSE, PAT 4,
Deep Resolve, 22 slices,
0,3 x 0,3 x 3 mm³,
FOV 160 mm, TA 1:21 min

PD TSE FatSat, PAT 4,
Deep Resolve, 22 slices,
0,5 x 0,4 x 3 mm³,
FOV 160 mm, TA 1:06 min

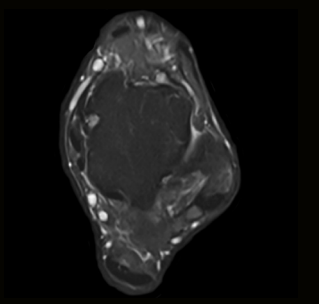

PD TSE FatSat, PAT 4,
Deep Resolve, 30 slices,
0,3 x 0,3 x 3 mm³,
FOV 160 mm, TA 1:30 min

T2 TSE, PAT 4,
Deep Resolve, 32 slices,
0,3 x 0,3 x 3 mm³,
FOV 160 mm, TA 1:33 min

[1]Deep Resolve Boost on MAGNETOM Free.Max is not yet commercially available in some countries. Due to regulatory reasons its future availability cannot be guaranteed. Please contact your local Siemens organization for further details.
[2]Deep Resolve Boost on MAGNETOM Free.Max is pending 510(k) clearance, and is not yet commercially available in the United States. Its future availability cannot be guaranteed.

The DICOM files of the figures in this gallery are available for download:

magnetomworld.siemens-healthineers.com/clinical-corner/protocols/dicom-images

Phoenix is a unique *syngo*-tool that allows you to click on an image, drag it into the measurement queue, and instantly duplicate the extracted protocol – TR, TE, bandwidth, number of slices, echo spacing, etc.

- Phoenix ensures reproducibility, e.g., for patient follow-up.
- Phoenix shares optimized protocols on the different MAGNETOM systems you work with.
- Phoenix supports multi-center protocol standardization.

You'll find DICOM images from various systems and all aspects of MRI at
magnetomworld.siemens-healthineers.com/clinical-corner/protocols/dicom-images

Intrahepatic Cholangiocarcinoma: Typical Imaging Findings at 0.55T

Manuel Teixeira Gomes, M.D.[1,2]; Ricardo Sampaio, M.D.[1,2]; Carina Silvestre, RT[1]; Catarina Pereira, RT[1]; Cristiana Araujo, M.Sc.[3]

[1]Hospital Lusíadas Albufeira, Portugal
[2]Hospital Lusíadas Porto, Portugal
[3]Siemens Healthineers Portugal

Introduction

Cholangiocarcinoma, a malignancy accounting for 15 to 20% of primary liver cancers, can be categorized based on location (intrahepatic, perihilar, or extrahepatic distal) or growth characteristics (mass-forming, periductal-infiltrating, or intraductal). These classifications are crucial due to their diverse clinical presentations and prognosis, which are contingent upon both factors. The cancer is predominantly found in the perihilar region, and less frequently in distal and intrahepatic locations, but the incidence of intrahepatic cases is on the rise [1–4].

Although major liver resection remains the primary treatment approach, eligibility for surgery is limited to only 12 to 40% of patients. After surgery, 5-year survival ranges from 25 to 40%, with tumor recurrence in 50 to 70% of cases. In instances of unresectable cholangiocarcinoma, the prognosis is grim, with survival rates as low as 35.4% at one year and 1.6% at three years. Unresectable criteria for intrahepatic cholangiocarcinoma (ICC) are distant or intrahepatic metastases, invasion or encasement of major vessels, or extensive regional lymph nodes [4, 5].

Magnetic resonance imaging (MRI) has the capability to differentiate the dissemination of tumors along bile ducts, owing to its exceptional soft-tissue contrast. Hence, it is the preferred imaging modality for both diagnosing and staging cholangiocarcinoma. In terms of precision, its efficacy rivals the combined accuracy of contrast-enhanced computed tomography (CE-CT) and direct cholangiography [6].

In recent times, there has been a resurgence in the popularity of low-field MRI systems, driven by improvements in image reconstruction – from parallel imaging and compressed sensing to deep learning image reconstruction. These developments mean clinicians can make optimal use of the available signal while exploiting the physical advantages of low-field MRI, such as reduced artifacts and increased patient comfort [7].

For a comprehensive assessment of cholangiocarcinoma, an ideal protocol should include magnetic resonance cholangiopancreatography (MRCP), conventional T1- and T2-weighted abdominal MRI pulse sequences (including T1 in- and out-of-phase imaging), diffusion-weighted imaging (DWI), and multiphase contrast-enhanced sequences acquired during the arterial, portal venous, and delayed phases. Our system, the 0.55T MAGNETOM Free.Max (Siemens Shenzhen Magnetic Resonance Ltd., Shenzhen, China), is capable of doing this, as we show in the case report [6].

Case report

We present the case of a 52-year-old woman with an unremarkable medical history, who presented to the emergency department with upper abdominal pain and notable weight loss.

During the physical examination, no indications of jaundice were evident. The laboratory results revealed anemia (hemoglobin 10.9 g/dL) and normal levels of AST, ALT, and total bilirubin.

The initial assessment using contrast-enhanced abdominal and pelvic CT imaging revealed a substantial hypo-attenuating mass situated in the left hepatic lobe, accompanied by distal intrahepatic bile duct dilation within hepatic segments II and III.

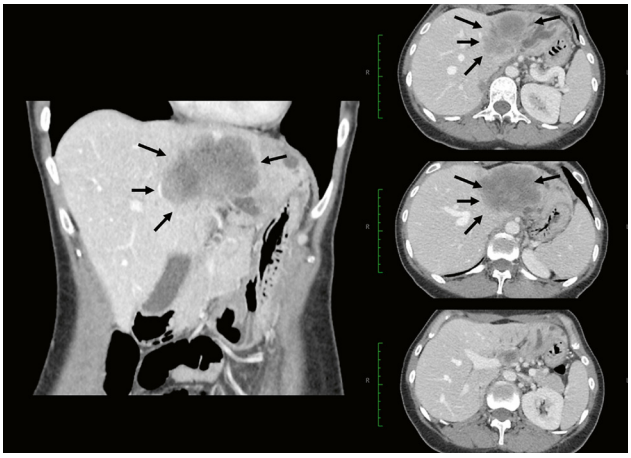

1 Abdominal CT showing a large mass (arrows).

Furthermore, a suspicious adenopathy measuring 2.2 × 1.5 cm was detected in the hilar/periceliac region, along with a right adrenal mass of 1.3 cm exhibiting a density surpassing 10 HU. Notably, no dilation was observed in the remaining intrahepatic bile ducts or the hepatic and common bile ducts.

Following the findings from the CE-CT, the patient was referred to undergo MRCP.

Further study with MRCP depicted a large heterogeneous intrahepatic left lobe mass, with low signal intensity on T1-weighted imaging, high signal intensity on T2-weighted imaging, and restricted diffusion on DWI, especially at the periphery of the mass ('target diffusion' on high b-values).

On dynamic contrast-enhanced MRI with extracellular contrast material, the mass also exhibits prominent peripheral rim enhancement with centripetal or gradual progressive enhancement. Central hypoattenuating areas in the mass represent necrosis and fibrosis, which are also responsible for the target diffusion appearance. The mass was also responsible for the dilated intrahepatic biliary ducts at the periphery of the left hepatic lobe.

Sequences/ Parameters	TR (ms)	TE (ms)	TA (s)	Matrix (mm)
Cor T2 TSE	2240	75	75	0.8 × 0.8 × 6
Tra T2 TSE	2800	75	68	0.8 × 0.8 × 6
Tra T2 TSE FS	3300	80	75	0.9 × 0.9 × 6
Tra T1 in/opp phase	213	6.5/13	79	0.7 × 0.7 × 6
MRCP	2500	702	320	0.6 × 0.6 × 1
Tra DWI (b50 / b800 s/mm²)	7800	93	336	1.5 × 1.5 × 6
Tra T1 VIBE Dixon (pre, arterial, venous, and delayed phase)	9.74	2.71	21	0.8 × 0.8 × 3

Table 1: Acquisition parameters for the 0.55T MAGNETOM Free.Max.

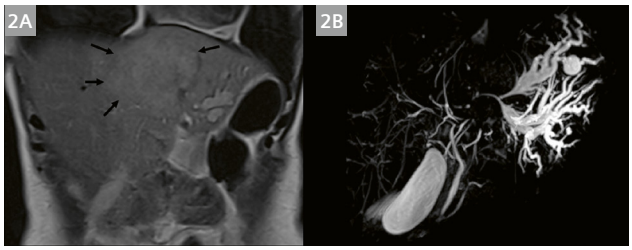

2 Coronal T2-weighted imaging **(2A)** and 3D MRCP maximum intensity projection (MIP) images **(2B)** showing a large left lobe hepatic mass with peripheral dilation of intrahepatic bile ducts – segments II and III).

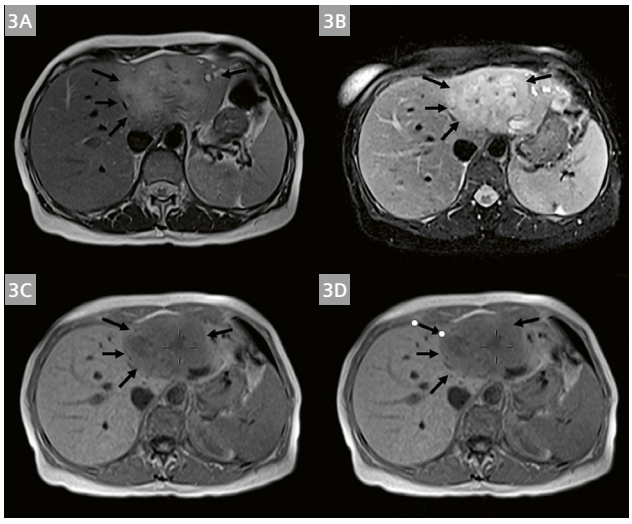

3 Axial T2 **(3A)**, T2 FS **(3B)**, T1 GRE in-phase **(3C)**, and GRE out-of-phase images **(3D)**.

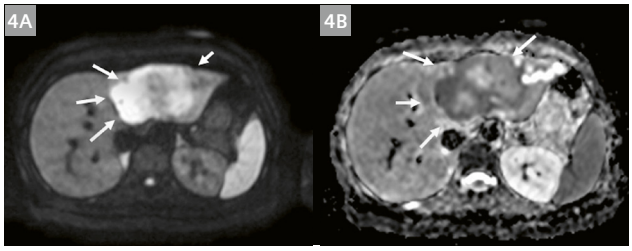

4 Axial DWI b800 s/mm² **(4A)** and ADC map **(4B)** showing 'target' restricted diffusion, more clearly appreciated on ADC map.

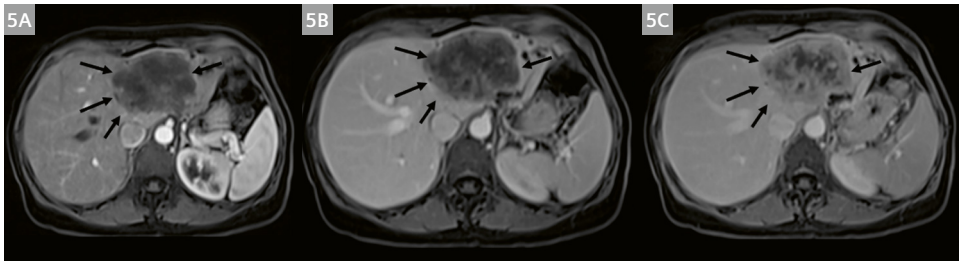

5 Dynamic study after intravenous contrast (**5A** arterial, **5B** venous, and **5C** delay phases) showing gradual enhancement of the mass.

High signal on T2-weighted imaging and restricted diffusion on DWI of the right adrenal mass and of the periceliac/hilar lymph nodes was also indicative of metastatic distant disease.

After multidisciplinary oncology consultation, the patient was diagnosed with unresectable disease and started systemic chemotherapy.

Conclusion

MRCP is considered the imaging modality of choice in the diagnosis of cholangiocarcinoma. This is because of its high contrast resolution, multiplanar capability, and its ability to evaluate biliary, parenchymal, and vascular extensions. Distant disease can also be clearly depicted, with a direct impact on treatment decisions.

Our case report shows the strengths of a 0.55T MR scanner in obtaining high-quality images, allowing the radiologist to perform accurate disease staging with a high level of confidence.

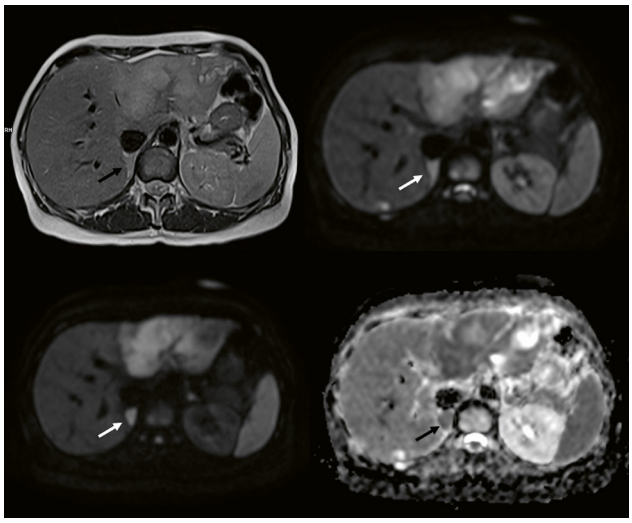

6 Small right adrenal mass showing restricted diffusion and high intensity on T2-weighted imaging, highly suspicious for metastatic disease (arrows).

Contact

Manuel Teixeira Gomes, M.D.
Hospital Lusíadas Albufeira
R. da Correeira
8200-112 Albufeira
Portugal
manuel.mantgomes@gmail.com

Ricardo Sampaio, M.D.
Hospital Lusíadas Albufeira
R. da Correeira
8200-112 Albufeira
Portugal
Rsampaio@gmail.com

References

1 Banales JM, Marin JJG, Lamarca A, Rodrigues PM, Khan SA, Roberts LR, et al. Cholangiocarcinoma 2020: the next horizon in mechanisms and management. Nat Rev Gastroenterol Hepatol. 2020;17(9):557–588.
2 Brindley PJ, Bachini M, Ilyas SI, Khan SA, Loukas A, Sirica AE, et al. Cholangiocarcinoma. Nat Rev Dis Primers. 2021;7(1):65.
3 Khan AS, Dageforde LA. Cholangiocarcinoma. Surg Clin North Am. 2019;99(2):315–335.
4 Gravely AK, Vibert E, Sapisochin G. Surgical treatment of intrahepatic cholangiocarcinoma. J Hepatol. 2022;77(3):865–867.
5 Tan JC, Coburn NG, Baxter NN, Kiss A, Law CH. Surgical management of intrahepatic cholangiocarcinoma – a population-based study. Ann Surg Oncol. 2008;15(2):600–608.
6 Jhaveri KS, Hosseini-Nik H. MRI of cholangiocarcinoma. J Magn Reson Imaging 2015;42:1165–1179.
7 Heiss R, Nagel AM, Laun FB, Uder M, Bickelhaupt S. Low-Field Magnetic Resonance Imaging: A New Generation of Breakthrough Technology in Clinical Imaging. Invest Radiol. 2021;56(11):726–733.

Exploring the Potential of Low-Field Musculoskeletal MRI at 0.55T: Preliminary Results in Patients with Large Metal Implants

Hanns-Christian Breit, M.D.[1]; Jan Vosshenrich, M.D.[1]; Martin Clauss, M.D.[2,3]; Markus M. Obmann, M.D.[1]; Michael Bach, Ph.D.[1]; Dorothee Harder, M.D.[1]; Ricardo Donners, M.D.[1]

[1]Department of Radiology, University Hospital Basel, University of Basel, Switzerland
[2]Center for Musculoskeletal Infections, University Hospital Basel, University of Basel, Switzerland
[3]Department for Orthopedics and Trauma Surgery, University Hospital Basel, University of Basel, Switzerland

Introduction

Low-field MRI scanners are currently experiencing a renaissance, thanks to technical innovations in gradient construction, coil design, and AI-based reconstruction methods [1]. Advantages over the 1.5T and 3T scanners used predominantly in clinical routine include lower acquisition and maintenance costs, and higher patient comfort [2, 3]. Potential advantages of low-field MR imaging include clinical scenarios where imaging using scanners with higher field strengths encounters technical limitations. This is especially the case when imaging patients with metal implants[1] where susceptibility artifacts are expected to be substantially less severe at 0.55T [4, 5]. This may be of particular interest in clinical routine, given an aging global population with an associated higher prevalence of metal implants, e.g., following joint replacement surgery [6]. This patient population has been shown to benefit from MR imaging [7].

The aim of this report is to provide a perspective on the possibilities and potential advantages of using a new-generation 0.55T low-field MRI system in imaging patients with large metal implants.

Materials and methods

Patient population
Three patients underwent complementary MR imaging at 0.55T in addition to their regular clinical imaging work-up.

MRI scanners
Low-field MR imaging was performed using a 0.55T MAGNETOM Free.Max scanner (Siemens Shenzhen Magnetic Resonance Ltd., Shenzhen, China, gradient amplitude 26 mT/m, slew rate 45 T/m/s, 80 cm bore). A six-channel flex coil was used for the examination of the knee and the upper limb.

The 1.5T examinations were performed using a MAGNETOM Avanto Fit system (Siemens Healthcare, Erlangen, Germany, gradient amplitude 45 mT/m, slew rate 200 T/m/s, 60 cm bore). The 3T examinations were performed on a MAGNETOM Skyra system (Siemens Healthcare, Erlangen, Germany, gradient amplitude 45 mT/m, slew rate 200 T/m/s, 70 cm bore).

[1]*The MRI restrictions (if any) of the metal implant must be considered prior to patient undergoing MRI exam. MR imaging of patients with metallic implants brings specific risks. However, certain implants are approved by the governing regulatory bodies to be MR conditionally safe. For such implants, the previously mentioned warning may not be applicable. Please contact the implant manufacturer for the specific conditional information. The conditions for MR safety are the responsibility of the implant manufacturer, not of Siemens Healthineers.*

A 59-year-old patient with several prior surgical procedures of the thoracic spine, including multi-level decompression and spinal fusion, presented with back pain refractory to medication. MR imaging of the thoracic spine was requested for the assessment of the spinal canal prior to epidural catheter placement. Routine imaging was performed at 1.5T, followed by a supplemental MR examination at 0.55T.

Due to severe susceptibility artifacts, the spinal canal was not assessable at 1.5T, neither on sagittal or axial T2-weighted sequences, nor on the T1-weighted sequence in the sagittal plane. At 0.55T, visibility and assessability of the spinal canal was substantially improved. Artifact superimposition was only minor, allowing for conclusive evaluation. Contraindications for epidural pain catheter placement could therefore be ruled out at 0.55T. Representative slices from 1.5T and 0.55T imaging are shown in Figures 1 and 2.

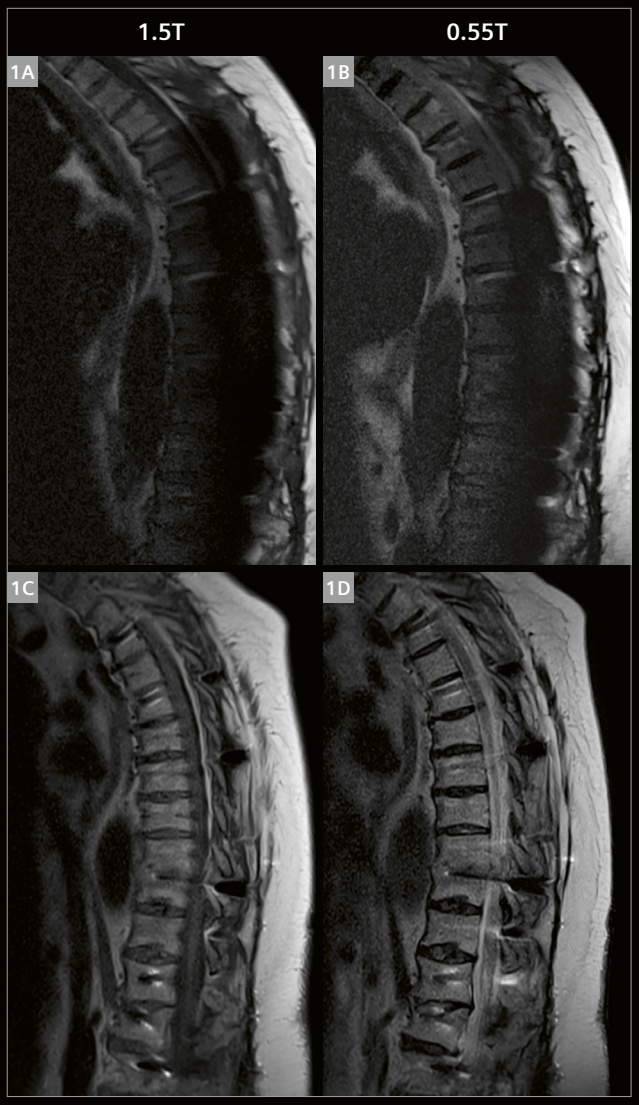

1 Preoperative imaging in a 59-year-old patient with multiple prior surgical procedures of the spine, prior to epidural pain catheter placement. Due to susceptibility artifact superimposition, the spinal canal was not assessable at 1.5T, neither in T2-weighted **(1A)** nor T1-weighted **(1C)** sequences. Artifact severity was substantially lower at 0.55T, allowing for assessment with high diagnostic confidence **(1B, 1D)**.

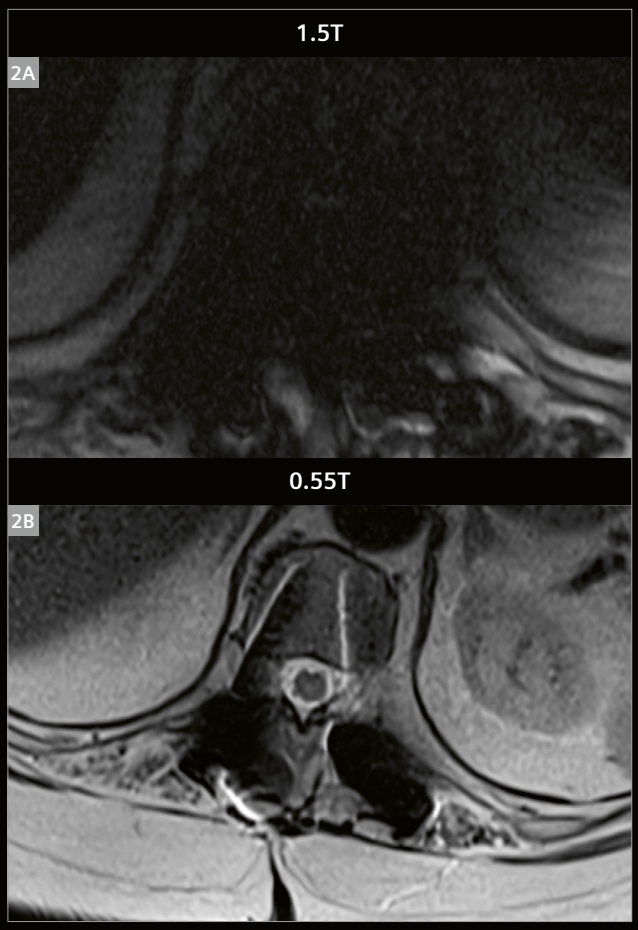

2 Similar to the sagittal images shown in Figure 1, the evaluation of the spinal canal was also only possible using the axial T2-weighted images acquired at 0.55T **(2B)**; while 1.5T did not allow for assessment due to artifact superimposition **(2A)**.

Case 2

A 59-year-old female patient presented with persistent knee pain five years after total knee arthroplasty. Given unremarkable radiographic examinations without signs of loosening, SPECT/CT and supplemental MR imaging at 0.55T were performed.

Radiography did not show signs of implant loosening or other postoperative complications (Fig. 3A). In contrast, MR imaging at 0.55T clearly depicted edema-equivalent signal changes adjacent to the tibial implant component in the lateral tibial plateau, and to a lesser extent also in the medial tibial plateau, indicative of implant loosening. Findings were consistent with the results from SPECT/CT imaging, which showed increased tracer uptake in the aforementioned locations. This was interpreted as implant loosening by a board-certified nuclear medicine physician (Figs. 3B, C).

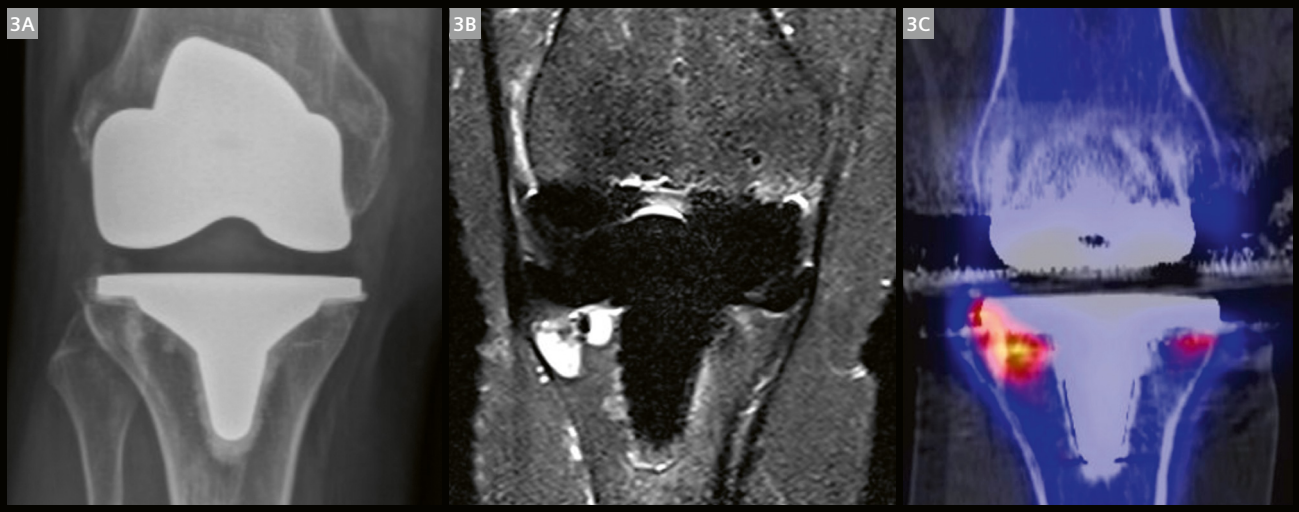

3 A 59-year-old female patient with persistent knee pain five years after total knee replacement. In contrast to conventional radiography **(3A)**, both 0.55T MR imaging **(3B)** and SPECT/CT imaging **(3C)** demonstrated implant loosening of the tibial implant component. The 0.55T MRI also allowed for assessment of ligamentous structures around the knee.

Case 3

A 39-year-old patient presented for routine follow-up imaging after resection of an osteosarcoma of the proximal left humerus and placement of a tumor prosthesis two years ago. Preoperative imaging was first performed at 3T. Follow-up imaging after surgery was performed at 1.5T and 0.55T.

The patient underwent regular postoperative follow-up imaging at 1.5T and supplemental imaging at 0.55T following osteosarcoma resection and tumor prosthesis implantation in the proximal left humerus. Preoperative imaging was performed at 3T (Figs. 4A, B). Comparing the follow-up MRI examinations, especially the soft tissues immediately adjacent to the tumor prosthesis shaft can be delineated clearly better at 0.55T (Fig. 3D) than at 1.5T (Fig. 3C) in the axial T2-weighted fat-suppressed sequences. In the scenario of patients undergoing follow-up imaging after bone tumor resection, potential local tumor recurrence close to the stem can be diagnosed or ruled out with greater confidence at low-field MRI, thanks to better delineation of adjacent structures due to fewer susceptibility artifacts.

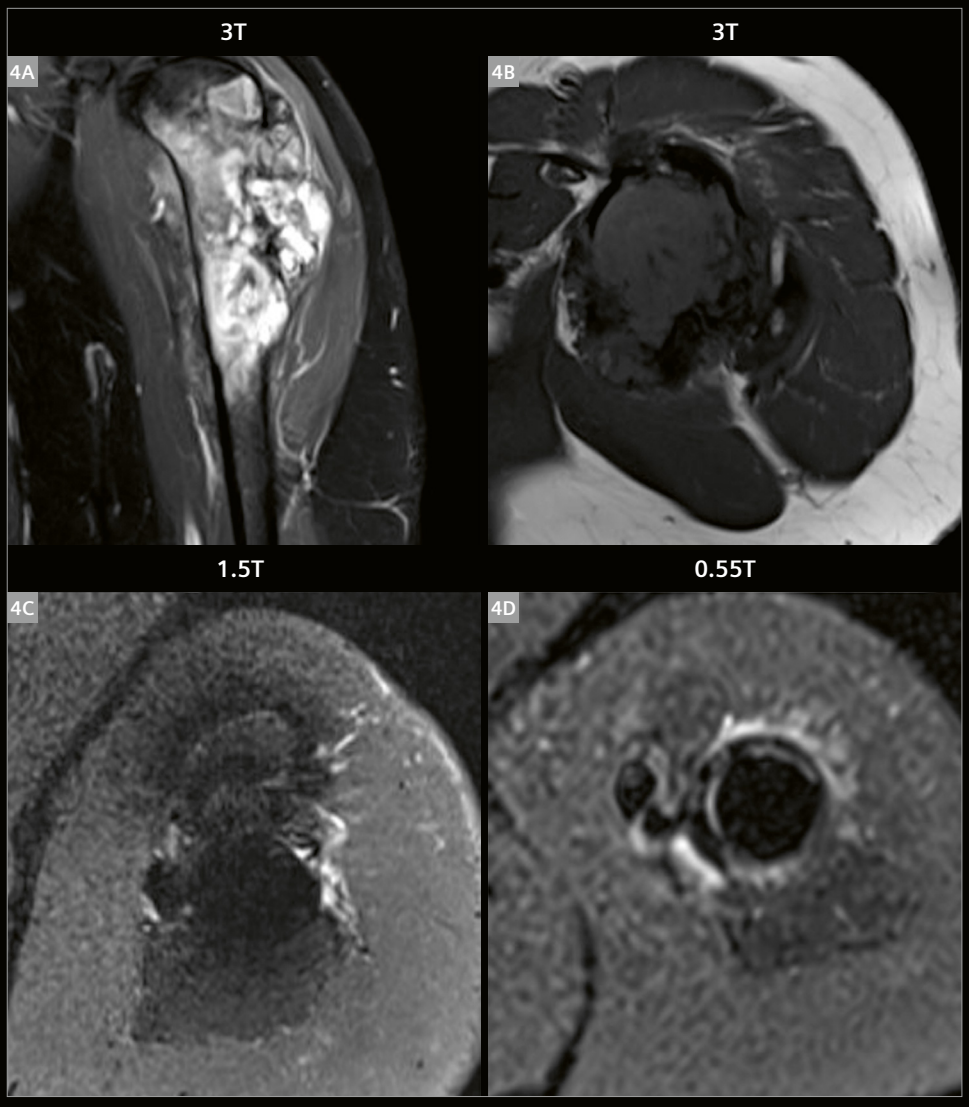

4 A 39-year-old patient who was diagnosed with osteosarcoma of the proximal humerus at 3T **(4A, 4B)**. Following tumor resection and tumor prosthesis implantation, follow-up imaging to assess for local tumor recurrence with axial T2-weighted fat-suppressed sequences is improved at 0.55T **(4D)** compared to 1.5T **(4C)**, with better delineation of the soft tissue structures immediately adjacent to the shaft.

Discussion

In order to achieve the best image quality, the acquisition protocol for handling metal implant imaging must be carefully optimized, regardless of the field strength. In the cases reported here, we employed our optimized clinical protocols for all field strengths used for the image acquisitions. Certain protocol features could contribute to more robust acquisition despite of the metal, while others can correct the resulting artifacts. Metal artifact correction methods, however, are often SAR intensive and result in longer acquisition times. By imaging at 0.55T one can also reduce the concern associated with increased SAR, while often being able to get good clinical results by employing a high-bandwidth protocol.

This brief case series emphasizes the potential of low-field MR imaging at 0.55T in patients with large metal implants. This is in accordance with recently published literature that outlines, for example, the advantages of low-field MR imaging over imaging at higher field strengths in patients with total hip arthroplasty [8]. Our initial experiences as demonstrated in this case series also suggest diagnostic benefits of 0.55T MR imaging in patient groups with other types of large metal implants, such as extensive thoracic or thoracolumbar spondylodesis. Reducing metal-implant-related susceptibility artifacts allows for improved assessment of structures and soft tissues immediately adjacent to the implants, which is of particular importance for detecting local recurrence following tumor resections. Additionally, low-field MR imaging may be helpful in the detection of implant loosening and could complement SPECT/CT imaging by providing details on soft-tissue structures around the knee prior to revising total knee replacements.

In conclusion, it appears to be worth conducting dedicated studies to asses potential applications and opportunities in metal implant imaging – especially in cases of large metal implants – to establish a role for 0.55T low-field MR imaging in clinical routine.

References

1 Runge VM, Heverhagen JT. Advocating the Development of Next-Generation, Advanced-Design Low-Field Magnetic Resonance Systems. Invest Radiol. 2020;55(12):747–753.
2 Vosshenrich J, Breit HC, Bach M, Merkle EM. Ökonomische Aspekte der Niederfeld-Magnetresonanztomographie : Anschaffung, Installation und Unterhaltskosten von 0,55 T-Geräten [Economic aspects of low-field magnetic resonance imaging: Acquisition, installation, and maintenance costs of 0.55 T systems]. Radiologe. 2022;62(5):400–404. German. Epub Mar 29
3 Rusche T, Vosshenrich J, Winkel DJ, Donners R, Segeroth M, Bach M, et al. More Space, Less Noise—New-generation Low-Field Magnetic Resonance Imaging Systems Can Improve Patient Comfort: A Prospective 0.55 T–1.5 T-Scanner Comparison. J Clin Med. 2022;11(22):6705.
4 Farahani K, Sinha U, Sinha S, Chiu LC, Lufkin RB. Effect of field strength on susceptibility artifacts in magnetic resonance imaging. Comput Med Imaging Graph. 1990;14(6):409–413.
5 Bernstein MA, Huston III J, Ward HA. Imaging artifacts at 3.0T. J Magn Reson Imaging. 2006;24(4):735–746.
6 Abdelaal MS, Restrepo C, Sharkey PF. Global Perspectives on Arthroplasty of Hip and Knee Joints. Orthop Clin North Am. 2020;51(2):169–176.
7 Jungmann PM, Agten CA, Pfirrmann CW, Sutter R. Advances in MRI around metal. J Magn Reson Imaging. 2017;46(4):972–991.
8 Khodarahmi I, Brinkmann IM, Lin DJ, Bruno M, Johnson PM, Knoll F, et al. New-generation low-field magnetic resonance imaging of hip arthroplasty implants using slice encoding for metal artifact correction: first in vitro experience at 0.55 T and comparison with 1.5 T. Invest Radiol. 2022;57(8):517–526.

Contact

Hanns-Christian Breit, M.D.
University Hospital Basel
Department of Radiology
Spitalstrasse 21
4031 Basel
Switzerland
Tel.: +41 61 328 56 33
hanns-christian.breit@usb.ch

Fetal Low Field MRI – the First 150 Cases

Jana Hutter, Ph.D.[1,2]; Jordina Aviles Verdera[1,2]; Raphaël Tomi-Tricot, Ph.D.[3]; Kelly Payette, Ph.D.[1,2]; Alena Uus, Ph.D.[1,2]; Sara Neves Silva[1,2]; Sebastien Ourselin, FREng[2]; Shaihan Malik, Ph.D.[1,2]; Mary Rutherford, M.D.[1,2]; Joseph Hajnal, Ph.D.[1,2]

[1]Centre for the Developing Brain, School of Biomedical Engineering, King's College London, UK
[2]Biomedical Engineering Department, School of Biomedical Engineering, King's College London, UK
[3]MR Research Collaborations, Siemens Healthcare Limited, Camberley, UK

Introduction

Fetal[1] magnetic resonance imaging (fetal MRI) has continuously increased its prominence in both research and clinical applications. The wide range of available contrasts, the high resolution, the ability to image the entire fetus up until late gestation, and operator-independence make it an essential research tool and an ideal complementary modality to ultrasound for clinical care. Fetal MRI is mainly used to image suspected clinical abnormalities found through ultrasound that require further clarification, such as neurological, spine, thorax, and abdominopelvic malformations or masses. It can also be used for detailed evaluations in cases of abnormal placentation, for antenatal surgical planning of spinal lesion closure in fetuses with spina bifida, and for laser ablations in monochorionic twin pregnancies or fetuses with congenital heart disease.

While anatomical imaging using turbo spin-echo (HASTE) sequences originally dominated, functional contrasts are increasingly being employed for a variety of indications in both research and clinical settings. They are either adapted from other parts of radiology or developed specifically for fetal indications, and include diffusion-weighted MRI [1, 2], T2* relaxometry [3], T1 relaxometry [4], and perfusion MRI [5]. As these complex functional techniques are being developed, they further increase the range of indications and hence applicability of fetal MRI.

While the current trend in MRI is to image at higher field strengths, some of the significant challenges encountered in fetal MRI may be addressed by operating at a lower field strength.

Advanced imaging techniques may be hampered by geometric distortion artifacts arising at air–tissue interfaces. This is made worse by the need to run highly efficient EPI-based read-outs for diffusion MRI, functional MRI, and multi-echo gradient echo sequences for T2* relaxometry, which leads to an increasing need for specialist image-based shimming techniques [6]. This increases examination time and the need for specialized fetal MRI technologists. Further challenges include B_1 inhomogeneity-related artifacts

1A

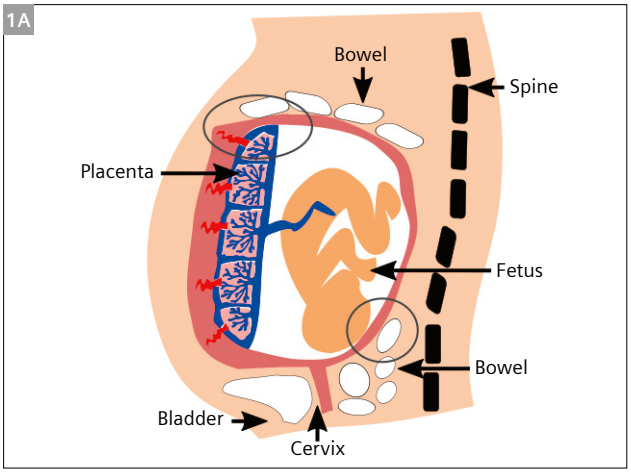

1B **Localizer**

Clinical protocol		
Anatomical MRI (T2-weighted HASTE)		11 min whole uterus
Diffusion MRI (Diffusion-weighted spin echo single shot EPI)		3 min whole uterus
Dynamic single-slice scan (cine)		1 min 1 slice
T2* Relaxometry (Multi-echo gradient echo single-shot (EPI)	*	4 min whole uterus
Research protocol		
T1 Relaxometry (Multi-echo gradient echo single-shot EPI)	*	3 min whole uterus
Combined T2*-Diffusion MRI (Multi-echo gradient echo single shot EPI)	*	8 min whole uterus
HARDI-Diffusion MRI (Diffusion-weighted spin echo single-shot EPI)	*	4 min placenta
No image-based shimming/calibration		

1 **(1A)** Schematic representation of the area of interest. The black circles signify areas of significant distortion due to air–tissue interfaces. **(1B)** Protocol overview for the clinical 20-minute exam and the research additions. The asterisks indicate custom-made sequences.

[1]*Siemens Healthineers disclaimer: MR scanning has not been established as safe for imaging fetuses and infants less than two years of age. The responsible physician must evaluate the benefits of the MR examination compared to those of other imaging procedures.*

enhanced by the presence of amniotic fluid, and specific-absorption-rate (SAR) limitations [7] resulting in inefficiencies in the sequences. Both B_0 and B_1 inhomogeneities increase with higher field strengths. Therefore, lower field strengths reduce both the impact of the aforementioned artifacts and the need for specialist correction tools.

T2* is quickly becoming a widely used functional modality, especially to assess the placenta in major pregnancy complications such as pre-eclampsia and fetal growth restriction. The increase in T2* at lower field strengths provides a clinically beneficial T2* dynamic range that is ideal for these assessments. Similarly, shorter T1 times at low field can potentially increase acquisition speed for T1 relaxometry, facilitating its application in fetal MRI.

While comfort and space are paramount for any patient undergoing an MRI scan, pregnant women in the later weeks of pregnancy present a population where space and comfort is both particularly important and challenging to achieve in a standard-sized MRI bore. In addition, the number of obese pregnant women is rising – with 24% of all pregnant women in the UK and U.S. considered obese as of 2020 [8]. This presents a currently underserved population that could benefit from fetal MRI, as these women often do not receive adequate prenatal imaging due in part to the detrimental effect of increased abdominal fat on ultrasound imaging. Lower-field strength MRI typically allows a homogeneous field even with a wider bore. Increasing the bore size to 80 cm and reducing the required length of the magnet may enable MRI to complement ultrasound in the routine clinical screening of the obese pregnant patient.

Finally, a field strength-independent challenge concerns unpredictable and uncontrollable fetal motion, especially in early-to-mid gestation when fetuses have enough space for large displacements. This can be particularly problematic for fetal functional MRI modalities, which rely on the acquisition of the same slice location multiple times in a time-series format, to then be combined for spatiotemporal analysis. Both post-processing base techniques such as slice-to-volume registration (SVR) [9, 10] and prospective motion-correction techniques based on localization and tracking may be employed at low field strengths.

Main benefits:

- 20-minute efficient and robust clinical imaging workflow at low field
- Improved patient comfort due to wide bore
- Increased magnetic field homogeneity and reduced imaging artifacts
- First evidence proving the efficacy of low-field clinical fetal MRI

Materials and methods

Patient preparation and comfort

Pregnant patients are consented for research by either a research midwife or obstetrician and then prepared for the scan. The weight of the pregnant uterus on the vena cava in supine position can in rare cases lead to vasovagal episodes. To mitigate this and allow early detection, tight blood pressure controls are performed in multiple positions. A first blood pressure reading is taken while the patient is sitting on the scanner table, after which they lie on their left side for a second blood pressure reading, and then slowly the patient is eased onto their back in head first supine position to limit the compression of the vena cava. Padding for the lower back, the head, and the legs is provided as requested. Throughout the scan, blood pressure readings are performed automatically at 10-minute intervals, the maternal heart rate and saturation are continuously monitored, and frequent verbal interaction is maintained.

Clinical protocol

The protocol was crafted to allow assessment of the fetal brain and body, the placenta, and the cervix (see Figure 1A for an overview). It consists of a clinical session (Fig. 1B), which lasts about 20 minutes, and a research session of up to 40 minutes. Both are designed specifically with the advantages and challenges of 0.55T in mind and are therefore modified from our standard fetal imaging at 1.5T and 3T in the following way:

The resolution for the anatomical HASTE scans was reduced, using a slice thickness of 4.5 mm instead of 2.5 mm (in-plane resolution 1.4 × 1.4 mm^2) and 9 stacks (3 uterus stacks, 3 fetal brain stacks, and 3 fetal body stacks) instead of 6 to allow robust SVR.

A multi-echo gradient echo EPI sequence was modified to include multiple echoes, allowing for motion-robust T2* mapping of the entire uterus with 20 dynamics. T2* shortens with advanced gestational age and with most major pathologies. Compared to higher field strengths, the increased T2* at low field allows longer read-outs and the conservation of signal over longer echo times at later gestation and in cases with placental disease. A diffusion MRI scan, allowing both apparent diffusion coefficient (ADC) and intravoxel incoherent motion (IVIM) calculations as typically used for fetal imaging, was acquired covering the entire uterus. Finally, a dynamic (CINE) single-slice HASTE scan was acquired (TR = 4 seconds) to visualize cardiac activity and limb and head motion.

Research protocol

The gradient echo sequence was modified with a global adiabatic inversion pulse and slice-shuffling to reap the benefits of the reduced T1 at this field strength for an efficient quantitative fetal T1 acquisition. A previously

proposed multi-echo diffusion MRI scan [11] was used to sample a large parameter space, combined synergistically with the longer T2* and allowing sampling for a longer time.

Importantly, none of these elements included image-based shimming or any other advanced shimming of the kind required on higher-field scanners, thus saving scanning time.

Analysis and quantities obtained

An anatomical brain report is obtained from the HASTE stacks and includes bi-parietal diameter, transcerebellar diameter, ventricular sizes, presence of orbits, ears, and more. The cervical length and the lung are segmented individually to obtain respective quantitative values. The stacks are also reconstructed to 3D volumes using SVR resulting in automatic segmentations and volumes for 16 brain regions. Mono-exponential fitting is performed on the T2* and T1 data to obtain quantitative maps for the brain and placenta. Finally, the dynamic T2* scans are processed using SVR and AI-based localization and segmentation to obtain organ-specific T2* maps and values for 10 organs of interest.

Results

Comfort and success of the examination

In the first nine months, a total of 150 fetal scans from 16+0 to 40+2 weeks of gestational age were performed on the 0.55T scanner, including 25 patients referred for clinical indications. This cohort includes patients with either significant claustrophobia or a BMI that does not

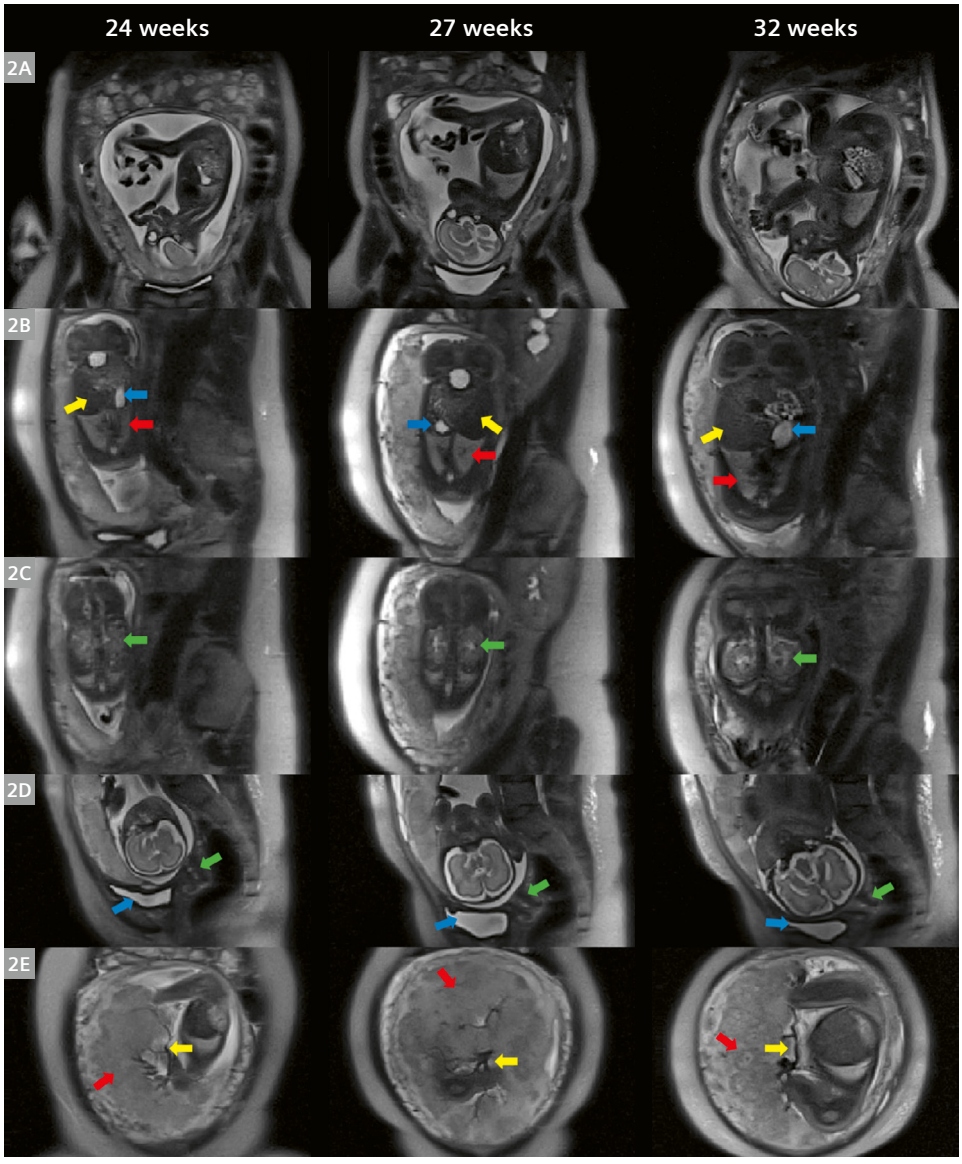

2 Fetal case scanned longitudinally at three time points during pregnancy (24, 27, and 32 weeks) illustrating **(2A)** a coronal whole uterus view; **(2B)** the fetal lung (red), stomach (blue), and liver (yellow); **(2C)** the kidney (green); **(2D)** the cervix (green arrow) and bladder (blue arrow); and **(2E)** a coronal whole uterus view through the placenta showing chorionic vessels connecting the placenta to the umbilical cord (yellow arrows) and the increasing heterogeneity with age within placental lobules (red arrow).

allow comfortable examination on any other available scanner (max BMI = 49.9 kg/m²). The pathologies studied included neurological abnormalities (ventriculomegaly, midline cysts, mega cisterna magna, scalp tumor), fetal body abnormalities (cystic kidney), and big obstetrical syndromes associated with the placenta (pre-eclampsia, fetal growth restriction). They also included findings such as funnels in the cervix, endometrial cysts, and fibroids. Patient feedback from a small cohort of pregnant women who had both a low-field and a high-field MRI scan during the same pregnancy revealed an increase in comfort (from 2.9 to 4.3 on a scale of 1 "not comfortable" to 5 "very comfortable"). This was also reflected in the large number of research patients choosing to come back for up to four scans.

Anatomical data obtained as illustrated in a longitudinal case (the same fetus was scanned at 24, 27, and 32 weeks) shown in Figure 2 clearly depicts all fetal structures (lungs, liver, stomach, and kidney are marked with arrows), the placental vasculature (yellow arrow), heterogeneity (red arrow), and the cervix (green arrow). Figure 3 shows more detailed views of the brain in radiological planes and after SVR at three time points. The results from automatic regional segmentation on these SVR results are shown for 60 healthy control cases in the bottom row, illustrating the ability of the data to accurately assess growth. Finally, Figure 4 shows zoomed images of the described pathologies, illustrating the ability of the low-field data to robustly visualize and quantify these.

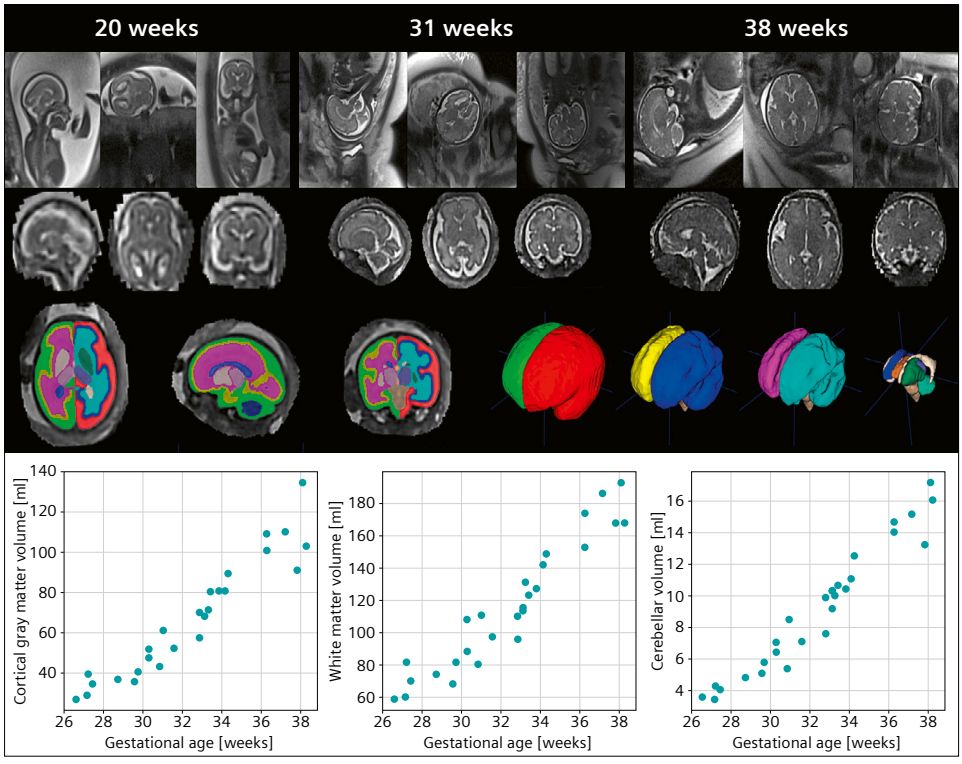

3 Detailed views of the HASTE data from the brain, acquired in radiological planes (top row) and after SVR (second row) at 20, 31, and 38 weeks. Results from the automatic subregion brain segmentation (third row) and volumetric brain assessment over gestational age (bottom row) from left to right: cortical grey matter volume, white matter volume, and cerebellar volume.

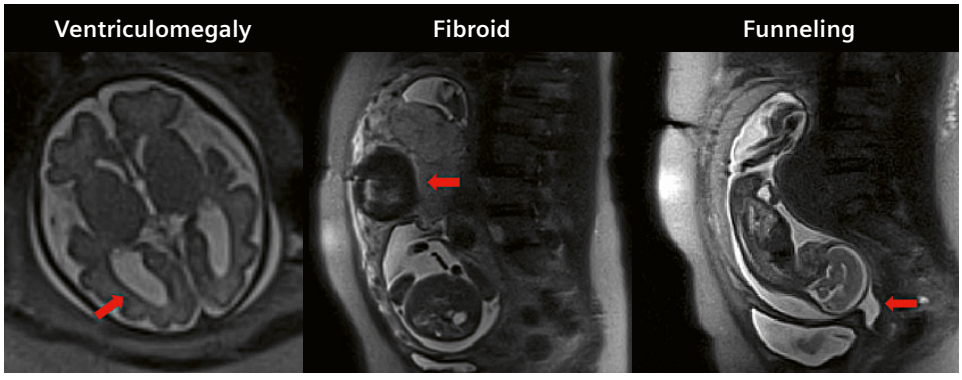

4 Fetal HASTE images of selected pathologies, including ventriculomegaly, an enlarged cisterna magna, a low signal-intensity fibroid, and funneling of the cervix.

Functional data and case study: BMI of 49.9 kg/m²
A total of 128 full sets of functional data were acquired, including T1 and T2* relaxometry and diffusion MRI. Imaging from a longitudinal case (same fetus scanned at 32 and 40 weeks) for T1 and for T2* (Fig. 5) depicts good delineation of major and fine brain structures. Finally, the T2* obtained for each fetal organ shows the ability of the proposed protocol at 0.55T to acquire quantitative information even for small fetal structures throughout gestation.

Results in a selected case with BMI = 49.9 kg/m² (Figure 6 for the anatomical and Figure 7 for the functional data) demonstrate the ability to obtain detailed results even in such challenging cases.

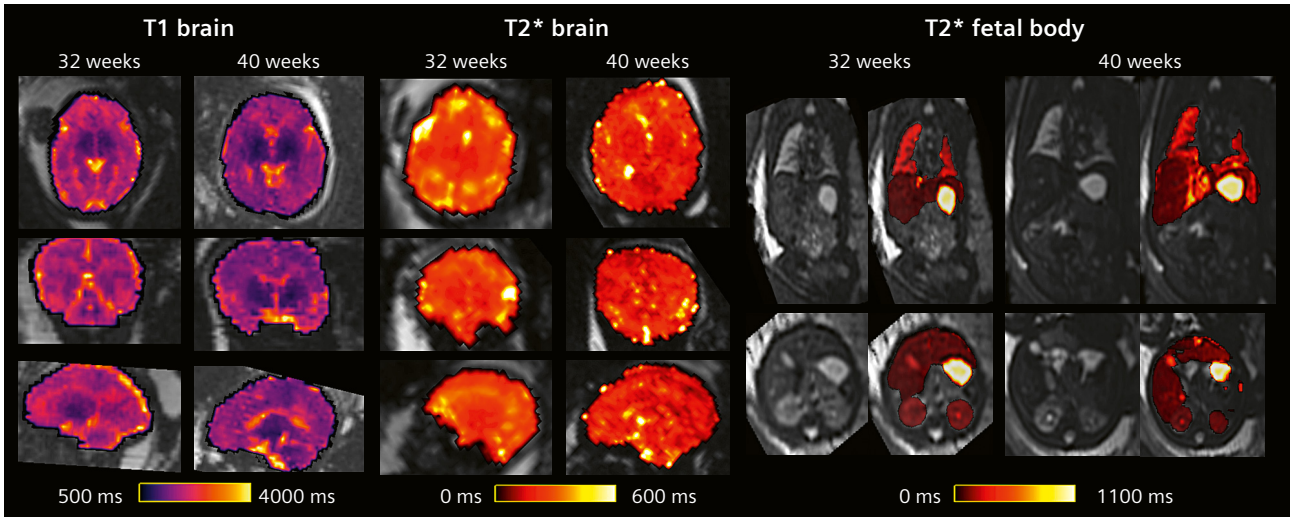

5 Longitudinal T1 (left) and T2* (middle) brain maps, and fetal organ T2* maps (right) for a subject scanned at 32 and 40 weeks' gestational age.

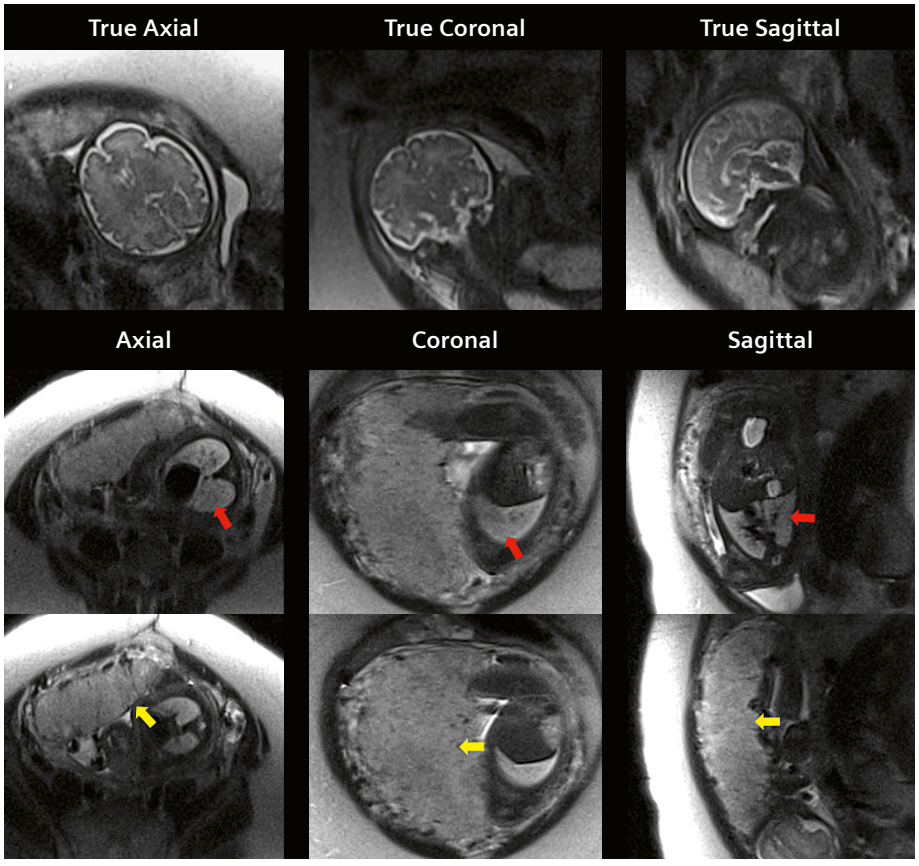

6 **Case study of fetal MRI at BMI 49.9 kg/m²: Part I:** Anatomical results for a participant with BMI = 49.9 kg/m² showing the ability to depict the brain structures (top row), the lungs (middle row, red arrows) and the placenta (bottom row, yellow arrows).

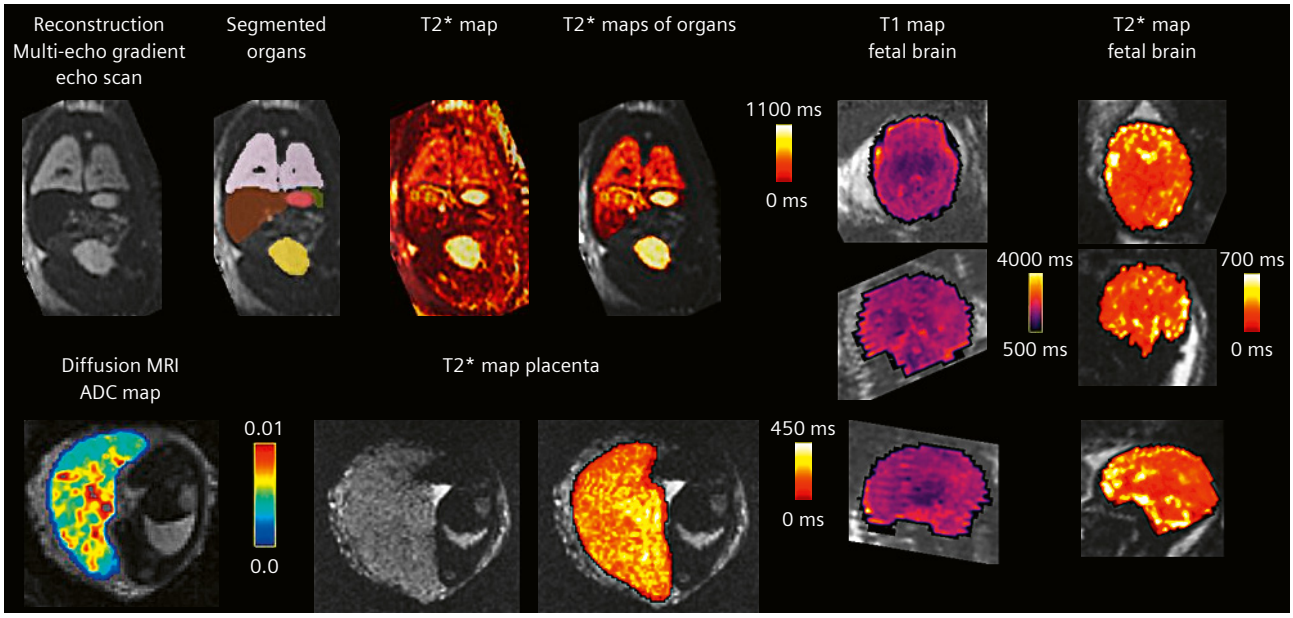

7 **Case study of fetal MRI at BMI 49.9 kg/m²: Part II:** Functional results from the same case for a participant with BMI = 49.9 kg/m² showing the individual organ T2* maps, the T1 and T2* maps of the brain, and the placental ADC and T2* map.

Discussion and conclusion

Fetal MRI at 0.55T is feasible, offers essential benefits, and is thus a promising direction for future antenatal imaging. The proposed short protocol allows anatomical and functional assessment of the fetus within 20 minutes. This is facilitated by foregoing any need for image-based shimming or other special correction tools, and carefully drafted to make use of the longer T2* and shorter T1 at low field. The research sequences allow further insights into desired regions of interest such as placental and lung microstructure and function. The wider bore size and shorter length increases comfort and thus increases access to fetal MRI until late gestation and in patients with higher BMIs. The fact that the scanner is a commercially available system makes it easy to integrate state-of-the-art techniques such as simultaneous multi-slice imaging, illustrated at 0.55T in Figure 8. Next steps will include adding fetal cardiac sequences; scanning further clinical cohorts such as patients with invasive placentation, preeclampsia, and congenital heart disease; and assessing the fetal placental unit prior to labor to assist in birth management. Other routinely used sequences for fetal MRI such as TrueFISP and T1-weighted contrasts will be added in the future.

An important future step is to further increase the availability of fetal MRI by allowing operation in hospitals and imaging centers without fetal MRI specialists. To come closer to this goal, a first step was the development of a prospective motion-correction technique that can detect fetal head translational displacements using deep learning and then feeds this information back to the scanner to continuously update the acquisition geometry in real time. This prospective motion correction shows great potential for applications that would highly benefit from precise correction of motion artifacts and immediate enhancement of the image quality during the scan. This can also be developed to be used to assess the tissue microstructure of the fetal brain through the quantification of the fetal brain's blood-oxygen-level-dependent (BOLD) response to maternal oxygenation and diffusion MRI.

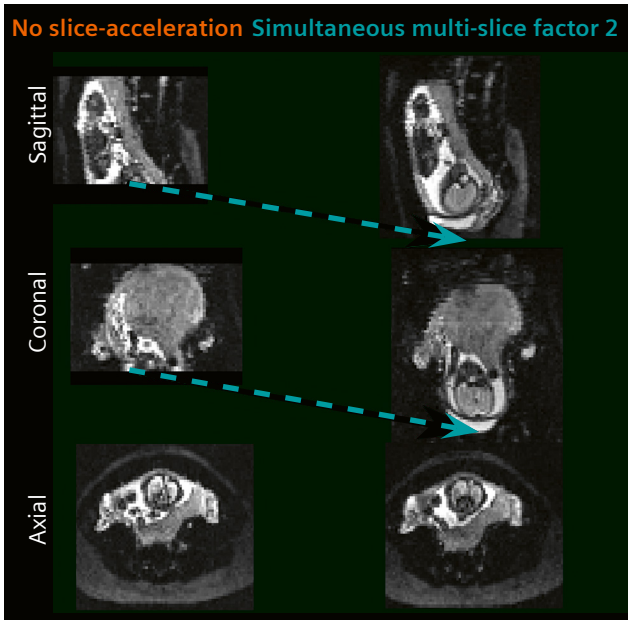

8 Simultaneous multi-slice imaging for T2* imaging at 0.55T illustrating the extension of the field of view by a factor of nearly two in the same scan time.

References

1 Bonel HM, Stolz B, Diedrichsen L, Frei K, Saar B, Tutschek B, et al. Diffusion-weighted MR imaging of the placenta in fetuses with placental insufficiency. Radiology. 2010;257(3):810–819.
2 Slator PJ, Hutter J, Palombo M, Jackson LH, Ho A, Panagiotaki E, et al. Combined diffusion-relaxometry MRI to identify dysfunction in the human placenta. Magn Reson Med. 2019;82(1):95–106.
3 Sørensen A, Hutter J, Seed M, Grant PE, Gowland P. T2*-weighted placental MRI: basic research tool or emerging clinical test for placental dysfunction?
Ultrasound Obstet Gynecol. 2020;55(3):293–302.
4 Gowland PA, Freeman A, Issa B, Boulby P, Duncan KR, Moore RJ, et al. In vivo relaxation time measurements in the human placenta using echo planar imaging at 0.5 T.
Magn Reson Imaging. 1998;16(3):241–247.
5 Zun Z, Limperopoulos C. Placental perfusion imaging using velocity-selective arterial spin labeling.
Magn Reson Med. 2018;80(3):1036–1047.
6 Gaspar AS, Nunes RG, Ferrazzi G, Hughes EJ, Hutter J, Malik SJ, et al. Optimizing maternal fat suppression with constrained image-based shimming in fetal MR.
Magn Reson Med. 2019;81(1):477–485.
7 Abaci Turk E, Yetisir F, Adalsteinsson E, Gagoski B, Guerin B, Grant PE, et al. Individual variation in simulated fetal SAR assessed in multiple body models.
Magn Reson Med. 2020;83(4):1418–1428.
8 Creanga AA, Catalano PM, Bateman BT. Obesity in Pregnancy.
N Engl J Med. 2022;387(3):248–259.
9 Uus A, Zhang T, Jackson LH, Roberts TA, Rutherford MA, Hajnal JV, et al. Deformable Slice-to-Volume Registration for Motion Correction of Fetal Body and Placenta MRI.
IEEE Trans Med Imaging. 2020;39(9):2750–2759.
10 Kuklisova-Murgasova M, Quaghebeur G, Rutherford MA, Hajnal JV, Schnabel JA. Reconstruction of fetal brain MRI with intensity matching and complete outlier removal.
Med Image Anal. 2012;16(8):1550–1564.
11 Hutter J, Slator PJ, Christiaens D, Teixeira RPAG, Roberts T, Jackson L, et al. Integrated and efficient diffusion-relaxometry using ZEBRA. Sci Rep. 2018;8(1):15138.

Contact

Jana Hutter, Ph.D.
Centre for the Developing Brain
School of Biomedical Engineering
King's College London
Westminster Bridge Road
London, SE1 7EH
United Kingdom
jana.hutter@kcl.ac.uk

Cardiac MRI on the MAGNETOM Free.Max: The Ohio State Experience

Orlando P. Simonetti[1], Juliet Varghese[1], Ning Jin[2], Daniel Giese[3], Yingmin Liu[1], Chong Chen[1], Rizwan Ahmad[1], Yuchi Han[1]

[1]The Ohio State University, Columbus, OH, USA
[2]Siemens Healthineers, Malvern, PA, USA
[3]Siemens Healthineers, Erlangen, Germany

Background

As the cardiovascular magnetic resonance (CMR) program at The Ohio State University has expanded, we added both a higher (3T, MAGNETOM Vida) and a lower (0.55T, MAGNETOM Free.Max) field system to our existing 1.5T MAGNETOM Sola. Having access to scanners with three different field strengths has enabled us to investigate the pros and cons of each across different CMR applications, with the aim to match the right field strength for the right patient and pathology. The first step in this process was to develop and implement cardiac imaging techniques for the MAGNETOM Free.Max, which was delivered without CMR product pulse sequences. We have worked closely with our colleagues at Siemens Healthineers to put together a comprehensive package of CMR techniques[1], which currently are still in the preliminary stage of development.

While signal-to-noise ratio (SNR) is directly proportional to the main magnetic field (B_0), lower B_0 offers a number of potential advantages for CMR [1, 2]. The higher field homogeneity and lower specific absorption rate (SAR) at lower-field benefits techniques that are dependent on balanced steady-state free precession (bSSFP), potentially increasing safety and reducing artifacts in patients with implanted devices[2]. Lower B_0 means lower Lorentz forces, reducing audible noise and potentially improving the patient experience. Reduced B_0 also offers greater flexibility in magnet design. The Free.Max platform has a unique, 80 cm diameter bore and an optional 705 lb / 320 kg patient table limit, which eliminates barriers to MRI for those with severe obesity. One of our primary motivations to pursue the development of CMR techniques on the MAGNETOM Free.Max is to increase the accessibility to CMR for obese patients, as well as those with severe claustrophobia who may benefit from the larger bore and quieter scans.

The United States Centers for Disease Control and Prevention (CDC) reports that the prevalence of obesity (body mass index (BMI) > 30 kg/m^2) now exceeds 40% and is projected to affect 50% of the U.S. population by 2025 [3]. The obesity epidemic is not unique to the USA, with a prevalence now exceeding 20% in most Western European countries. Obesity increases the risk of cardiovascular disease (CVD) [4] and these risks are even greater in those with severe obesity, i.e., BMI > 40 kg/m^2, which now accounts for more than 9% of the adult USA population. This significant population segment faces serious healthcare challenges, especially in terms of access to non-invasive cardiovascular imaging. Most cardiac imaging equipment is not designed to accommodate the weight and girth of severely obese patients; furthermore, radiation-based modalities such as CT and SPECT require excessive radiation for adequate image quality, while attenuation of ultrasound by adipose tissue limits the utility of echocardiography [5, 6]. If not for the bore diameter (60 cm – 70 cm) and table weight limits (typically < 450 lbs / 200 kg) of standard magnetic resonance imaging (MRI) systems, MRI could provide a safe, comprehensive assessment of CVD in even the most severely obese patients. The 80 cm bore and optional 705 lb / 320 kg table weight limit of MAGNETOM Free.Max offer this possibility.

Several years ago, our group recognized the potential for low-field cardiovascular MRI [1], and demonstrated the feasibility of CMR at 0.35T in comparison with standard field strengths [7]. Our work, together with preliminary results published by others using a prototype scanner

[1]Work in progress: the application is currently under development and is not for sale in the U.S. and in other countries. Its future availability cannot be ensured.
[2]The MRI restrictions (if any) of the metal implant must be considered prior to patient undergoing MRI exam. MR imaging of patients with metallic implants brings specific risks. However, certain implants are approved by the governing regulatory bodies to be MR conditionally safe. For such implants, the previously mentioned warning may not be applicable. Please contact the implant manufacturer for the specific conditional information. The conditions for MR safety are the responsibility of the implant manufacturer, not of Siemens Healthineers.

ramped-down to 0.55T [2, 8], supported the concept that high quality CMR could be feasible at reduced field strength. We hypothesized that the ultra-wide bore MAGNETOM Free.Max system could deliver the proven benefits of CMR to the severely obese patient population, i.e., patients who face significantly limited diagnostic image quality and radiation dosing challenges from other imaging modalities, and set a goal of developing a comprehensive suite of CMR techniques for the MAGNETOM Free.Max. To achieve this goal, however, requires overcoming two primary technical challenges;

1) the deficit in SNR as compared to higher field systems, and
2) the reduced gradient performance (26 mT/m max. amplitude and 45 mT/m/ms max. slew rate) of MAGNETOM Free.Max, resulting in longer echo times (TE) and repetition times (TR).

Taken together, these performance differences can lead to significantly longer scan times, and compromised spatial and temporal resolution. These factors are especially critical in CMR where scan time is often limited to a short breath-hold to avoid respiratory motion, and sufficient temporal resolution is required to avoid cardiac motion artifact, or to accurately resolve cardiac motion and flow. The initial steps we have taken to address these limitations include the implementation of dedicated pulse sequences, optimization of scan parameters, judicious use of advanced reconstruction strategies, and machine learning driven denoising. Preliminary results are shown in the following sections where we review the various component techniques that comprise the comprehensive cardiac package, and present example results we have obtained to date in animal models, healthy volunteers, and patients with cardiovascular disease, including those with severe obesity.

Our cardiac package

Overview

As the MAGNETOM Free.Max does not include dedicated sequences released for cardiac imaging, all of the following sequences and reconstruction techniques are research packages[1] that were enabled and/or developed by our group in collaboration with Siemens Healthineers. Furthermore, the MAGNETOM Free.Max does not have an integrated ECG triggering system; yet, it is capable of accepting an external triggering signal, and this can be provided by a variety of third-party patient monitoring systems.

At this early stage of the project, we have developed working techniques covering all of the clinical CMR applications shown in Figure 1. Our ultimate goal is to run protocols that obviate the need for patient breath-hold, and can be completed within 30 minutes; however, at this stage of development, some methods still rely on conventional segmented *k*-space, breath-hold acquisition. As we continue to innovate and combine advanced compressed sensing (CS) and deep learning-based reconstruction techniques paired with custom data acquisition strategies, we fully expect to achieve our goal of a rapid, comprehensive free-breathing CMR suite.

Morphology

Dark-blood turbo spin echo (TSE) based techniques are useful to distinguish morphological features and to characterize masses and tumors. The limited SNR and gradient speed available on MAGNETOM Free.Max impact the performance of some CMR techniques more than others. Given that TSE images tend to have relatively high SNR and the sequence is not reliant on fast gradients, the translation from higher field and faster gradient systems was

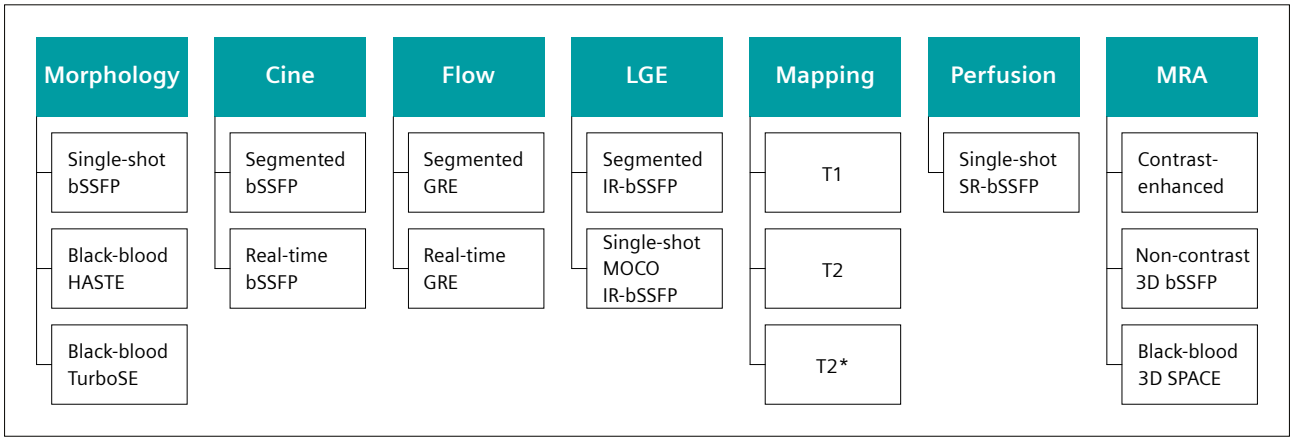

1 Shown are the primary components of the comprehensive cardiac imaging package[1]. All of the basic components are in place, although many of these techniques rely on breath-hold, segmented *k*-space acquisitions. Optimization of techniques and scan parameters is ongoing in our effort to maximize SNR, contrast, and image quality. We also continue working to develop strategies to support free-breathing image acquisition across all categories.

straightforward, and the technique performed well at low field with little modification. Example images in a healthy volunteer are shown in Figure 2, demonstrating the commonly used variants of black-blood T1 and T2-weighted TSE, and STIR. These are standard acquisitions with each 2D slice acquired in a short breath-hold of 10 to 12 heartbeats, and employed the Deep Resolve AI-based image denoising technique provided by Siemens Healthineers. Exemplary scan parameters used at 0.55T and 1.5T are listed in Table 1. Example images (Fig. 3) at both 1.5T and 0.55T in a patient with Harrington rods in their spine illustrate the reduced artifact surrounding metal implants[2] that can be expected at lower B_0 field strength.

Cine

Cine imaging is at the core of every CMR exam, providing information on cardiovascular morphology and function. Measurements can be made on the cine images to quantify global and regional cardiac function. Cine typically relies on balanced steady-state free precession, (bSSFP) and therefore has inherently high SNR relative to other techniques. Thus, the reduced SNR at low field is not a significant obstacle; however, bSSFP cine does require short TR for high temporal resolution, thus presenting a challenge on this scanner where gradient performance is limited. We have addressed this challenge through the utilization of CS reconstruction methods [9]. Table 2 lists the imaging parameters achieved at 0.55T, in comparison to a 1.5T scanner with faster gradients. With highly accelerated CS-based sequences, we have been able to achieve high-quality cine results with segmented breath-hold techniques, as well as real-time, free-breathing imaging. Segmented *k*-space, breath-hold cine images acquired in the same patient at 1.5T and at 0.55T are shown in Figure 4. This patient has an artificial aortic valve with metallic components[2]. The size of the signal void around the valve is less in the 0.55T images, as might be expected due to the reduced susceptibility gradients surrounding the metal. The degree of metal artifact is highly dependent on the specific material used to construct the implant[2].

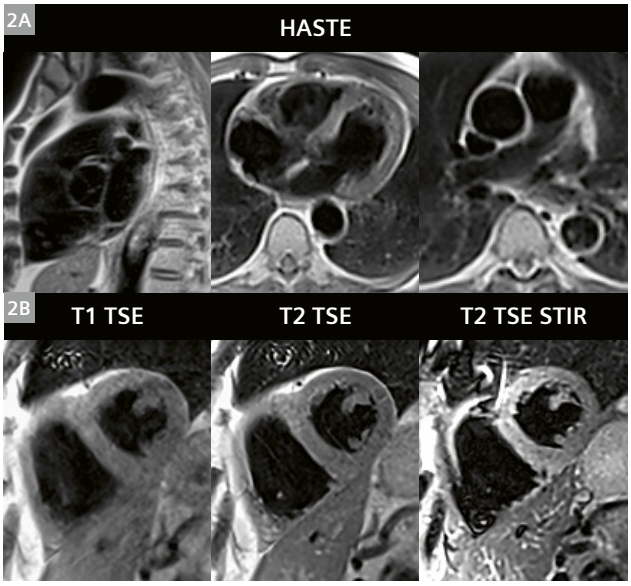

2 Dark-blood images acquired in a volunteer. Single-shot HASTE images in different cardiac views are shown in the top row **(2A)**. The bottom row shows T1 TSE, T2 TSE and T2 TSE STIR images in a mid-short axis view **(2B)**. Each TSE image was acquired in a 12-heartbeat breath-hold.

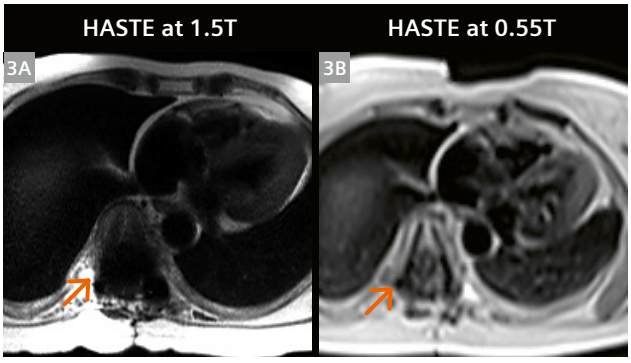

3 Single-shot axial images acquired in a patient with Harrington rods post spinal fusion[2]. HASTE images acquired on a 1.5T MAGNETOM Avanto system **(3A)** from a prior exam demonstrate significant susceptibility artifact (orange arrows) compared to localized artifact on the corresponding HASTE image at 0.55T **(3B)**.

	Scanner	Flip angle (deg)	TE (ms)	Echo spacing (ms)	RBW Hz/pixel	Turbo factor	Temporal resolution (ms)	Slice thickness (mm)	Pixel size (mm)	Acceler-ation	Scan time
T2 TSE	1.5T MAGNETOM Sola	180	60	3.54	849	17	60	5	1.3 × 1.3	G 2	10 HB
	0.55T MAGNETOM Free.Max	180	43	5.36	401	14	75	6	2.0 × 2.0	G 2	12 HB
HASTE	1.5T MAGNETOM Sola	120	35	3.94	501	104	409	6	1.3 × 1.3	none	1 HB
	0.55T MAGNETOM Free.Max	160	16	4.1	1502	72	295	10	3.6 × 3.6	G 2	1 HB

Table 1: Acquisition parameters for breath-hold segmented turbo spin echo (TSE) (top rows) and single-shot HASTE (bottom rows) shown for 1.5T MAGNETOM Sola and 0.55T MAGNETOM Free.Max.

It is also dependent on TE and TR, and therefore will be affected by gradient performance as well as field strength. Figure 5 shows a comparison of breath-held segmented *k*-space cine images and real-time cine images, all acquired at 0.55T using the scan parameters listed in Table 2. Despite the high acceleration rates used to overcome slower gradient performance, SNR and overall image quality are maintained with CS reconstruction.

Flow quantification

Phase contrast (PC) imaging is the standard MRI method used to measure blood flow. While low-field offers advantages of reduced susceptibility and greater field homogeneity, the inherently low SNR of the spoiled gradient echo (GRE) sequences used for PC MRI can be challenging at low-field, and higher acceleration is needed to overcome slower gradients. We have successfully implemented segmented *k*-space, breath-hold flow quantification on the MAGNETOM Free.Max [10] and sample results

	Scanner	Flip angle (deg)	TE (ms)	TR (ms)	RBW Hz/pixel	Segments	Temporal resolution (ms)	Slice thickness (mm)	Pixel size (mm)	Acceleration	Scan time
BH-Cine	1.5T MAGNETOM Sola	75	1.16	2.71	930	12	32.5	6	1.8 × 1.8	CS 4.3	3 HB
	0.55T MAGNETOM Free.Max	110	1.95	4.65	930	6	27.9	8	1.8 × 1.8	CS 4.3	6 HB
RT-Cine	1.5T MAGNETOM Sola	75	1.04	2.43	1184	18	43.7	8	2.0 × 2.0	CS 7.4	1 HB
	0.55T MAGNETOM Free.Max	110	1.84	4.55	1002	10	45.5	8	2.0 × 2.0	CS 9.7	1 HB

Table 2: Acquisition parameters for breath-hold segmented *k*-space cine (top rows) and real-time free-breathing cine (bottom rows) shown for 1.5T MAGNETOM Sola with faster gradients than the 0.55T MAGNETOM Free.Max. Higher acceleration rates are used for real-time cine on the MAGNETOM Free.Max to overcome the slower gradients.

4 End-diastole (ED) and End-systole (ES) cine frames acquired in a three-chamber view (3CH) and left ventricular outflow tract (LVOT) are shown. The 1.5T (MAGNETOM Avanto) **(4A)** images shown were acquired in the same patient in a prior exam using a GRAPPA-based breath-held segmented SSFP method. Images at 0.55T **(4B)** were acquired using a compressed sensing-based breath-held segmented SSFP method. Note that the patient has an artificial valve[2], and the metal artifacts in proximity to the valve are reduced at 0.55T.

in comparison with GRAPPA parallel imaging are shown in Figure 6. In preliminary testing, CS-based reconstruction provides the high acceleration rates needed while maintaining spatial and temporal resolution and SNR. Real-time flow imaging requires significantly higher acceleration rates and is still under development, but free-breathing acquisition can be achieved through the use of signal averaging to suppress respiratory motion artifact, as also shown in Figure 6. Exemplary PC-MRI scan parameters are listed in Table 3. Although initial results demonstrate the feasibility of flow quantification on the MAGNETOM Free.Max, several sources of errors related to low-field and/or lower gradient performance (e.g., Maxwell-Terms and Flow Displacement Artifacts) are still under investigation.

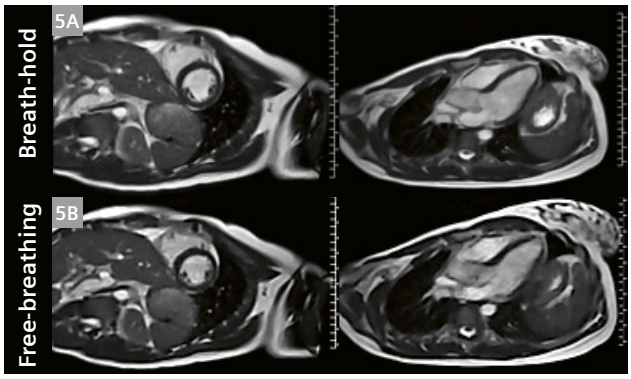

5 Breath-held segmented *k*-space cine frames **(5A)** and real-time free-breathing cine frames **(5B)** acquired in a healthy volunteer. Despite use of a high under-sampling rate of near 10× in real-time cine, CS reconstruction provides sufficient image quality at 0.55T.

	Scanner	Flip angle (deg)	TE (ms)	TR (ms)	RBW Hz/pixel	Segments	Temporal resolution (ms)	Slice thickness (mm)	Pixel size (mm)	Acceleration	Scan time
BH Flow	1.5T MAGNETOM Sola	15	2.26	4.23	501	5	42.3	6	2.0 × 2.0	G 2	10 HB
	0.55T MAGNETOM Free.Max	12	4.49	7.64	427	3	45.8	6	1.8 × 1.8	CS 3	13 HB
FB Flow	1.5T MAGNETOM Sola (RT)	12	2.51	4.41	560	6	52.9	10	2.8 × 2.8	CS 16	1 HB
	0.55T MAGNETOM Free.Max (avg)	12	3.67	6.55	427	3	39.3	8	1.9 × 1.9	G 2	58 HB

Table 3: Acquisition parameters for breath-hold segmented *k*-space flow quantification sequence (top rows) and free-breathing acquisition (bottom rows) shown for 1.5T MAGNETOM Sola and 0.55T MAGNETOM Free.Max. Free-breathing (FB) acquisition is currently achieved by signal averaging to suppress respiratory motion on MAGNETOM Free.Max, while real-time (RT) flow data acquisition is possible at 1.5T using compressed sensing. Real-time flow requires significantly higher acceleration, which is challenging in face of the reduced SNR at 0.55T.

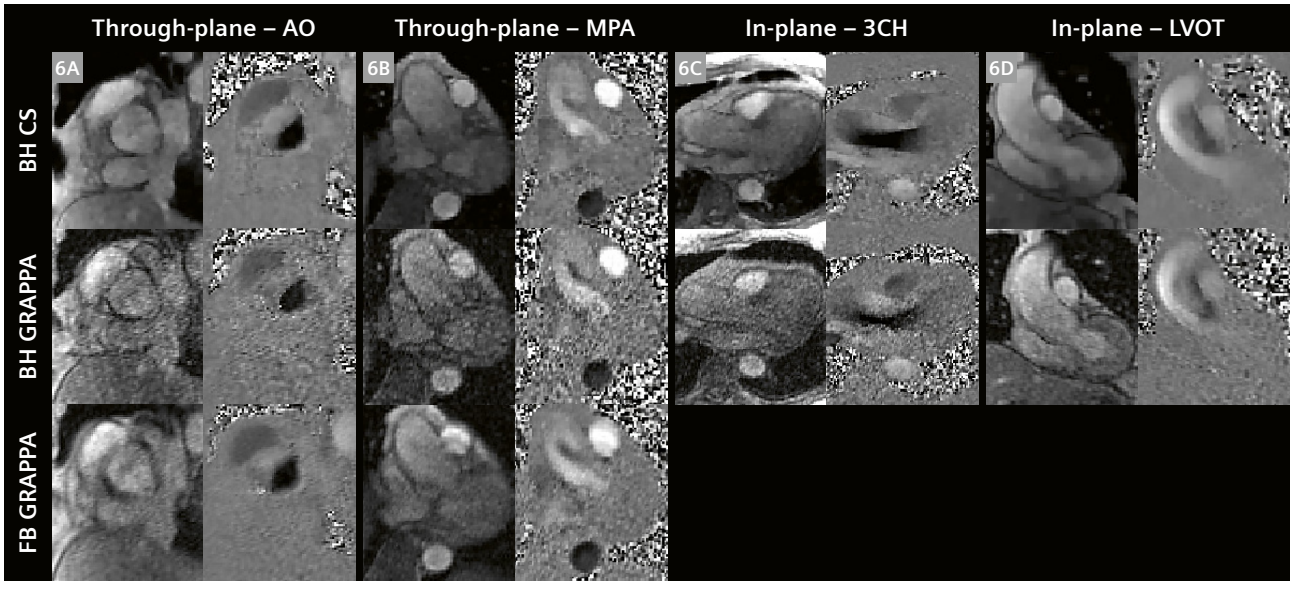

6 Through-plane (**6A** aortic root and **6B** main pulmonary artery) and In-plane (**6C** 3-chamber view and **6D** left ventricular outflow tract) 2D phase contrast flow images acquired in a patient with a bicuspid aortic valve, aortic dilatation and aortic regurgitation. The top row shows magnitude and phase images acquired with a breath-held compressed sensing-based 2D PC MR sequence, while the middle row shows images from a breath-held GRAPPA sequence. Images in the bottom row were acquired free-breathing using a GRAPPA sequence with four averages to boost SNR. AO = aorta, MPA = main pulmonary artery, 3CH = cardiac 3-chamber view, LVOT = left ventricular outflow tract view.

Late Gadolinium Enhancement (LGE)

LGE provides unique information on myocardial tissue changes, including scar, fibrosis, and edema. We are currently optimizing both breath-hold segmented LGE and single-shot free-breathing LGE with motion correction and averaging, all based on bSSFP readout which provides high SNR. Exemplary scan parameters are listed in Table 4, along with 1.5T parameters for reference. Example images from two patients with non-ischemic cardiomyopathies showing segmented breath-hold, single-shot, and free-breathing, motion corrected LGE at 0.55T, along with comparative images acquired at 1.5T and 3T, are shown in Figure 7. Additional improvements in acquisition speed and image quality are anticipated as we incorporate compressed sensing into LGE image acquisition and reconstruction.

Gadolinium contrast agent T1 relaxivity is generally a function of field strength, and as shown by Campbell-Washburn et al., relaxivity at 0.55T may be slightly higher or lower than at 1.5T, depending on the particular agent [2]. All of the contrast-enhanced images shown here used gadobutrol, which may have a slightly lower (worse) relaxivity at 0.55T than at 1.5T. Additionally, because the native T1 times are shorter, the differential contrast enhancement at lower field may be less. Thus far, in our preliminary studies, we have observed the use of gadolinium-based contrast agent to be effective for the visualization of myocardial scar, perfusion defects, and blood pool in MRA, but careful studies are required to evaluate the diagnostic efficacy.

Myocardial relaxation parameter mapping

Myocardial longitudinal (T1) and transverse (T2) relaxation times are elevated with fibrosis, edema, and inflammation. Quantitative myocardial parameter mapping methods are being used clinically at higher field to evaluate these pathological changes in myocardium that can accompany a variety of diseases. We implemented parameter mapping schemes for T1 and T2 taking into consideration the shorter T1 relaxation times and longer T2 relaxation times at 0.55T in comparison to higher field. The T1-mapping scheme was based on that typically used for post-contrast T1 mapping at 1.5T (4(1)3(1)2), with the addition of a fourth inversion pulse and two more images at the shorter

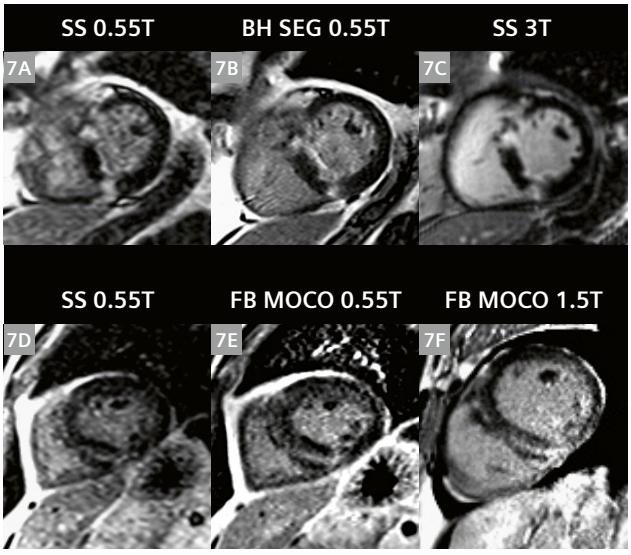

7 Top row **(7A–7C)** shows LGE images acquired in a patient with hypertrophic cardiomyopathy with fibrosis of the left ventricle. **(7A)** Single-shot inversion recovery prepared bSSFP image at 0.55T, **(7B)** breath-held segmented LGE image at 0.55T, and **(7C)** single-shot IR-prepared bSSFP LGE acquired on a 3T MAGNETOM Vida system for comparison.
Bottom row **(7D–7F)** shows LGE images acquired in a different patient with non-ischemic septal mid-wall fibrosis. Single-shot **(7D)** and free-breathing motion-corrected averaged **(7E)** LGE images were acquired on MAGNETOM Free.Max, while the corresponding MOCO LGE image, shown in **(7F)**, was acquired on a 1.5T MAGNETOM Sola system.

	Scanner	Flip angle (deg)	TE (ms)	TR (ms)	RBW Hz/pixel	Segments	Temporal resolution (ms)	Slice thickness (mm)	Pixel size (mm)	Acceleration	Scan time
BH LGE	1.5T MAGNETOM Sola (GRE)	20	1.55	4.06	465	31	142	8	1.4 × 1.4	none	8 HB
	0.55T MAGNETOM Free.Max (bSSFP)	80	2.48	6.66	200	21	140	10	1.6 × 1.6	none	12 HB
MOCO LGE	1.5T MAGNETOM Sola (bSSFP)	50	1.18	2.79	1085	86	240	8	1.4 × 1.4	G 2	16 HB
	0.55T MAGNETOM Free.Max (bSSFP)	50	1.84	4.69	698	63	295	8	1.5 × 1.5	G 2	24 HB

Table 4: Acquisition parameters for breath-hold segmented *k*-space LGE (top rows) and free-breathing LGE based on single-shot acquisition with motion correction (MOCO) and averaging (bottom rows) shown for 1.5T MAGNETOM Sola and 0.55T MAGNETOM Free.Max. Additional averages were used at 0.55T in the MOCO LGE scan to boost SNR. Note also that the standard segmented breath-hold approach at 1.5T and 3T typically utilizes a GRE readout, while bSSFP is employed at 0.55T to boost SNR. The higher B_0 homogeneity allows broader utilization of bSSFP without risk of dark band artifacts that could confound the interpretation of LGE, first pass perfusion, and other techniques where changes in myocardial signal intensity are of interest.

inversion times (4(1)3(1)2(1)2). The T2 mapping scheme was modified to acquire 6 source images at 3 different T2 preparation times (0, 25, and 60 ms). Scan parameters are listed in Table 5, along with typical parameters used at 1.5T for comparison. Results shown in Figure 8 acquired in a porcine infarct model at 0.55T utilized an increased number of source images to boost SNR through the pixel-wise parameter fitting process. We are continuing to work on applying the same CS strategies that have been instrumental in boosting SNR and acceleration rates in cine and flow, and expect that this will improve SNR and sharpness in the resulting parameter maps, while reducing the scan duration. Prospective respiratory motion compensation techniques based on the Pilot Tone technology [11] are under development and will be used to further improve free-breathing methods.

	Scanner	Flip angle (deg)	TE (ms)	TR (ms)	RBW Hz/pixel	Segments	Temporal resolution (ms)	Slice thickness (mm)	Pixel size (mm)	Acceleration	Scan time
T1 mapping	1.5T MAGNETOM Sola	35	1.01	2.42	1085	60	145	8	2.0 × 2.0	G 2	11 HB
	0.55T MAGNETOM Free.Max	50	1.77	4.3	539	60	258	10	2.4 × 2.4	G 2	14 HB
T2 mapping	1.5T MAGNETOM Sola	70	1.04	2.43	1184	55	133	8	2.1 × 2.1	G 2	7 HB
	0.55T MAGNETOM Free.Max	70	1.69	4.18	558	60	250	10	2.4 × 2.4	G 2	16 HB

Table 5: Acquisition parameters for myocardial T1 mapping (top rows) and T2 mapping (bottom rows) listed for both 1.5T MAGNETOM Sola and 0.55T MAGNETOM Free.Max. Additional source images are acquired at 0.55T to boost SNR, leading to slightly longer scan times. Longer TR due to slower gradients also degrades temporal resolution, and this can cause some motion artifact at higher heart rates. Approaches to increase acceleration rate to improve temporal resolution are being developed using Compressed Sensing.

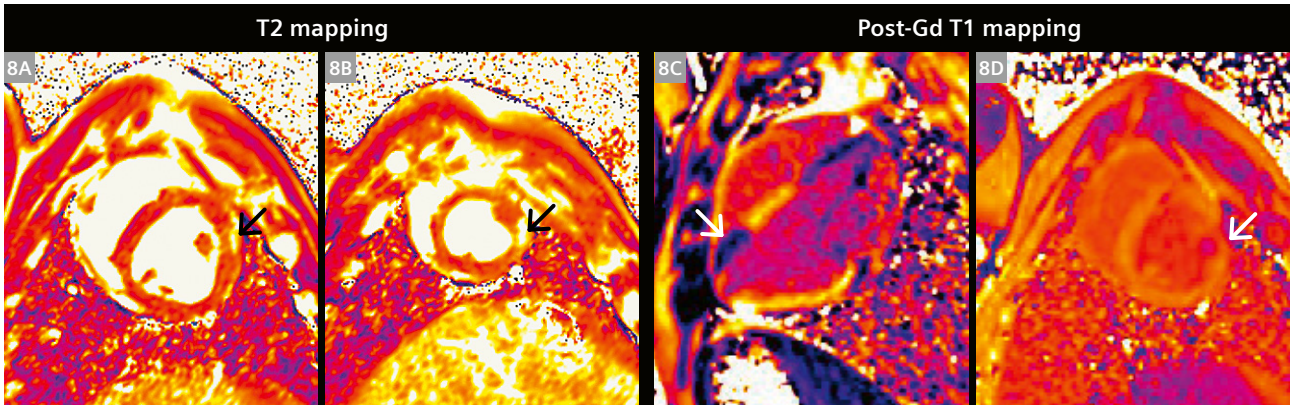

8 Myocardial T2 **(8A, 8B)** and post-Gd T1 **(8C, 8D)** maps acquired in a porcine model of acute myocardial infarction. These images, acquired five days post 90-minute occlusion-reperfusion of the left circumflex coronary artery, illustrate the feasibility of parameter mapping at 0.55T. Antero-lateral infarct is visible as regionally elevated T2 (black arrows in panels 8A and 8B), and shortened post-contrast T1 (white arrows in panels 8C and 8D).

	Scanner	Flip angle (deg)	TE (ms)	TR (ms)	RBW Hz/pixel	Segments	Temporal resolution (ms)	Slice thickness (mm)	Pixel size (mm)	Acceleration	Scan time
First-pass Perfusion SR-bSSFP	1.5T MAGNETOM Sola (bSSFP)	50	1.04	2.5	1085	37	92.5	8	1.9 × 1.9	G 3	50 HB
	0.55T MAGNETOM Free.Max (bSSFP)	90	1.81	4.04	868	25	101	8	3.0 × 3.0	CS 4	50 HB

Table 6: Acquisition parameters for myocardial first-pass perfusion imaging for 1.5T MAGNETOM Sola (top row) and 0.55T MAGNETOM Free.Max (bottom row). Saturation-recovery (SR) bSSFP is used on both scanners. Compressed Sensing is used on MAGNETOM Free.Max to push the acceleration rate to 4× to overcome the longer TR, and to maintain SNR. Even with higher acceleration there is some compromise in spatial and temporal resolution when compared to 1.5T. Further investigation is required to determine the impact of these parameter differences.

First-pass perfusion

Gadolinium-enhanced first-pass perfusion imaging, combined with vasodilator stress, is the most critical component of the CMR evaluation of patients with known or suspected ischemic heart disease. With the requirements of delivering multi-slice coverage within a single heartbeat, and high T1-contrast images with little motion artifact, first-pass perfusion imaging pushes the speed and SNR limits of CMR even at higher field. Whether or not these requirements can be met at lower field with reduced

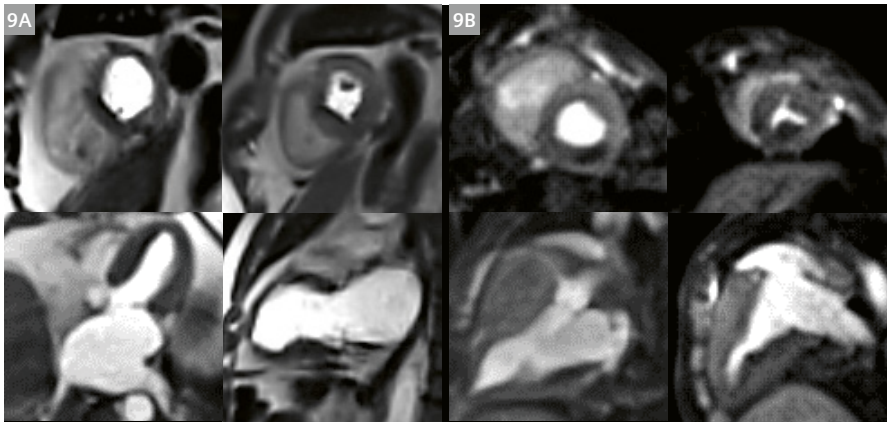

9 Rest perfusion images indicate perfusion defect in a patient with hypertrophic cardiomyopathy **(9A)** and in a porcine model with left circumflex artery infarct **(9B)**.

	Scanner	Flip angle (deg)	TE (ms)	TR (ms)	RBW Hz/pixel	Segments or turbo factor	Temporal resolution (ms)	Slice thickness (mm)	Pixel size (mm)	Accel-eration	Scan time
non-contrast MRA navigator bSSFP	1.5T MAGNETOM Sola	90	1.45	3.38	592	35	118	1.3	1.6 × 1.6	G 2	78 HB
	0.55T MAGNETOM Free.Max	110	1.89	4.61	501	35	161	1.5	1.6 × 1.6	G 2	142 HB
non-contrast MRA navigator SPACE	1.5T MAGNETOM Sola	variable	23	1RR	744	35	130	1.3	1.3 × 1.3	G 2	205 HB
	0.55T MAGNETOM Free.Max	variable	23	1RR	630	25	214	1.3	1.6 × 1.6	G 2	289 HB
Gd ce-MRA ECG gated GRE	1.5T MAGNETOM Sola	30	1.25	2.97	591	100	297	1.4	1.4 × 1.4	CS 9	10 HB
	0.55T MAGNETOM Free.Max	30	1.71	3.68	781	80	294	1.5	1.6 × 1.6	CS 7	13 HB

Table 7: Acquisition parameters for 3D MR angiography (MRA) sequences used on the 1.5T MAGNETOM Sola and 0.55T MAGNETOM Free.Max. Three different techniques are listed: 3D navigator respiratory gated bSSFP (top rows), 3D navigator gated dark-blood SPACE (middle rows), and 3D contrast enhanced ECG-gated MRA. Some compromises are made in spatial resolution on the MAGNETOM Free.Max to offset reduced SNR and gradient speed.

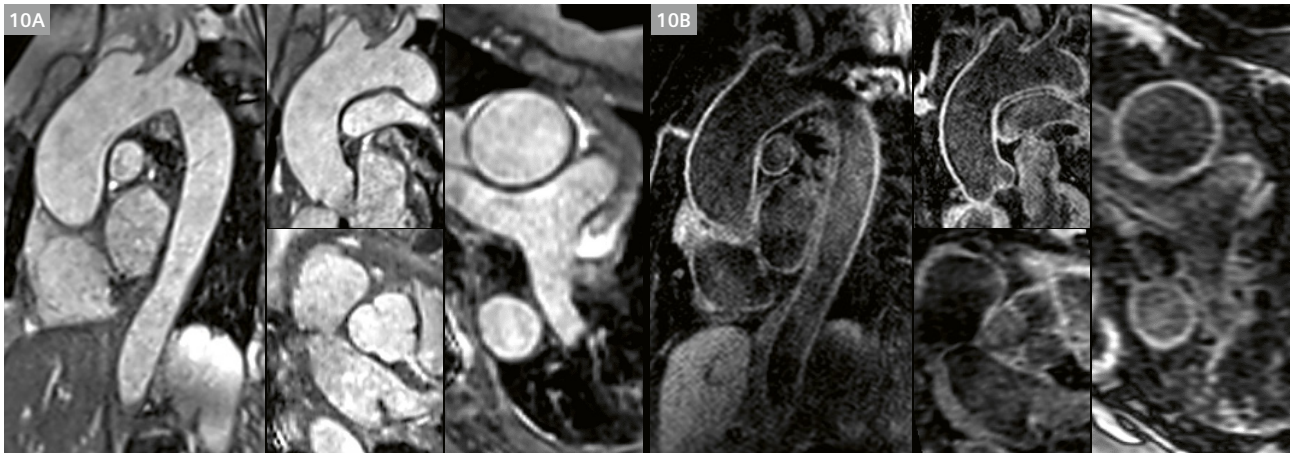

10 2D reformatted images from non-contrast 3D MRAs acquired in a patient with Harrington spinal rods[2] being evaluated for aortic dilatation. Images in **(10A)** show reconstructions from a bright-blood ECG-triggered, navigator gated bSSFP MRA, while **(10B)** shows reconstructions from a dark-blood 3D SPACE sequence used to highlight vessel wall anatomy.

gradient performance is an important question. We have experimented with a bSSFP perfusion sequence (parameters listed in Table 6) that applies the same CS-based approach to data sampling and reconstruction [9] that has been successfully utilized to accelerate real-time cine imaging without sacrificing SNR. While this method has yet to be tested with vasodilator stress, initial results acquired at rest in a porcine model of myocardial infarction, and in volunteers and patients, are promising (Fig. 9).

MR Angiography

Thoracic MR angiograms of the aorta, pulmonary arteries, and pulmonary veins form an important component of the comprehensive cardiovascular imaging exam in many of our patients. While the standard method is contrast-enhanced MR angiography (ce-MRA), non-contrast MRA using a 3D bSSFP sequence with navigator respiratory gating is now being utilized more frequently at our institution. We also frequently employ a 3D dark blood SPACE sequence to visualize vessel wall morphology; SPACE is also less sensitive to metal artifact around implants[2]. Parameters for all three methods are listed in Table 7 for 0.55T and 1.5T. We have implemented and investigated all three of these MRA techniques in volunteers and patients. Contrast-enhanced MRA has been tested both with and without ECG gating, while the non-contrast technique is always ECG-triggered. ECG-gated ce-MRA places high demands on acceleration and we have employed a CS-based technique to maintain high spatial resolution and a reasonable breath-hold duration of 18 heartbeats or less.

Navigator-gated non-contrast MRA data were acquired during free-breathing with scan times of 6 minutes or less, depending on heart rate and the extent of anatomical coverage. 3D SPACE acquisition times are longer as signal averaging is used at both 1.5T and 0.55T. Examples of non-contrast and contrast-enhanced MRA acquired at 0.55T are shown in Figures 10, 11, and 12.

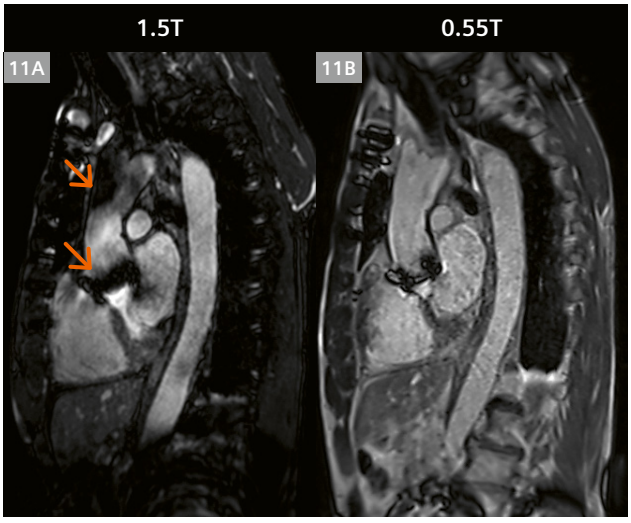

11 2D reformatted images from ECG triggered, navigator gated non-contrast enhanced 3D bSSFP MRA scans acquired in the same patient at 1.5T **(11A)** and at 0.55T **(11B)**. This patient has an artificial aortic valve[2] and sternal wires. The extent of signal dephasing artifacts (orange arrows) seen at 1.5T are reduced at 0.55T. Cine images from this patient are shown in Figure 4.

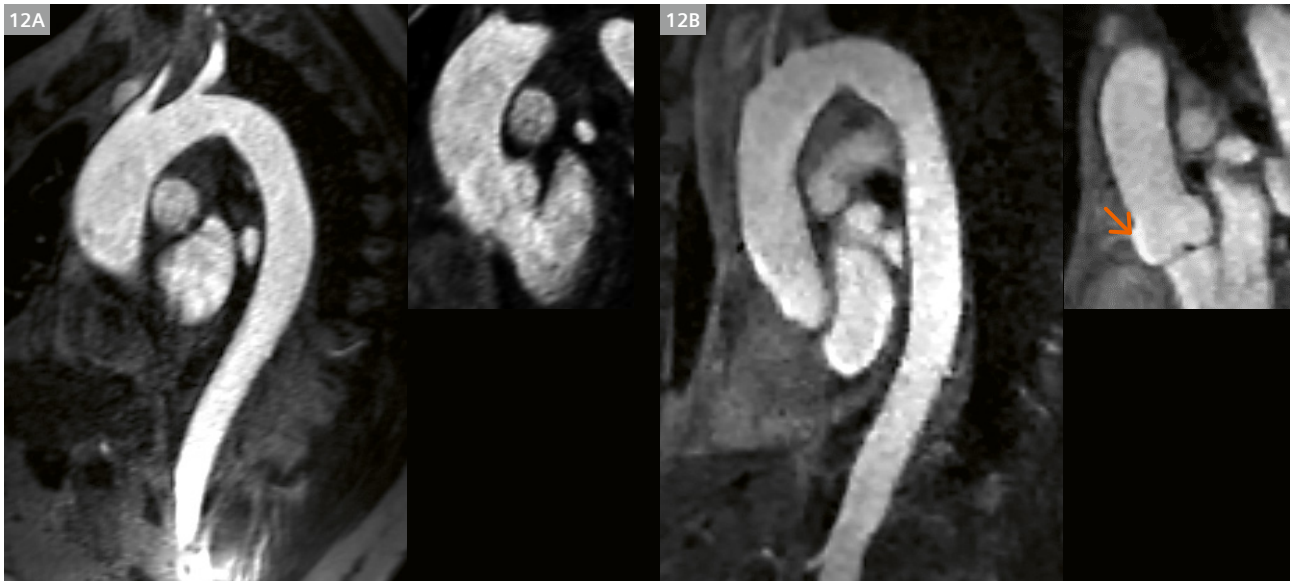

12 2D reformatted images from 3D contrast-enhanced (ce-)MRA scans in two different subjects. On the left **(12A)** a non-gated contrast-enhanced 3D MRA acquired in an obese patient shows a dilated thoracic aorta. The patient was unable to proceed with a cardiac MR exam in a standard 70 cm bore MR system but successfully completed an evaluation on the MAGNETOM Free.Max; additional images from this patient are shown in Figure 13. On the right **(12B)** is an ECG-gated ce-MRA scan from a healthy volunteer. Note the clear delineation of the aortic root and valve leaflets in the gated MRA (orange arrow), as compared to the non-gated MRA.

Putting it all together

After compiling the sequences required to cover all of the basic cardiac imaging applications, we have recently begun to identify and scan severely obese patients who were referred for clinical CMR, but whose body habitus made it impossible, or too uncomfortable, to be scanned on systems with a standard 70 cm bore diameter. In Figure 13, images acquired on the MAGNETOM Free.Max are shown from a patient weighing 350 lbs / 159 kg with BMI > 48 being evaluated for possible cardiomyopathy and dilated

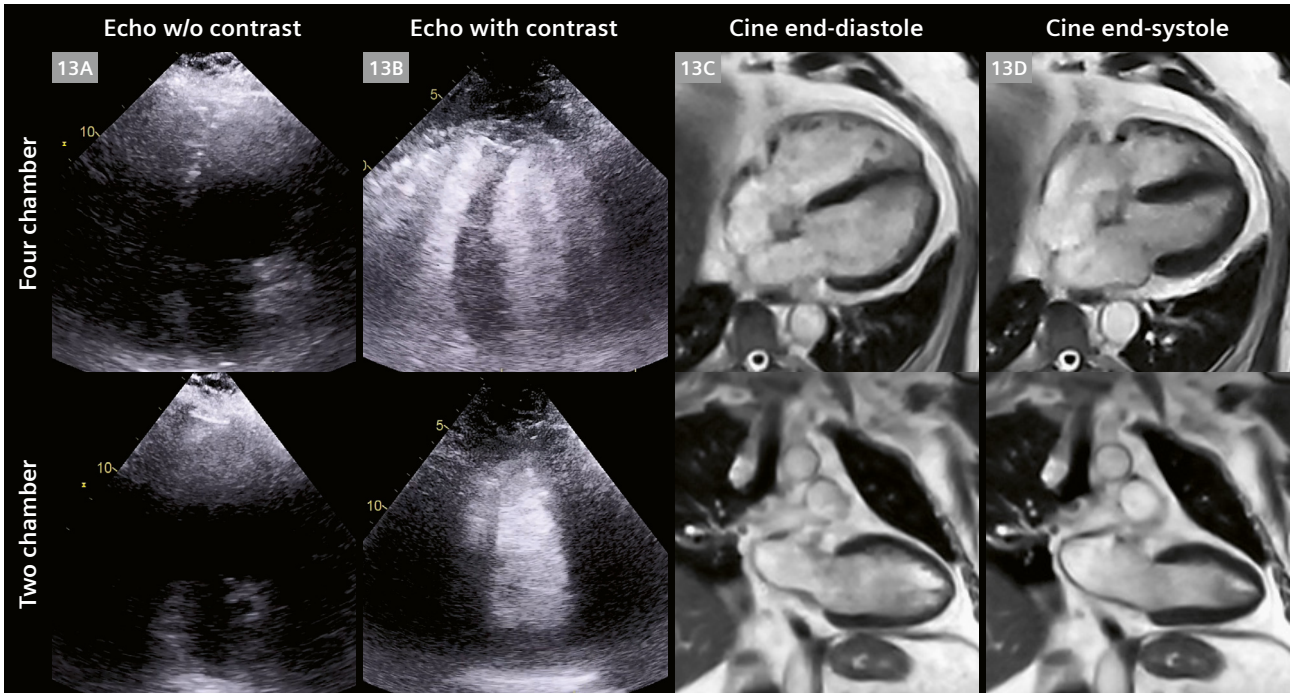

13 4-chamber view (top row) and 2-chamber view (bottom row) echocardiographic (**13A** without contrast, and **13B** with contrast) and CMR images (**13C** end-diastole, and **13D** end-systole) acquired in an obese patient with BMI > 48 kg/m^2. Echo image quality is degraded by large body habitus, and this patient could not fit into a 70 cm magnet bore. The MAGNETOM Free.Max provides access to MRI for severely obese patients for whom no other good options exist for cardiac imaging. MRA for this patient is shown in Figure 12.

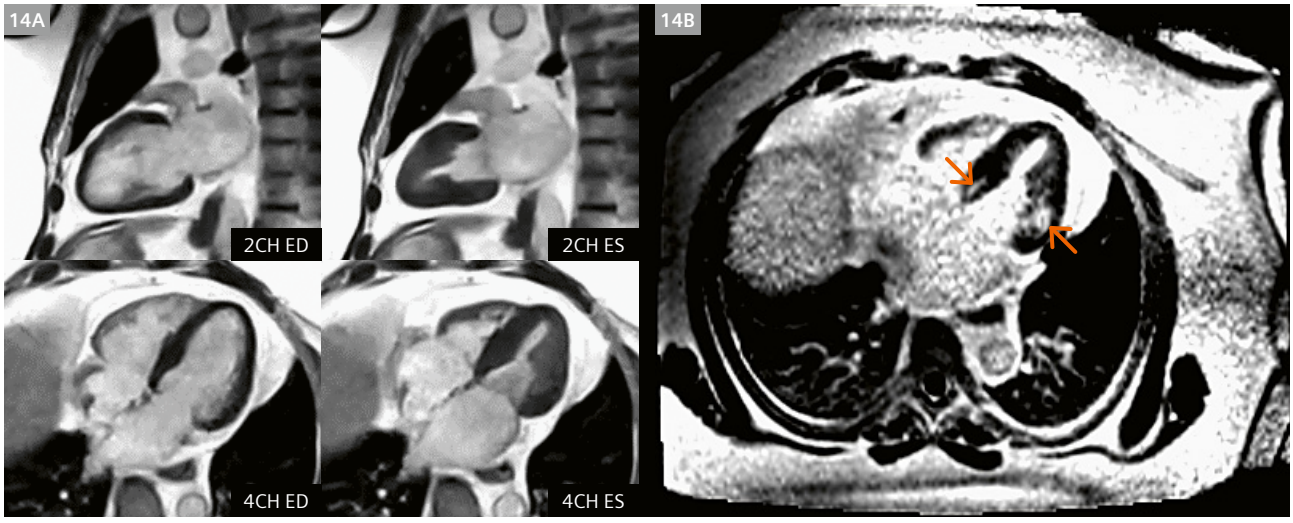

14 Example images from a patient weighing 410 lbs / 186 kg with BMI 57 kg/m^2. This patient being evaluated for cardiomyopathy, was unable to complete the exam on a 70 cm bore system. Compressed Sensing-based breath-held segmented bSSFP cine images acquired on the MAGNETOM Free.Max are shown in panel **(14A)** on the left. End-diastolic and end-systolic cardiac phases are shown. In panel **(14B)** on the right is shown an LGE image acquired during free-breathing using the technique of single-shot motion corrected (MOCO) imaging with averaging. Basal regions of enhancement (orange arrows) indicate areas of fibrosis.

aorta. While the weight of this patient can be accommodated by most scanners, their body habitus prevented them from fitting into a 70 cm bore. They were comfortably scanned on the MAGNETOM Free.Max, and the bSSFP cine images are shown here in comparison to echocardiography images acquired with and without echo contrast. The echo image quality is poor, and MAGNETOM Free.Max offers the potential for high-quality cardiac imaging for these severely obese patients in whom other modalities including echo and CT may be limited. The contrast-enhanced MR angiogram acquired in this patient is shown in Figure 12. MAGNETOM Free.Max images from another patient with a BMI of 57 (weight 410 lbs / 186 kg) diagnosed with heart failure with preserved ejection fraction (HFpEF) being evaluated for cardiomyopathy are shown in Figure 14. This patient was able to initially enter the bore of a 70 cm scanner, but was too uncomfortable to complete the exam. The patient reported being comfortable in the MAGNETOM Free.Max. The exam, including cine and LGE imaging was successfully completed, revealing normal biventricular function, but scarring evident at the base of the left ventricle.

Summary

While this project to develop and optimize cardiac imaging techniques for the 0.55T MAGNETOM Free.Max is still in relatively early stages, the images and results obtained thus far show great promise for the breadth of techniques and image quality that this system will be able to deliver in the future. We will continue to explore the cardiac imaging potential for this ultra-wide bore 0.55T system and anticipate that in the near future it will provide a solution to accurately diagnose and guide clinical cardiovascular care of patients with severe obesity, as well as those with severe claustrophobia.

Acknowledgements

The entire OSU CMR team, and Siemens Healthineers collaborators. Funding support from National Heart Lung and Blood Institute (R01HL161618) and The Robert F. Wolfe and Edgar T. Wolfe Foundation. Columbus, Ohio, USA.

References

1 Simonetti OP, Ahmad R. Low-Field Cardiac Magnetic Resonance Imaging: A Compelling Case for Cardiac Magnetic Resonance's Future. Circ Cardiovasc Imaging. 2017;10(6):e005446.
2 Campbell-Washburn AE, Ramasawmy R, Restivo MC, Bhattacharya I, Basar B, Herzka DA, et al. Opportunities in Interventional and Diagnostic Imaging by Using High-Performance Low-Field-Strength MRI. Radiology. 2019;293(2):384-393.
3 Hales CM, Carroll MD, Fryar CD, Ogden CL. Prevalence of Obesity and Severe Obesity Among Adults: United States, 2017-2018. NCHS Data Brief. 2020;(360):1-8.
4 Virani SS, Alonso A, Aparicio HJ, Benjamin EJ, Bittencourt MS, Callaway CW, et al. Heart Disease and Stroke Statistics-2021 Update: A Report From the American Heart Association. Circulation. 2021;143(8):e254-e743.
5 Fursevich DM, Limarzi GM, O'Dell MC, Hernandez MA, Sensakovic WF. Bariatric CT Imaging: Challenges and Solutions. RadioGraphics. 2016;36(4):1076-1086.
6 Finkelhor RS, Moallem M, Bahler RC. Characteristics and impact of obesity on the outpatient echocardiography laboratory. Am J Cardiol. 2006;97(7):1082-1084.
7 Varghese J, Craft J, Crabtree CD, Liu Y, Jin N, Chow K, Ahmad R, Simonetti OP. Assessment of cardiac function, blood flow and myocardial tissue relaxation parameters at 0.35 T. NMR Biomed. 2020;33(7):e4317.
8 Bandettini WP, Shanbhag SM, Mancini C, McGuirt DR, Kellman P, Xue H, et al. A comparison of cine CMR imaging at 0.55 T and 1.5 T. J Cardiovasc Magn Reson. 2020;22(1):37.
9 Chen C, Liu Y, Schniter P, Jin N, Craft J, Simonetti O, et al. Sparsity adaptive reconstruction for highly accelerated cardiac MRI. Magn Reson Med. 2019;81(6):3875-3887.
10 Jin N, Liu Y, Chen C, Giese D, Ahmad R, Simonetti O. Highly accelerated 2D phase contrast imaging on a low-field 0.55T MRI system. ISMRM Workshop on Low Field MRI, March 2022.
11 Speier P, Fenchel M, Rehner R. PT-Nav: a novel respiratory navigation method for continuous acquisitions based on modulation of a pilot tone in the MR-receiver. ESMRMB 2015, 32nd Annual Scientific Meeting, Edinburgh, UK, 1-3 October: Abstracts, Thursday, Magnetic Resonance Materials in Physics, Biology and Medicine. 2015; 28:1–135.

Contact

Orlando P. Simonetti, Ph.D., MSCMR, FISMRM, FAHA
John W. Wolfe Professor in Cardiovascular Research
Professor of Internal Medicine and Radiology
The Ohio State University
Biomedical Research Tower
460 W. 12th Ave.
Columbus, OH 43210
USA
Tel.: +1 614-293-0739
Orlando.Simonetti@osumc.edu

Low Field MRI Impact on Interventions

Paul J.A. Borm, Ph.D.[1,2]; Orlando P. Simonetti, Ph.D., MSCMR, FISMRM, FAHA[3]; Aimee K. Armstrong, M.D., FAAP, FACC, FSCAI, FPICS[3,4]

[1]Nano4Imaging GmbH, Aachen, Germany
[2]Heinrich Heine University (HHU), Düsseldorf, Germany
[3]The Ohio State University College of Medicine, Columbus, OH, USA
[4]The Heart Center, Nationwide Children's Hospital, Columbus, OH, USA

Cathlab and MRI

While X-ray fluoroscopy continues to be the mainstay imaging method for cardiac catheterization procedures, it has numerous disadvantages, including poor soft tissue visualization, need for repeated injections of iodinated contrast to depict the anatomy, inability to visualize the anatomy during interventions, harmful effects of radiation, and the need for lead protection that can induce orthopedic injuries. The adverse effects of radiation are compounded in children, due to their greater mitotic activity. In addition, many congenital heart disease (CHD) patients need repeated cardiac catheterizations and radiation-based imaging throughout their lives, sometimes receiving accumulated lifetime doses that are associated with a detectable increased risk of cancer [1]. Children also have longer lifespans than adults, thereby having more time to develop radiation-induced cancer.

Cardiac magnetic resonance (CMR) eliminates many of the disadvantages of X-ray, but it comes with its own challenges for real-time interventional imaging. The field of interventional CMR (ICMR) has been slow to advance, due to safety hazards from radiofrequency-induced heating of catheterization equipment during scanning, inability to visualize standard catheters with MRI, and large metallic artifacts from interventional wires that obstruct the imaging. The many drawbacks of X-ray imaging, however, continue to push clinicians, researchers, and industry to overcome these limitations in the field of ICMR.

Advantages and Needs

To date, the vast majority of ICMR work has been performed in 1.5 Tesla scanners. Clinical investigators at the National Institutes of Health (NIH) performed right heart catheterizations (RHC) in adults [2], and Ratnayaka and colleagues were the first to move ICMR into a pediatric hospital on a large scale, reporting 50/50 successful RHC procedures in children[1] [3]. As the field progressed, specific equipment was developed for catheterization to make wires and catheters safe and conspicuous in MRI. Nano4Imaging (Düsseldorf, Germany) has produced the first CE and FDA-approved guidewire (EmeryGlide MRWire) for ICMR by placing passive markers on the distal tip of fibre-polymer composite wire. The composite material removes concerns for device heating and metal artifact, and the markers are visible under both MRI and X-ray fluoroscopy, allowing for use in both settings. This technology has helped to bring ICMR to the evaluation of patients with CHD, enabling procedures to measure pressure gradients across stenoses with real-time MR guidance [4] and assess hemodynamics during Fontan fenestration test occlusion [5]. In addition to these procedures in CHD, diagnostic catheterization is routinely performed for pulmonary hypertension patients in many hospitals in the United Kingdom, France, and Scandinavia. Procedure time has been shown to be equivalent to similar catheterizations with X-ray fluoroscopy, while radiation exposure is reduced to both patients and staff [6].

[1]*Siemens Healthineers disclaimer: MR scanning has not been established as safe for imaging fetuses and infants less than two years of age. The responsible physician must evaluate the benefits of the MR examination compared to those of other imaging procedures.*

ICMR TOP INDICATIONS IN 2019	PREDICTED ICMR TOP INDICATIONS IN 2023
Evaluation of pulmonary hypertension	Balloon angioplasty of branch pulmonary artery
Evaluation of post-heart transplant patients	Myocardial biopsy
Diagnostic evaluation of post-Fontan/single-ventricle patients	Fontan fenestration test occlusion and device closure
Pre-Fontan surgical evaluation	Balloon angioplasty of RV-PA conduit
Diagnostic right- or left-heart cath before shunt closure procedures	Balloon pulmonary valvuloplasty

Table 1: Current and future indications of ICMR, as indicated by 132 pediatric interventional cardiologists in a 2019 survey.

Current and future indications

While diagnostic catheterizations with MR guidance are being performed on a regular basis at some institutions, interventional procedures, such as angioplasty, stenting, and septal defect closures, are not part of clinical practice today, primarily due to the lack of equipment that is both visible and safe in the MR environment, the absence of supporting software, and uncertainty about reimbursement. An international survey of members of the pediatric interventional cardiology community at 175 centers in 2019 revealed that 14 centers have active ICMR programs, and physicians at 72 other centers are interested in starting a program. The major problems they envisaged or encountered were lack of a scanner in a location for safe ICMR procedures (26%), MR-safe medical devices (18%), physician training (13%), and training of key team members (12%). Hands-on training and workshops were mentioned as the prime needs to get started, while medical devices were also seen as important. The wish list of devices was topped by more MR conditional guidewires, followed by access kits, torque control catheters, angioplasty catheters, and a bioptome [7]. The current and future clinical indications, which were outlined in 2019, are shown in Table 1; as it is now almost five years beyond the date of the survey, some of the "future" indications have been executed in animal and/or clinical studies.

Groundwork

Early work in low-field (0.55T) MR scanners suggests that it has great potential to overcome some of the long-standing problems with ICMR. The lower field strength may allow the safe use of commercially available catheterization equipment. Campbell-Washburn et al. [8] showed that two types of nitinol non-exchange length glidewires and two types of stainless-steel braided catheters were safe at 0.55T (< 1°C heating) during 2 minutes of continuous scanning. They then performed low field MR-guided RHC successfully in 7/7 patients using a commercially available nitinol glidewire (180 cm 0.035" Micro J-tip Glidewire, Terumo, Tokyo, Japan) without complication or evidence of heating [8]. These studies were performed on an investigational, modified commercial MRI system that operated at 0.55T but retained the high gradient performance of the original 1.5T system (MAGNETOM Aera, Siemens Healthineers AG, Erlangen, Germany).

Low Field MRI available now

Since these studies were performed, a low field scanner has become commercially available (0.55T MAGNETOM Free.Max, Siemens Shenzhen Magnetic Resonance Ltd., Shenzhen, China). The system has a wide, 80 cm bore diameter, facilitating patient access, but limited gradient performance (maximum gradient amplitude 26 mT/m, maximum slew rate 45 mT/m/ms). The system is more affordable than higher field, 1.5T and 3T scanners, as it is less expensive to manufacture, transport, and install and easier to operate. Most importantly for interventionalists, it may be the breakthrough that is needed to enable MR-guided interventional procedures, because of the decreased RF-induced heating that can allow the use of standard equipment, improved access to the patient in the wider bore, and multiple simpler safety and maintenance features. With FDA approval of the MAGNETOM Free.Max and multiple installations around the world, there is renewed energy in ICMR by clinicians and industry alike. The current platform still needs considerable development, such as imaging techniques and pulse sequences required for cardiovascular and interventional imaging but is expected to make the difference for MRI-guided procedures in cardiology and interventional radiology.

Live case at PICS

Dr. Aimee K. Armstrong from Nationwide Children's Hospital (NCH) in Columbus, Ohio, USA and a team at The Ohio State University (OSU) led by Dr. Orlando P. Simonetti, were the first to test the feasibility of performing right and left heart catheterization, inferior vena cava (IVC) angioplasty, and IVC stenting with realtime imaging in pre-clinical studies performed on the 0.55T MAGNETOM Free.Max [9]. While many types of standard catheterization equipment can be used safely at low field, the devices must be made conspicuous, and this was accomplished by adding MagnaFy MR-visible markers (Nano4Imaging GmbH, Düsseldorf, Germany) to the standard equipment. Three different sizes of proprietary MagnaFy MR-visible markers were evaluated on Z-Med balloons (NuMED Inc., Hopkinton, NY, USA). One of these cases was performed live during the Pediatric Interventional Cardiology

1 Dr. Aimee Armstrong (right) and Jason Swinning, RT(R)(CI), RCIS (left) (Nationwide Children's, Columbus, OH) during PICS 2022 live case stenting the IVC of a large animal with low field MRI guidance and being questioned by Dr. Suren Reddy (Dallas Children's- UT Southwestern).

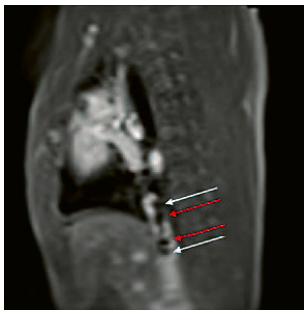

2 Low field (0.55 Tesla) CMR still frame showing MagnaFy ®markers (white arrows) placed at the ends of the tapered tips of the 20 mm × 3 cm Z-Med balloon well distinguished from ends of crimped 26 mm long Mega LD stent (red arrows).

Symposium (PICS) Chicago 2022 (Fig. 1), and Figure 2 shows how a marked angioplasty catheter can be well distinguished in MRI from the ends of a crimped 26 mm long Mega LD stent (red arrows) to facilitate stenting of the IVC.

If low field MRI is going to be used clinically for ICMR in the future, further development and optimization of cardiac and interactive real-time imaging techniques is required to overcome the limitations of low signal-to-noise ratio and limited gradient performance. Fortunately, pre-clinical and clinical testing has already shown that a comprehensive CMR imaging protocol is feasible, including compressed-sensing 2D phase-contrast cine, dynamic contrast-enhanced imaging for myocardial perfusion, 3D MR angiography, and late gadolinium enhanced tissue characterization [10].

Open field lab in Ohio

In 2022, a dedicated collaboration was formed by clinicians at NCH, researchers at OSU, and multiple industry partners, and is already making positive steps towards bringing low-field MRI to the interventional space. In 2023, OSU continues to function as a field-laboratory for pre-clinical testing of devices and software from Siemens Healthineers, Nano4Imaging, Cook Medical, and NuMed. Together, these organizations continue to develop, optimize, and evaluate the hardware and software necessary to bring interventional procedures with real-time MR-guidance into routine clinical practice.

References

1 Stern H, Seidenbusch M, Hapfelmeier A, Meierhofer C, Naumann S, Schmid I, et al. Increased Cancer Incidence Following up to 15 Years after Cardiac Catheterization in Infants under One Year between 1980 and 1998-A Single Center Observational Study. J Clin Med. 2020;9(2):315.

2 Rogers T, Ratnayaka K, Khan JM, Stine A, Schenke WH, Grant LP, et al. CMR fluoroscopy right heart catheterization for cardiac output and pulmonary vascular resistance: results in 102 patients. Journal of Cardiovascular Magnetic Resonance 2017;19:54.

3 Ratnayaka K, Kanter JP, Faranesh AZ, Grant EK, Olivieri LJ, Cross RR, et al. Radiation-free CMR diagnostic heart catheterization in children. J Cardiovasc Magn Reason. 2017;19(1):65.

4 Meierhofer C, Belker K, Shehu N, Latus H, Mkrtchyan N, Naumann S, et al. Real-time CMR guidance for intracardiac and great vessel pressure mapping in patients with congenital heart disease using an MR conditional guidewire – results of 25 patients. Cardiovasc Diagn Ther 2021;11(6):1356-1366.

5 Reddy SRV, Arar Y, Zahr RA, Gooty V, Hernandez J, Potersnak A, et al. Invasive cardiovascular magnetic resonance (iCMR) for diagnostic right and left heart catheterization using an MR-conditional guidewire and passive visualization in congenital heart disease. J Cardiovasc Magn Reason 2020;22(1):20.

6 Knight DS, Kotecha T, Martinez-Naharro A, Brown JT, Bertelli M, Fontana M, et al. Cardiovascular magnetic resonance-guided right heart catheterization in a conventional CMR environment – predictors of procedure success and duration in pulmonary artery hypertension. J Cardiovasc Magn Reson. 2019;21(1):57.

7 Reddy S, Ewert P, Ratnayaka K, Halperin H, Gotto J, Hussain T, et al. Current and future application of interventional CMR as alternative to the cathlab in congenital heart diseases. Results of an online survey. Poster presentation at PICS/AICS 2019, San Diego.

8 Campbell-Washburn A, Ramaswamy R, Restivo MC, Bhattacharya I, Basar B, Herzka DA, et al. Opportunities in Interventional and Diagnostic Imaging by Using High-Performance Low-Field-Strength MRI. Radiology 2019;293(2):384-393.

9 Armstrong A, Krishnamurthy R, Swinning J, Liu Y, Joseph M, Simonetti O. Feasibility of MRI-Guided Cardiac Catheterization, Angioplasty, and Stenting in a 0.55T Scanner with Limited Gradient Performance. PICS-AICS 2022, Chicago, IL, September 2022. Selected Abstracts from the PICS Society Symposium 2022 Marriott Chicago Downtown September 7–10, 2022. Pediatr Cardiol 43, 1934–2029 (2022). https://doi.org/10.1007/s00246-022-02969-y

10 Varghese J, Jin N, Giese D, Chen C, Liu Y, Pan Y, et al. Building a comprehensive cardiovascular magnetic resonance exam on a commercial 0.55T system: A pictorial essay on potential applications. Front Cardiovasc Med. 2023;10:1120982.

Contact

Prof. Dr. Paul J.A. Borm, Ph.D.
CTO and Cofounder of Nano4Imaging GmbH
Life Sciences Centre
Merowingerplatz 1
40225 Düsseldorf
Germany
Tel.: + 31 641725351
pbo@nano4imaging.com
www.nano4imaging.com

Paul J.A. Borm, Ph.D.

Orlando P. Simonetti, Ph.D., MSCMR, FISMRM, FAHA

Aimee K. Armstrong, M.D., FAAP, FACC, FSCAI, FPICS

MAGNETOM Free.Star: Initial Experience in a Tier 3 Indian City

V. Suresh, M.D.

Dolphin Diagnostic Centre, Vishakhapatnam, India

Why MAGNETOM Free.Star fits

India is now the world's most populous country, home to more than 1.4 billion people. The private healthcare sector is the major healthcare provider [1], and patients usually pay their healthcare expenses directly because health insurance coverage is very limited [2]. Recently, the operating costs of diagnostic centers have increased significantly, partially as a result of rising equipment and maintenance costs, inflation, and higher wage costs. However, patients' financial resources remain largely the same.

On another note, we do not have an appointment system in India. Patients always walk in for exams and prefer to move to another diagnostic center if the waiting time is too long. Infrastructure-related challenges like space and power requirements are also a critical consideration for healthcare providers.

At our diagnostic center, we were handling over 60 cases per day using our 1.5T MAGNETOM ESSENZA system, and we had the potential to handle close to 90 cases per day – this means we were turning away 30 patients in a given day either needing to schedule them to a later time or having them travel to the next available imaging center. To increase our throughput and minimize patient waiting time, we began looking for a second MRI scanner that would be able to perform more exams with good image quality, but with a lower total cost of ownership. This was around the time that Siemens Healthineers was launching its new scanner that requires just 0.7 liters of helium.

I have always had an affinity for new technology, so I was very interested to learn about the innovations behind the new MAGNETOM Free.Star scanner. We were the first center in our region to invest in a MAGNETOM ESSENZA in 2007, and we are always looking to explore new technologies that can deliver on our practical needs. MAGNETOM Free.Star is very practical: Its DryCool technology, which makes it possible for this MRI system to operate on only 0.7 liters of helium, addresses the current challenges of rising helium prices and declining availability, and the scanner also has a very small footprint with no quench pipe. In addition, its simple BioMatrix Select&Go workflow, myExam Autopilot, and contour coils are forward looking technologies that are likely to have a positive impact on daily routines.

> *"I'm also a big admirer of the latest technology. When I heard from the team at Siemens Healthineers that they had designed a new machine with virtually no helium, less space and power requirements, and lower maintenance costs, I was very curious about this product. After learning about the features, I placed an order for not one but two scanners to be installed across my centers. The magnet requires only 24 square meters and it weighs just 3.1 tons. This is relevant, because I have installed this scanner on the first floor."*

Workflow with MAGNETOM Free.Star

MAGNETOM Free.Star allows us to easily handle over 40 cases a day, and we're consistently doing more than 30. Our cases are approximately 60% neuro, 20% body, 18% musculoskeletal, and 2% special studies.

Minimizing patient positioning times and having faster scan times, thanks to the built-in Deep Resolve technology, are important for our MRI exams schedule. Our MAGNETOM Free.Star is equipped with AI-enabled BioMatrix Select&Go, which enables one-touch patient positioning without laser light landmarking. It also has lightweight and conformable contour coils, which are easy to setup and enhance patient experience. We can do brain and spine positioning (about 60% of our routine work) in less than 30 seconds, body positioning in under 40 seconds, and MSK positioning in roughly 40 seconds. Afterwards, myExam Autopilot allows the radiographer to perform multiple tasks, while a single person can handle the scanner.

> *"I am performing about 40 cases with MAGNETOM Free.Star. The overall workflow is seamless and allows me to handle more cases. Now everything is automatic, my team can do automatic positioning, automatic planning, and automatic scanning. This helps us save more time."*

Image quality

The image quality in MRI must be diagnostic: Images must have an adequate signal-to-noise ratio, good in-plane and through-plane resolution, and should not miss any potential pathologies. MAGNETOM Free.Star is equipped with modern technology to make the most of the field strength. This includes Deep Resolve (for denoising and matrix improvement), Simultaneous Multi-Slice (SMS), and Compressed Sensing. These features allow us to produce the good diagnostic images we need. Table 1 lists our protocols for brain, spine, knee, shoulder, and abdomen exams. The following cases demonstrate the benefits of MAGNETOM Free.Star:

Protocol	Sequences	Prep time	Scan time	Total time
Routine brain	Axial: T2 TSE, DWI, T2-FLAIR, GRE; sagittal: T1 SE	~30 sec	~12 min	~15 min
Contrast brain	Routine brain + 3D MPRAGE	~30 sec	~17 min	~20 min
Brain with 3D-TOF	Routine brain + 3D Time Of Flight	~30 sec	~17 min	~20 min
IAC/Cranial nerves	Routine brain + 3D T2-SPACE+3D TOF/post-contrast T1 (if required)	~30 sec	~16/21 min	~25 min
C-spine with whole-spine screening	Sagittal: T2 (2-station), T1 (cervical), STIR; axial: T2 TSE	~30 sec	~20 min	~22 min
LS-spine with whole-spine screening	Sagittal: T2 (2-station), T1 (cervical), STIR; axial: T2 TSE	~30 sec	~20 min	~22 min
Liver + MRCP	Axial: T2 HASTE/BLADE TSE, DWI, TrueFISP, VIBE Dixon; coronal: 3D MRCP/radial MRCP	~40 sec	~15 min	~17 min
Whole abdomen	2-station coronal TrueFISP/HASTE and VIBE Dixon; axial: TrueFISP/HASTE, DWI, VIBE Dixon	~40 sec	~18 min	~20 min
Male pelvis	Axial: T2, T2 FS, T1 TSE, DWI; sagittal: T2 TSE; coronal: T2 TSE, STIR	~40 sec	~28/40 min (for CE)	~30/42 min
Female pelvis	Axial: T2, T2 FS, T1 TSE; sagittal: T2 TSE; coronal: T2 TSE, STIR, DWI	~40 sec	~28/40 min (for CE)	~30/42 min
Knee	Axial, coronal, sagittal PD FS; coronal T1 TSE; sagittal/coronal T2	~40 sec	~14 min	~16 min
Shoulder	Axial, coronal, sagittal PD FS; coronal T1 TSE; sagittal/coronal T2	~40 sec	~16 min	~18 min
Hip joint	Coronal: STIR, T1, T2; sagittal PD FS; axial: T2/PD FS, T1 TSE	~40 sec	~20 min	~22 min

Table 1: Common protocols at Dolphin Diagnostic

1. Routine brain

Our routine brain examination consists of transverse or sagittal T2-weighted (T2W), T1W, T2FLAIR, GRE, and diffusion-weighted (DWI) sequences. Apart from being quantitative, DWI is one of the most important sequences in pathologies such as stroke, tumors, and infection [3–6]. However, it is known that distortions related to echo-planar imaging that originate from static B_0 field inhomogeneities caused by magnetic susceptibility variations within the object increase with magnetic field strength [7] and can result in missing lesions or cause uncertainty in diagnoses.

One of the most important features of MAGNETOM Free.Star is its excellent DWI capabilities. These are extremely helpful in cases where lesions are in difficult areas of the brain, such as at the skull base or in the temporal lobes. We are also able to do 3D post-contrast imaging in under five minutes using MPRAGE or T1 SPACE sequences.

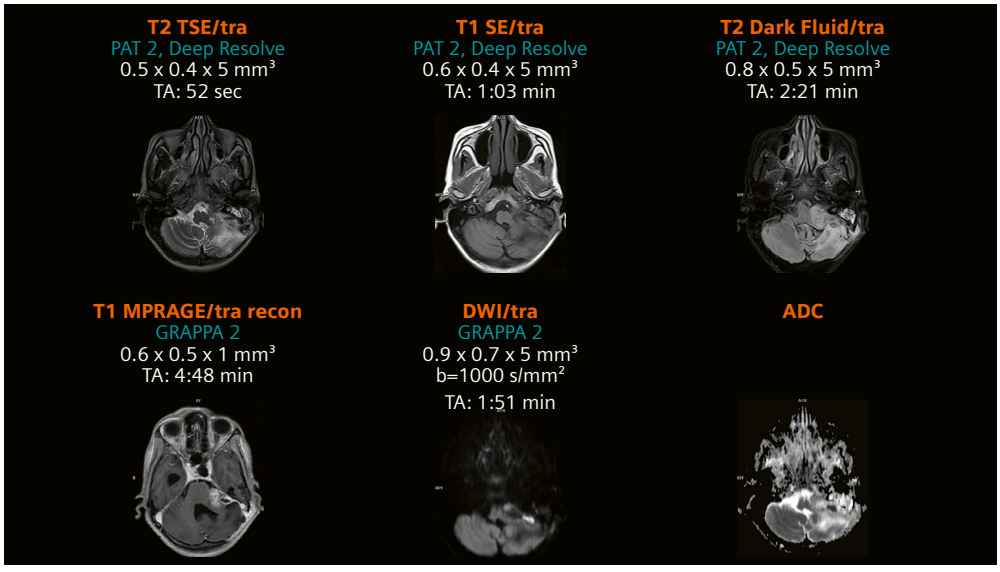

1 A 48-year-old female patient. Post-operative case showing enhancing lesion (on post-contrast T1 MPRAGE) in the left cerebellum, suggestive of residual tumor. The rim-enhancing lesion shows high restriction on DWI and reduced ADC. The transverse T2-FLAIR shows significant edema in the left cerebellar region.

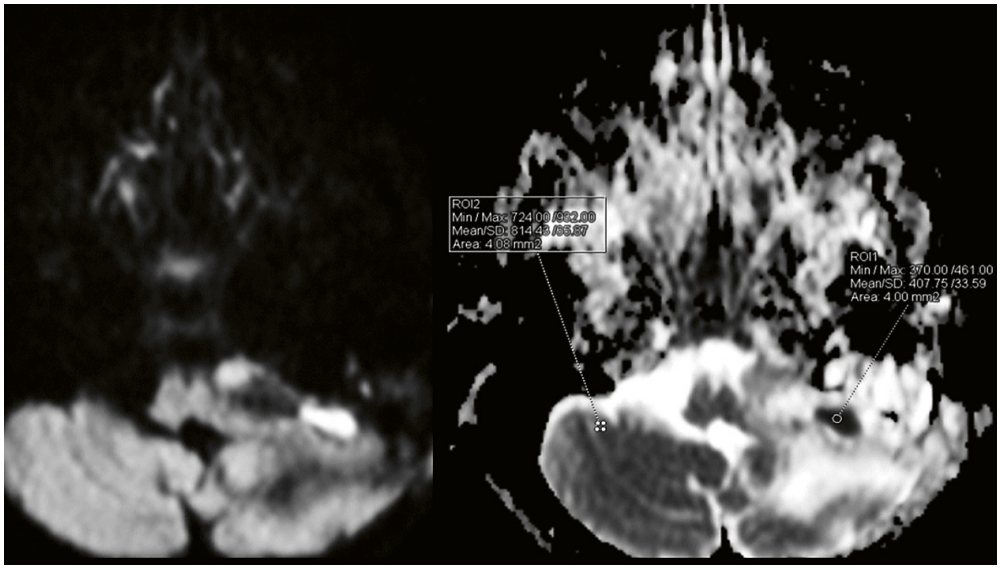

2 The ADC map shows a significant reduction in ADC values (407×10^{-6} mm²/s compared to contralateral normal with 814×10^{-6} mm²/s) of high diffusion restriction in the cystic component.

2. Pediatric brain

Pediatric[1] imaging benefits from MAGNETOM Free.Star in a number of ways. Above all, the exams inherently produce very little noise, while also providing excellent T1 tissue contrast. The very short bore length helps reduce patient anxiety and premature exam termination due to claustrophobia.

[1] *MR scanning has not been established as safe for imaging fetuses and infants less than two years of age. The responsible physician must evaluate the benefits of the MR examination compared to those of other imaging procedures.*

3. Spine imaging (including single setup whole spine acquisition)

Spine imaging is one of the 'bread-and-butter' imaging applications for us, and the most important requirement for us is the ease of performing this examination. As mentioned earlier, the patient setup for this examination takes less than 30 seconds, in addition, the inline composing and automatic numbering allow our radiographer to perform several tasks at once. In addition, flow artifacts are minimal, and T1W images have better tissue-T1 contrast. Furthermore, we have found that the contrast between the spinal cord and Cerebral Spinal Fluid (CSF) is excellent.

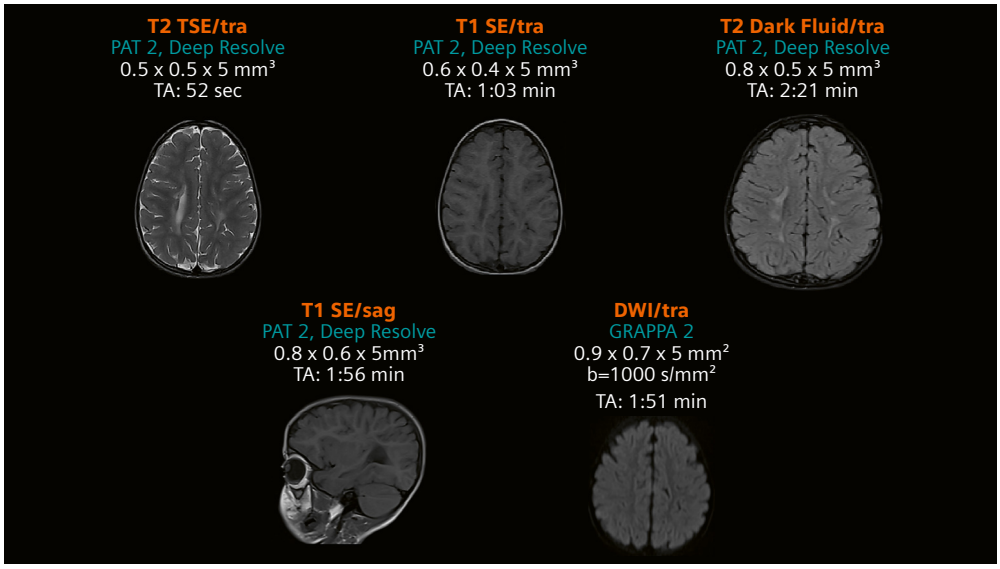

3 A 2-year-old girl. Exam includes transverse plane T2W, T1W, T2-FLAIR, and DWI sequences, showing bilateral symmetric T2/T2-FLAIR hyperintensities in periventricular white matter. The likely cause for the anomaly appears to be periventricular white matter leukomalacia.

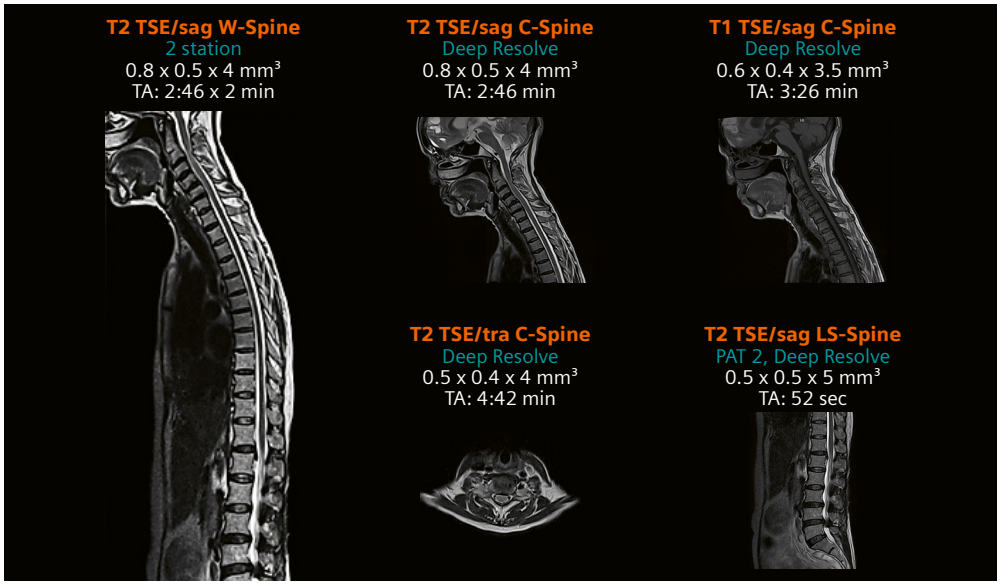

4 A 48-year-old female patient. Exam includes 2-station whole-spine T2W TSE screening, and sagittal T1W and axial T2W sequences for the cervical spine showing cervical spondylotic changes, disc desiccation at multiple levels, and disc bulges with thecal sac indentation at multiple levels in the cervical and lumbar spine.

4. MSK imaging

Musculoskeletal MRI requires a very high resolution to enable diagnosis of various clinical conditions. Deep Resolve and SMS help us optimize both image quality and scan time without compromising on either aspect. Another benefit of MAGNETOM Free.Star are the Contour coils, which are light weight coils designed to improve patient comfort and support quick positioning. The dedicated MSK positioning cushions help immobilize the patient and allow us to achieve very good image quality. We are able to do knee and shoulder exams in under 15 minutes, with excellent fat suppression even in off-center anatomies such as the shoulder.

5. Body imaging

We have found that it is advantageous to perform abdominal MRI on our MAGNETOM Free.Star, as it produces fewer susceptibility, motion, and chemical shift artifacts, and the images are very homogenous without any shading artifacts. The availability of advanced techniques like Compressed Sensing allows faster 3D MRCP acquisition, and we can examine patients with large accumulations of fluid (or ascites) without artifacts. Performing DWI of the abdomen is a major challenge, and even 1.5T scanners can produce shading and distortion artifacts which may obscure lesions in susceptibility-prone areas. With MAGNETOM Free.Star, we get excellent DWI and ADC maps.

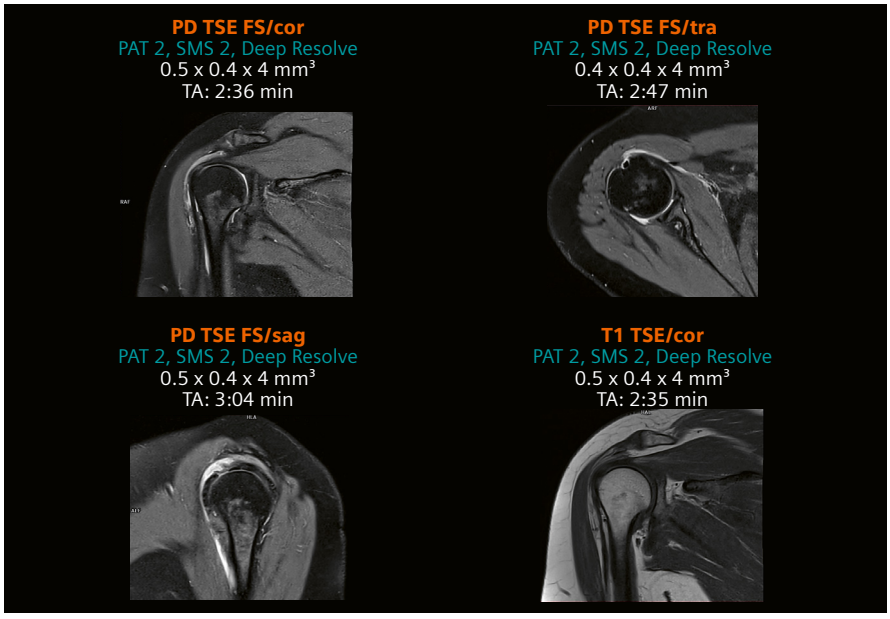

5 A 42-year-old female patient. Exam includes transverse, sagittal, and coronal PD-weighted TSE with fat suppression, and a coronal T1W sequence. The images show thin lumen with fluid, and subacromial, subdeltoid, and sub-coracoid bursitis. The supraspinatus tendon shows mild signal intensity changes, suggestive of chronic subtendinosis.

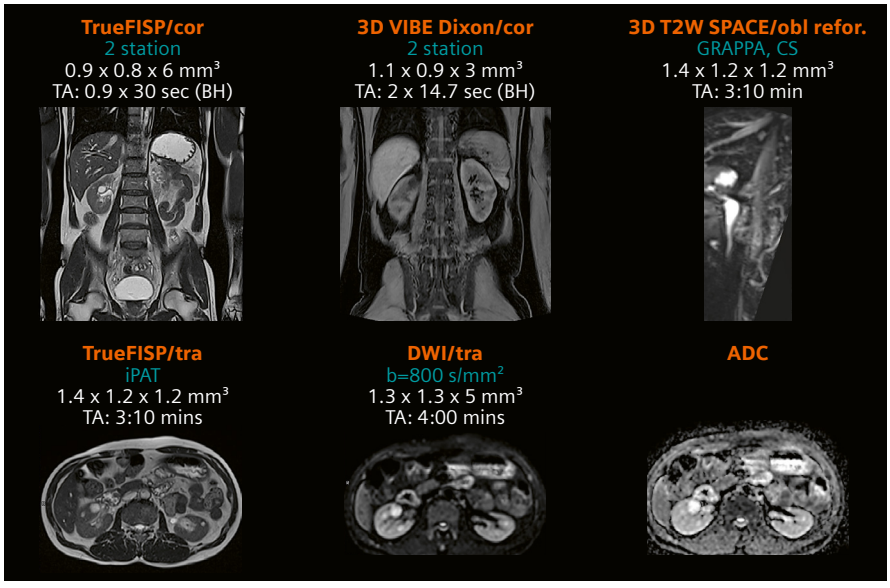

6 A 46-year-old male patient. Exam includes whole-abdomen (2 stations) TrueFISP and 3D VIBE Dixon (T1W) in coronal plane, 3D T2W SPACE in sagittal plane, TrueFISP and DWI in axial plane, and an ADC map. The images show normal structure and signal intensities for the hepatobiliary system, gall bladder, spleen, pancreas, urinary bladder, peritoneum, and prostate. The kidneys show multiple bilateral cystic lesions.

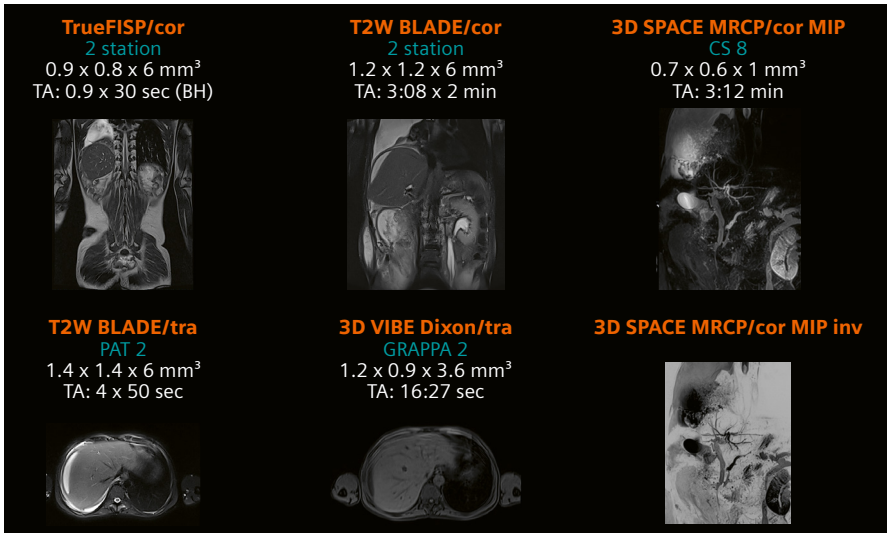

7 A 40-year-old male patient. Exam includes whole-abdomen (2 stations) TrueFISP and T2 BLADE TSE in coronal plane, 3D SPACE MRCP in coronal plane, and T2 BLADE TSE and TrueFISP in axial plane. The images show a large lobulated plural effusion with associated collapse-consolidation of the right lung. The liver shows perifissural atrophy, a loculated collection over the surface of the liver parenchyma. Free fluid is visible in the right external and internal oblique muscle, the paracolic gutter, and the pelvic and peritoneal cavity. The 3D MRCP shows slight dilation in the common hepatic and bile ducts.

> *"We have been operating six 1.5T MRI scanners across our centers. I must say the image quality on this system is excellent. We have been using the system for a wide range of applications, including neonatal[1] scans, fetal MRI, bariatric exams, and for patients with metal implants[2]."*

Conclusion

MAGNETOM Free.Star brings many benefits to radiology departments. It delivers a similar performance to our MAGNETOM ESSENZA 1.5T MRI system, from the perspective of scan time and image quality, and the total cost of ownership is about 30% less. It also allows reliable scanning of patients with implants[2] and is suitable for use in gynecological, gastroenterological, and pulmonological cases, which have not traditionally been the focus for MRI scans. Being able to handle more cases benefits our patients and leads to more revenue and faster break-even. It is important to mention that the system does not have some applications. These include MR spectroscopy, cardiac MRI, and functional MRI. However, in small regions like Visakhapatnam, we mainly require good diffusion, fast workflows, better safety, user-friendly systems, and above all a low total cost of ownership and no challenges when servicing this complex equipment. MAGNETOM Free.Star fulfills all these requirements, and the advantages outweigh the few missing applications.

Contact

V. Suresh, M.D.
Dolphin Diagnostic Services
18-1-18, KGH Down Rd,
Near KGH Down Road,
Maharani Peta, Visakhapatnam,
Andhra Pradesh 530002
India
sureshtez@yahoo.co.in

Acknowledgment

I would like to acknowledge the support of Dr. Rishi Awasthi, Mr. Anto Alwine, and Mr. R. Vinoth Kumar from Siemens Healthineers for this article.

References

1 International Institute for Population Sciences and Macro International. National Family Health Survey (NFHS-3), 2005–06 [Internet]. Mumbai, India: Ministry of Health and Family Welfare, Government of India. September 2007;436–440. Available from: https://dhsprogram.com/pubs/pdf/FRIND3/FRIND3-Vol1AndVol2.pdf
2 Berman P, Ahuja R, Bhandari L. The Impoverishing Effect of Healthcare Payments in India: New Methodology and Findings. Economic and Political Weekly. 2010;45(16):65–71.
3 Guo AC, Cummings TJ, Dash RC, Provenzale JM. Lymphomas and high-grade astrocytomas: comparison of water diffusibility and histologic characteristics. Radiology. 2002;224(1):177–183.
4 Le Bihan, Breton E, Lallemand D, Grenier P, Cabanis E, Laval-Jeantet M. MR imaging of intravoxel incoherent motions: Application to diffusion and perfusion in neurologic disorders. Radiology. 1986;161(2):401–407.
5 Warach S, Chien D, Li W, Ronthal M, Edelman RR. Fast magnetic resonance diffusion-weighted imaging of acute human stroke. Neurology. 1992;42(9):1717–1723.
6 Le Bihan D, Iima M. Diffusion Magnetic Resonance Imaging: What Water Tells Us about Biological Tissues. PLoS Biol. 2015;13(6):e1002203.
7 Jezzard P, Balaban RS. Correction for geometric distortion in echo planar images from B0 field variations. Magn Reson Med. 1995;34:65–73.

[2]The MRI restrictions (if any) of the metal implant must be considered prior to patient undergoing MRI exam. MR imaging of patients with metallic implants brings specific risks. However, certain implants are approved by the governing regulatory bodies to be MR conditionally safe. For such implants, the previously mentioned warning may not be applicable. Please contact the implant manufacturer for the specific conditional information. The conditions for MR safety are the responsibility of the implant manufacturer, not of Siemens Healthineers.

MAGNETOM Free.Max: Access to MRI – How to Make it Big Inside and Small Outside

Stephan Biber, Ph.D.

Senior System Architect & Principal Key Expert at Siemens Healthineers, R&D AEP, Erlangen, Germany

MR systems have always been known to be large, heavy machines that require a complex infrastructure such as the supply of liquid helium and a highly reliable supply of electricity and cooling. While the new DryCool magnet technology has been presented in detail by Simon Calvert [1], this article will focus on how the MAGNETOM Free.Max system is able to be big on the inside with the first-ever 80 cm patient bore on the market, making it at the same time one of the smallest whole-body MRI systems on the market. With a footprint of just 23 m^2, a transportation height of less than 2 meters, and a weight of only 3.2 tonnes we believe the system defines a new class of MRI systems. This paper will present a number of technical innovations, which in isolation could be seen as simple engineering tasks, but together they help to overcome long-established issues with the installation process and therefore can realize unmet customer needs. Furthermore, we would like to demonstrate how only a holistic system-perspective, which aligns all the engineering disciplines behind a common goal, is able to accomplish this.

How to make it big: Combining field strength and gradient power with new imaging techniques

MR systems with solenoid magnets have been available with 60 cm patient bores since the early 1990s. In 2004, Siemens Healthineers introduced MAGNETOM Espree, the first 1.5T system with a 70 cm bore and MAGNETOM Verio in 2007, the first 3T system with a 70 cm bore. This broadened access to MRI for growing patient groups by improving comfort, counteracting claustrophobia, and accommodating obese patients in the bore. Despite the larger bore on the 70 cm systems, the need remained for even more space in the bore for the same reasons that first triggered the development of 70 cm systems. But whereas 20 years ago, the market was able to deal with the associated increased costs of 70 cm systems versus 60 cm systems, the situation is different today. Radiology is under severe cost pressure, which calls for new ways of providing high-value imaging with improved patient access at an affordable cost.

The belief in MRI has long been that higher field strengths and gradient powers together with a high receive system channel count delivers better image quality and higher speeds. This belief still holds true but there are other ways to serve markets that require the diagnostic quality of a 1.5T system but not necessarily at exactly the same speed and contrast. A larger bore diameter is essentially what drives up the costs of MRI systems. This, in turn, reduces the accessibility of MRI to a large part of the worldwide population. The costs of the magnet (mainly the superconductive wire) increase rapidly as the size rises. Gradient coil power increases with ~R^5, which would quadruple the power needed when going from a 60 to 80 cm patient bore. The only way out is to go against the grain and question existing assumptions on field strength and gradient power.

During an early prototyping phase back in 2016, a 1.5T MAGNETOM Aera system was ramped down to 0.55T and equipped with modified RF-electronics. With *in vivo* imaging, it was then possible to assess image quality and analyze the impact of different types of gradient engines.

Designed as our most compact whole-body MRI MAGNETOM Free.Max

The in-house prototype and a replica of this system installed at the National Institutes of Health (NIH) helped to demonstrate that routine clinical questions in general radiology can be answered at a field strength of 0.55T [2]. Our internal analysis indicated that acceptable image quality and measurement times could be achieved with a gradient engine of 45 T/m/s and a gradient field of approximately 26 mT/m for this application field. In contrast to the 1990s, we were able to combine this MRI system with new imaging techniques that help overcome some of the drawbacks of mid-field imaging. These negative aspects had originally stimulated the design of 1.5T scanners, e.g., DeepResolve Gain and Sharp are image reconstruction methods enabling intelligent, iterative denoising using individual noise maps and an increase in image resolution using a deep neural network. These technologies can be used to reduce acquisition times and improve image quality simultaneously. At the same time, Deep Resolve can be combined with image acceleration techniques such as parallel imaging – which was not available in the 90s – and Simultaneous Multi-slice (SMS) on MAGNETOM Free.Max. In addition, Compressed Sensing has also proven to be a valuable tool for acquisition acceleration. For clinical examples, please refer to the Image Gallery [3].

The unique combination of a 0.55T scanner with various powerful new acquisition and reconstruction techniques laid the foundation for the innovation, MAGNETOM Free.Max. The reduced field strength on both the magnet and the gradient engine allowed the bore diameter to be scaled up from 60 to 80 cm, while still keeping the superconductive wire length and gradient power within a range that would make the system more affordable.

Figure 1A shows the optimization in the multiparameter space: superconductive wire length and costs increase with field strength and magnet bore diameter. When starting with an 80 cm patient bore (1), the thickness needed for the gradient coil and the body coil dictate the magnet bore diameter. For the sake of simplicity here, we assume a range of different thicknesses shown by the blue and green areas, with a slight tendency of gradient coils with higher G_{max} and SR to also require more radial space (2). With the magnet bore diameter derived from the outer diameter of the gradient coil, the impact on wire length for 0.5T and 1.5T are shown by the yellow and red curves (3), assuming similar boundary conditions on the stray field. These two curves show the huge scale of the nonlinear increase in the superconductive wire for the magnet when field strength and bore diameter are increased.

Starting from the 80 cm bore diameter, looking into the lower right quadrant (4), it becomes evident that the gradient power not only increases with higher SR and G_{max}, but it increases disproportionally with patient bore diameter.

Increased gradient power usually goes hand in hand with the additional power needed for the cooling system, which has to extract the heat from the gradient coil and the gradient power amplifier (GPA) and dissipate it in the

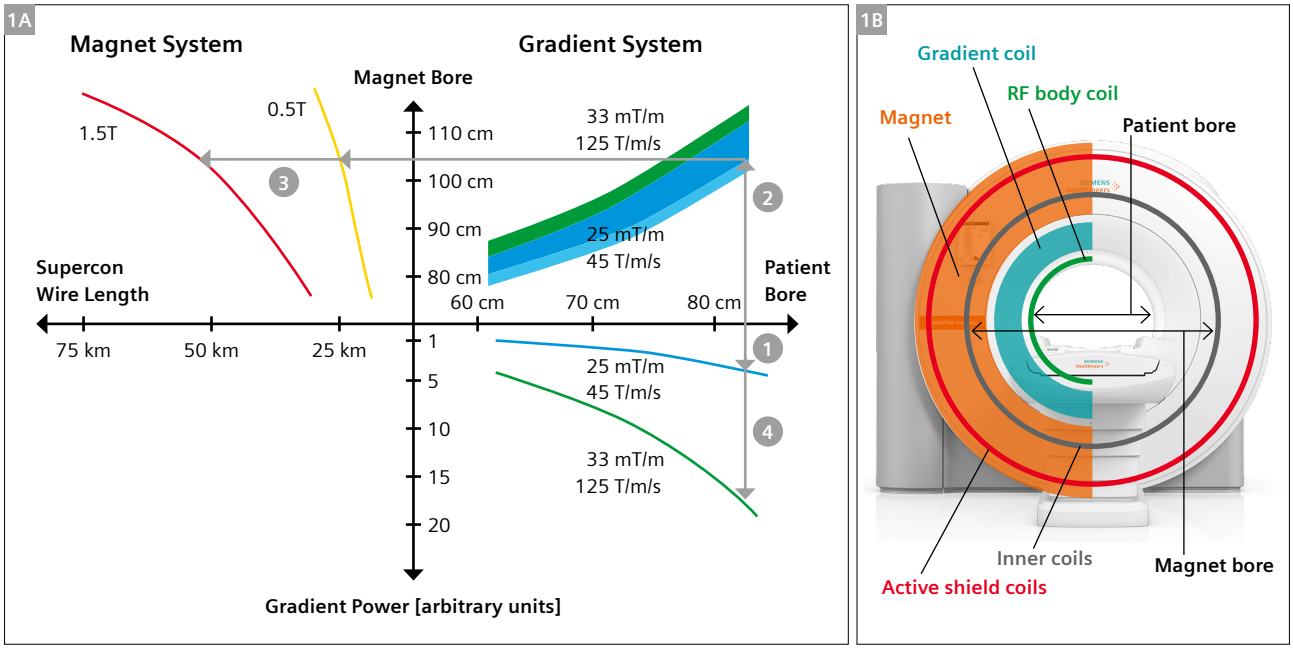

1 **(1A)** Scaling of superconductive wire length and gradient power with patient bore and field strength. Figures are merely illustrative to show the main correlations. Please note that the numbers in this article are also indicative to explain the physics and not related to a special design. **(1B)** When starting with an 80 cm patient bore, the thickness needed for the gradient coil and the body coil dictate the magnet bore diameter.

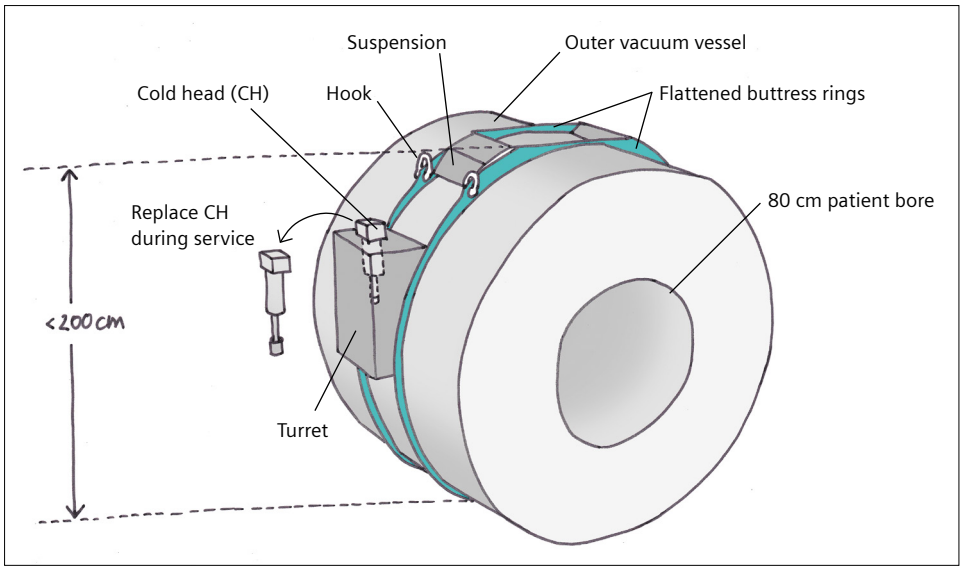

2 Figure 2 shows the flattened buttress rings, the outer vacuum vessel (OVC) with the shield coils, and the turret with the cold head that is moved further down on the side of the system.

air. Therefore, stronger gradients have a quadruple effect on the system design: They require more power to generate the fields, they require more cooling to extract the resulting heat and together this drives needs on local infrastructure up (connection power, space for chiller, etc.). They tend to also drive the gradient coil thickness and therefore the inner diameter (4) of magnet.

Scaling the Tx subsystem to provide sufficient B_1 amplitude on a 23 MHz system with an 80 cm patient bore is – compared with the magnet and gradient design – the easiest piece in this puzzle. Luckily, a lower Lamor frequency also requires less power to achieve the same B_1 field. Therefore, an existing 63 MHz amplifier can be tuned to 23 MHz and the additional power can be invested in overcoming the lower efficiency $\eta = B_1/P_{BC}$ of a body coil with a larger diameter. The lower conductivity of tissue at a lower frequency also makes SAR an almost negligible issue.

How to keep it small

While the inside of an MRI system should be as large as possible to provide space for the patient, it is more difficult to identify what the system should look like from the outside. When observing an installation process, it immediately becomes clear that the height of the system is a critical parameter: The system should be easily movable through doors. In the past, even removing doors often did not help and MRI installations frequently meant breaking up concrete structures, affecting the structural integrity of the building. Naturally, this was often associated with high costs and organizational efforts as well as other unwanted consequences. In many countries, two-meter high door openings are standard. Here is the simple but effective recipe with five major ingredients how to make sure the MRI system stays below 2 m height:

1. Outer vacuum vessel: Limit shield coil diameter
Underneath the plastic cover of an MRI system is the outer vacuum chamber (OVC), which contains the cryoshield and the superconductive magnet coils (dry magnets do not need a helium vessel). When the inner coils of the magnet are moved outward to accommodate the large patient bore, the shield coils also tend to move further out. Setting a boundary of ~1.95 m for the diameter of the OVC sets a clear design goal for the position of the shield coils. If the OVC is to be within the two-meter limit, it is essential that no other parts of the system design exceed this limit.

2. Buttress rings and magnet suspension
For the OVC to withstand the 1 bar atmospheric pressure from the outside, it is reinforced using circumferential buttress rings. These rings are flattened at the top of the magnet without any negative impact on their structural stiffness, which in turn allows the shield coils to be moved out as far as possible inside the OVC. Another structure that potentially affects the overall height of the system are the suspensions that hold the magnet coils in place. A tensile suspension connects the 4 K cold inside of the magnet with the warm outer vacuum chamber (OVC). The mechanical structure required to mount the tensile suspension to the outside of the OVC needs to be very slim so that this is not the highest point.

3. Quench pipe
The dry magnet does not need a quench pipe. It follows that there is no pipework on top of the magnet that could require extra height on top of the OVC and would require the connection of the magnet to the ceiling. This makes the new SkyView option possible (Fig. 3), which gives the system a unique visual impression by removing any connection between the MR scanner and the ceiling.

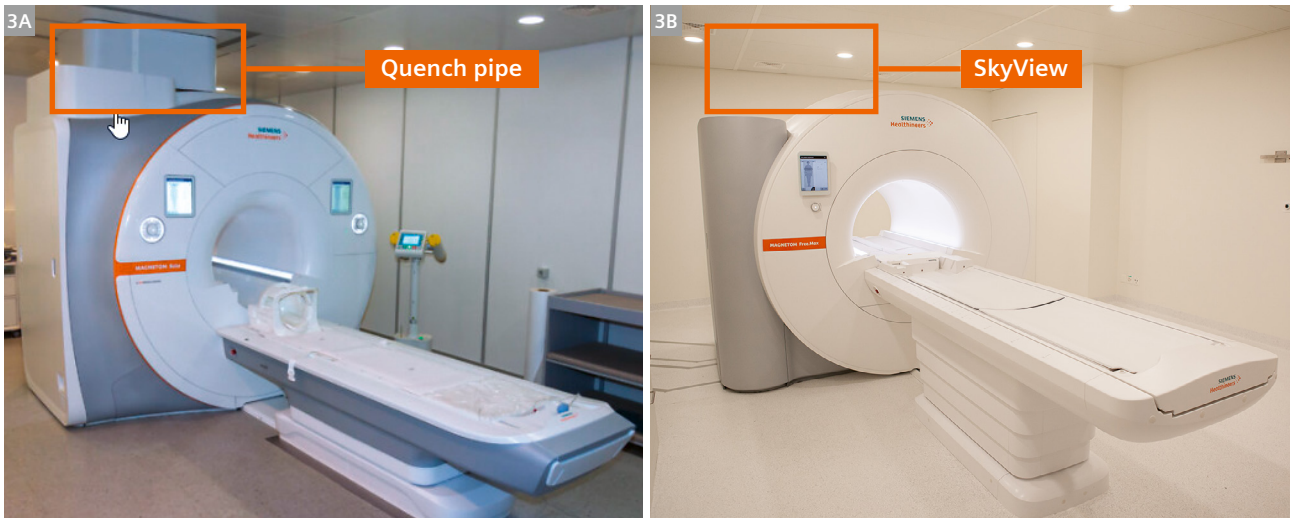

3 **(3A)** Conventional system with quench pipe. **(3B)** MAGNETOM Free.Max with DryCool magnet technology and easy siting.

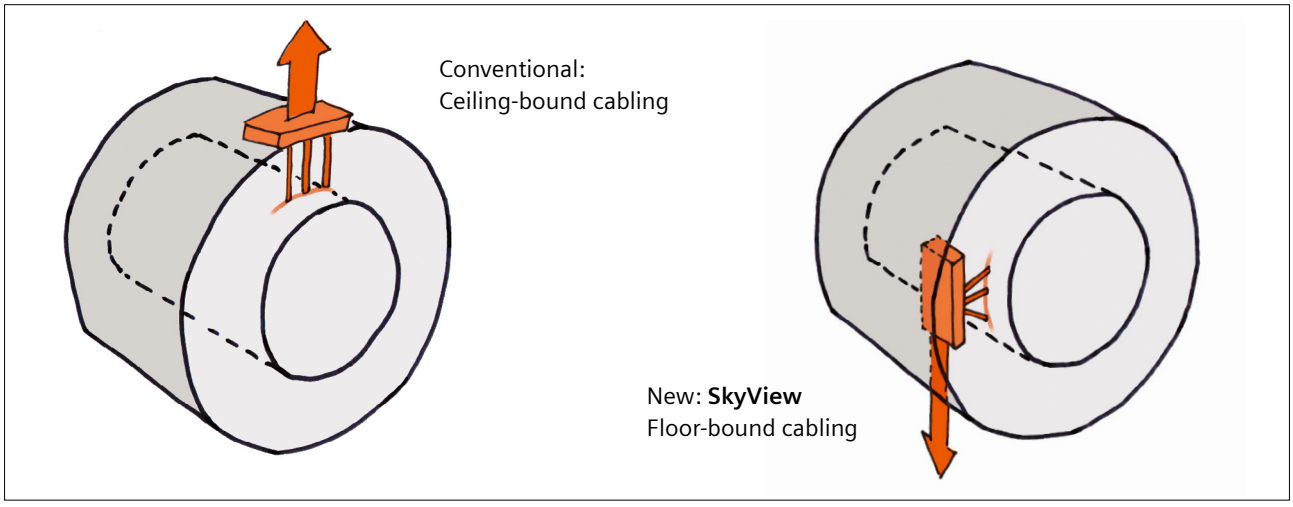

4 Gradient connection and SkyView

4. Gradient connections

The gradient coil needs to be connected to the gradient cables that deliver the current from the gradient power amplifier (GPA). As in every electrical connection, the point where two cables are joined together is critical to maintaining good electrical contact. The gradient cables carry currents over 300 A and voltage up to 1200 V, so any loose connections could generate sparks that must be avoided. The connection of gradient cables is particularly critical due to the high Lorenz forces:

$$|\vec{F}_L| = |I|\,|\vec{\ell}|\,|\vec{B}|\,\sin\alpha$$

Locally, the actual field at the end of the magnet can be higher by up to a factor of 2–3 than the nominal field at the isocenter. For a 1.5T system with a strong gradient engine (I = 900 A), a 40 cm long gradient cable at the end of the magnet will experience a force of approx. 500–1500 N (equaling 50–150 kg) oscillating with the gradient pulses. This is why, historically, the connection of the gradient cables from the GC to the cables from the GPA on scanners from Siemens Healthineers was on top of the magnet. Here, the fields perpendicular to the wires and the resulting Lorenz forces are lower. This location for the gradient connection was never an issue on wet MRI magnets, because other parts (e.g., the cold head or pipework for the quench line) were located even higher.

I = current, ℓ = length of wire/cable, B = magnetic flux density aka magnetic field, α = angle between wire/cable and B

5 MAGNETOM Free.Max installation at University Hospital Basel in Switzerland. Even during one of the very first installations, the small size of the system and the eliminated quench pipe paid off to make the installation process much easier.

With the lower field strength and the lower gradient current, it was possible to reduce the forces by almost one order of magnitude. This facilitates a gradient connection on the rear side of the magnet rather than on the top. This is also required for the SkyView siting option. Here, gradient cables are routed together with all other cables through the floor rather than the ceiling (Fig. 3B).

5. Cold head

The cold head in conventional MRI magnets, where the superconductive coils are submerged in a liquid helium bath, needs to be located above the liquid helium level to allow recondensation of the gaseous helium. In dry magnets that have just a small helium reservoir as a liquid heat buffer rather than a large helium vessel, the cold head can sit in any vertical position. On MAGNETOM Free.Max, the cold head is located inside a turret, mounted on the side ~30 cm below the upper boundary of the OVC. This not only allows unhindered transportation through 2 m high doors, but also means that all later service activities (e.g., cold head replacement) can be performed within a ceiling height of just 2.2 m – even after the system has been installed in its final location. Since MAGNETOM Free.Max can be both installed and serviced in low-height premises, MR diagnostics can now be brought to new places such as small imaging centers. These are often located in residential buildings with limited available space.

This overview shows how a complete design overhaul of the magnet and gradient system together with the use of new imaging and reconstruction techniques results in an MRI system that achieves somewhat contradictory goals: A large 80 cm bore for the patient with a scanner that delivers diagnostic image quality AND easy installation with a small physical footprint and low connection power.

More background information on MAGNETOM Free.Max and DryCool magnet technology will be available soon on: www.siemens-healthineers.com/magnetom-world.

References

1 Calvert S. A Brief History of the DryCool Magnet Development. MAGNETOM Flash. 2020; MAGNETOM Free.Max special issue. Available at https://www.magnetomworld.siemens-healthineers.com/hot-topics/lower-field-mri

2 Campbell-Washburn AE, Ramasawmy R, Restivo MC, et al. Opportunities in Interventional and Diagnostic Imaging by Using High-Performance Low-Field-Strength MRI. Radiology. 2019;293(2):384-393.

3 MAGNETOM Free.Max Image Gallery. MAGNETOM Flash (78) 1/2021. Available at https://www.magnetomworld.siemens-healthineers.com/publications/magnetom-flash

Contact

Stephan Biber, Ph.D.
Siemens Healthineers
SHS DI MR R&D AEP
Postbox 32 60
91050 Erlangen
Germany
stephan.biber@siemens-healthineers.com

MAGNETOM Free.Max: Keeping a Hot System Cool

Stephan Biber, Ph.D.

Senior System Architect & Principal Key Expert at Siemens Healthineers, R&D AEP, Erlangen, Germany

Helium is a rare element on Earth. Once released into the atmosphere, it is so lightweight that it leaves Earth's gravitational field and diffuses into space. DryCool technology, one of the key innovations on MAGNETOM Free.Max, reduces the helium demand in MR systems and removes the need to handle liquid helium during system installation. It also saves helium and prevents it from being released into the atmosphere during both normal system operation and failures such as quench events. However, the dramatic reduction of liquid helium to 0.7 liters contained in each MR magnet reduces the heat capacity of the magnet. If a conventional magnet loses cooling – e.g., due

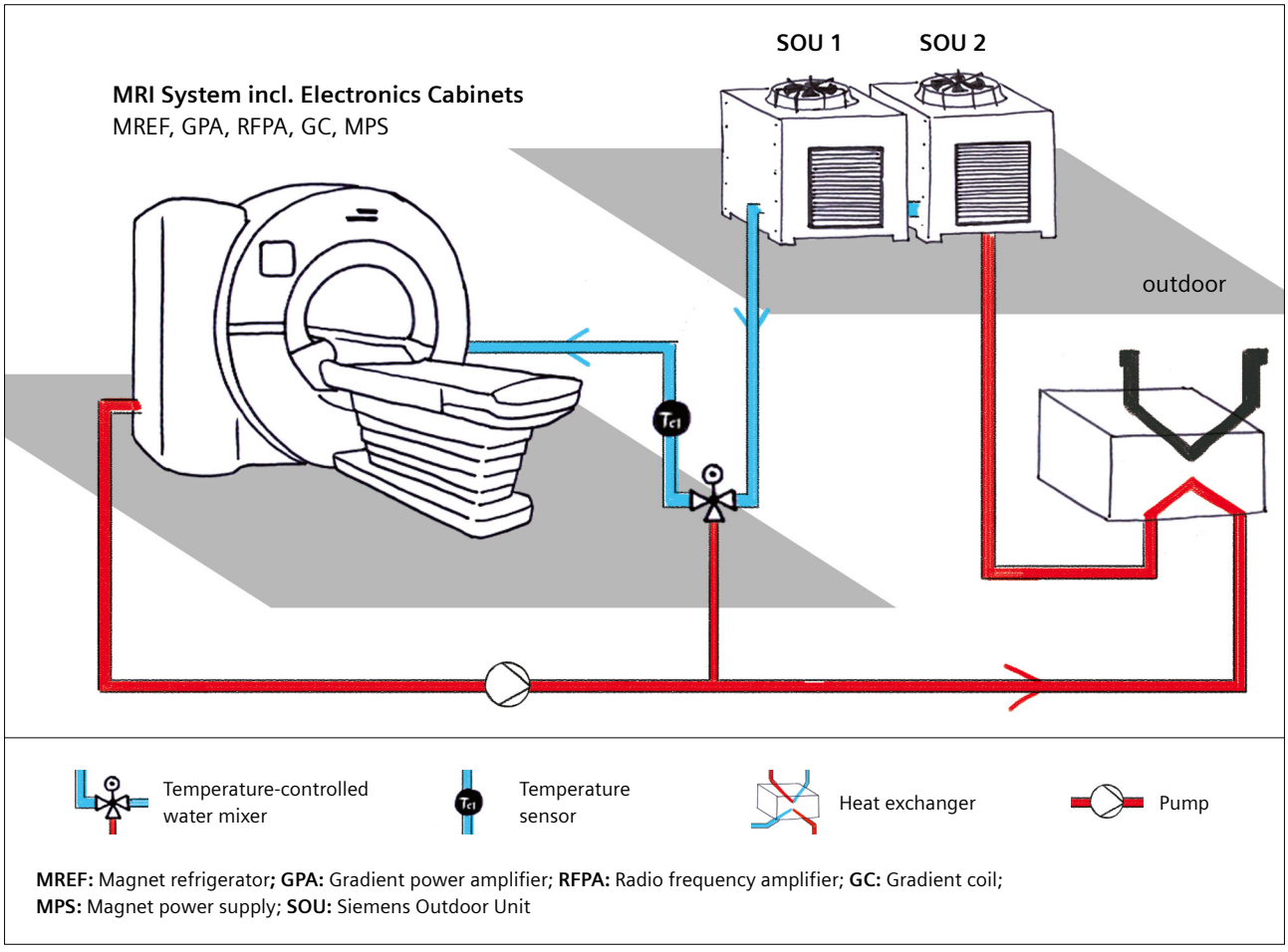

1 Active cooling system with external chillers.

to a power outage or a failure of the cooling system – the liquid helium slowly starts evaporating. Once a certain pressure threshold is exceeded (usually after less than 1 hour), the magnet loses helium into the ambient atmosphere. Depending on the filling level, a conventional magnet can stay cold by continuously evaporating its helium reservoir for many days without losing superconductivity. This is because the helium reservoir contains several hundred liters of helium. Reducing the helium down to less than 1 liter for DryCool magnets therefore also reduces the tolerance of such systems against infrastructure failures. The main types of failure are power outages and failures of the cooling system. This paper describes how MAGNETOM Free.Max can provide high availability of the MRI scanner despite a liquid helium inventory of only 0.7 liters.

Power outages

Power outages are external events, out of control of the MRI system. The system can only react accordingly; it cannot avoid the situation itself. With DryCool technology, a small integrated uninterruptible power supply (UPS) keeps the magnet electronics running even during a power outage. If the power outage persists, the magnet electronics will ramp down the magnet after a certain waiting time in order to avoid a quench event, which would turn all the energy in the magnetic field into heat and warm up the system significantly. With MAGNETOM Free.Max, ramping the magnet down and then back up to field is now an automatic procedure which no longer requires an onsite visit from a service technician, due to the integrated magnet power supply. After a controlled ramp down, the magnet heats up very slowly. Once power returns, it can be recooled and ramped up again [1]. In regions where power reliability is poor, the system can also be buffered with a large UPS which not only keeps the system cold, but also enables continuous scanning even during brownouts or blackouts of the power grid.

Cooling system failures

Unlike power outages, the reliability of the cooling system is very much under the control of the MRI system design. For an imaging modality like MRI, which relies so much on cooling, the reliability of the cooling system is essential for guaranteeing high availability of the MRI system. The MAGNETOM Free.Max cooling system was developed with the need for high reliability in mind from the very beginning. The following section explains the redundancy-focused architectural measures which were applied to MAGNETOM Free.Max.

A liquid helium temperature of 4 K is achieved using a cryocooler ("cold head") which is driven by a compressor. The compressor (magnet refrigerator = MREF) requires approximately 6–8 kW of power to generate ~1 W cooling power on the 4 K level. In order to ensure permanent operation of the compressor, which keeps the magnet cold, the MREF must be supplied with electricity and cooling water. Cold water for MAGNETOM Free.Max can be provided by two different options:

Active cooling system

One option is to buy an external chiller which is tailored to operate with the MRI system. The flow diagram in Figure 1 shows that, in this case, the same water running through the MR components (MREF, gradient coil, amplifiers) is also running through the outdoor units SOU 1 and SOU 2. In such a configuration, the MRI system is self-contained and does not rely on any external water supply. This makes the setup very reliable because it avoids clogging of water flow or corrosion due to dirt and debris from external cooling water.

Chillers are located outside the building, often on rooftops or parking lots, where they use the ambient air to dissipate the heat from the MRI system. As they are located outdoors, chillers are exposed to all kinds of weather conditions: Temperatures can range from -20°C to +45°C, and dirt, dust, or leaves can block the heat exchangers. In highly reliable cooling systems, the outdoor units are a weak point in the chain. If an outdoor unit fails, the helium compressor will stop working and this will soon cause the magnet to ramp down. For the new DryCool technology, the chillers were designed with built-in redundancy to overcome this problem. During heavy-load scanning (mainly diffusion imaging) MAGNETOM Free.Max can

2 Active cooling system with two ~17 kW Siemens Outdoor Units (SOU).

require up to 33 kW of cooling power, with demand primarily coming from the gradient system (coil and amplifier), the magnet cooling, and the RF amplifier. The cooling power is provided by two separate ~17 kW outdoor units (Siemens Outdoor Unit: SOU 1 and SOU 2; Fig. 2), which can work mostly independently from one another. During times when the system is in standby or scanning with less power-demanding sequences (TSE, GRE), only one of the two chillers is needed and the other one is turned off to save energy. If there is a failure with one of the 17 kW chillers, the second one automatically takes over to guarantee a permanent cold water supply and avoid a magnet ramp-down and the associated system downtime. The system can even continue scanning in this mode. Furthermore, during normal operation when one chiller is enough, the chillers are switched on and off in alternating mode to make sure both chillers are always operational and the energy consumption is optimized.

The splitting of the cooling modules requires little additional effort, as the 33 kW cooling power is needed anyway for system operation. This means that there is no extra cooling power added to provide redundancy for the magnet cooling, because the 6–8 kW required for magnet cooling is less than half of the total cooling power of a single unit. Redundancy can therefore be achieved just by providing the overall cooling power from two separate units with half the total system power – without the need to install any unused cooling power, which would add extra effort and costs.

Passive cooling system

In many large institutions, cooling water is centrally supplied and the MRI system can profit from the fact that no extra chillers are needed. The so-called "passive cooling option" cools the MRI system using a heat exchanger which separates the water provided by the central cooling supply from the water circulating through the MRI system components (Fig. 3A).

In cases where the central water supply from the hospital is not considered to be reliable enough, there is also a possibility to connect a locally sourced "backup chiller" to the system. This can provide the cooling power needed to keep only the magnet refrigeration running in case the central water supply fails. The cold water for the MREF coming from the backup chiller is provided to the system through an additional heat exchanger. The system automatically detects cases where the cooling power from the central water supply is insufficient and sends a signal to trigger the backup chiller (Fig. 3B).

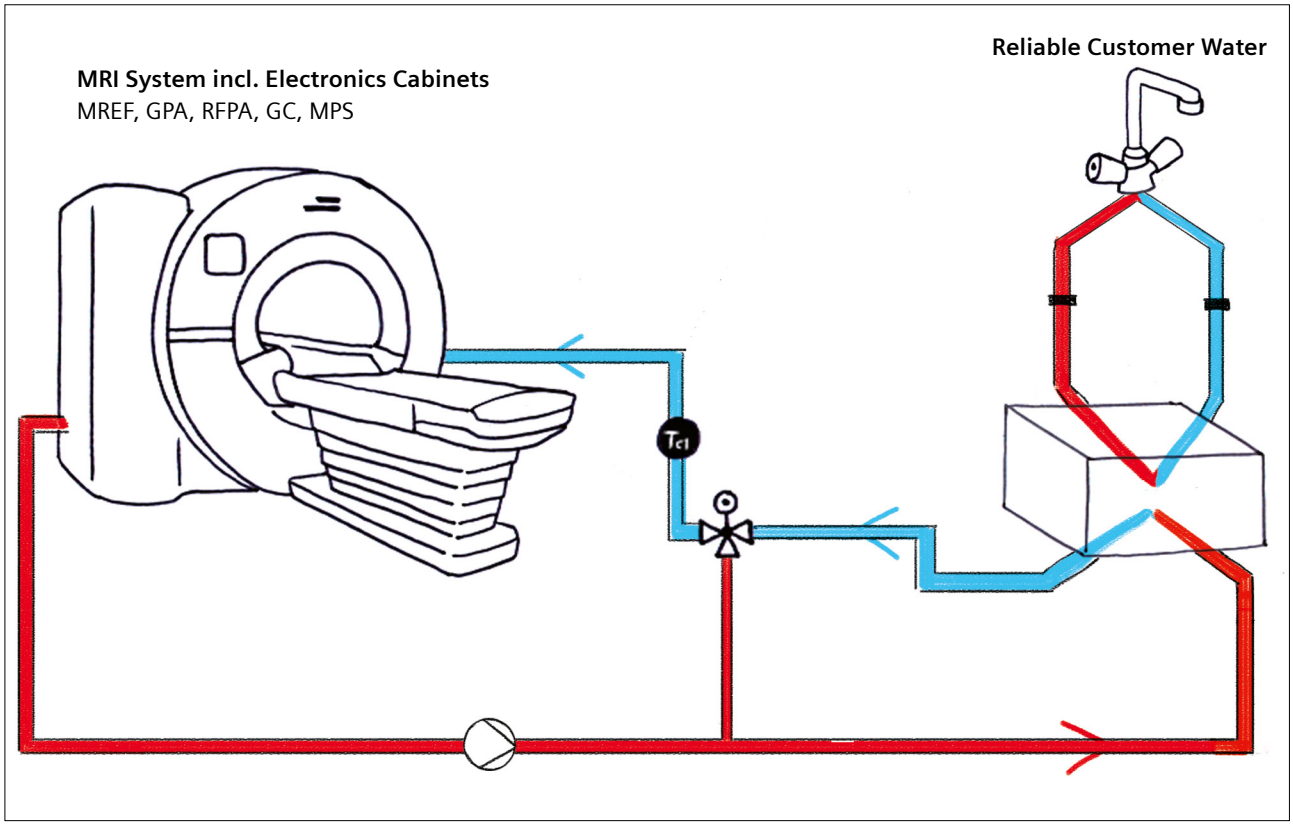

3A Passive cooling system with reliable water from a central customer supply.

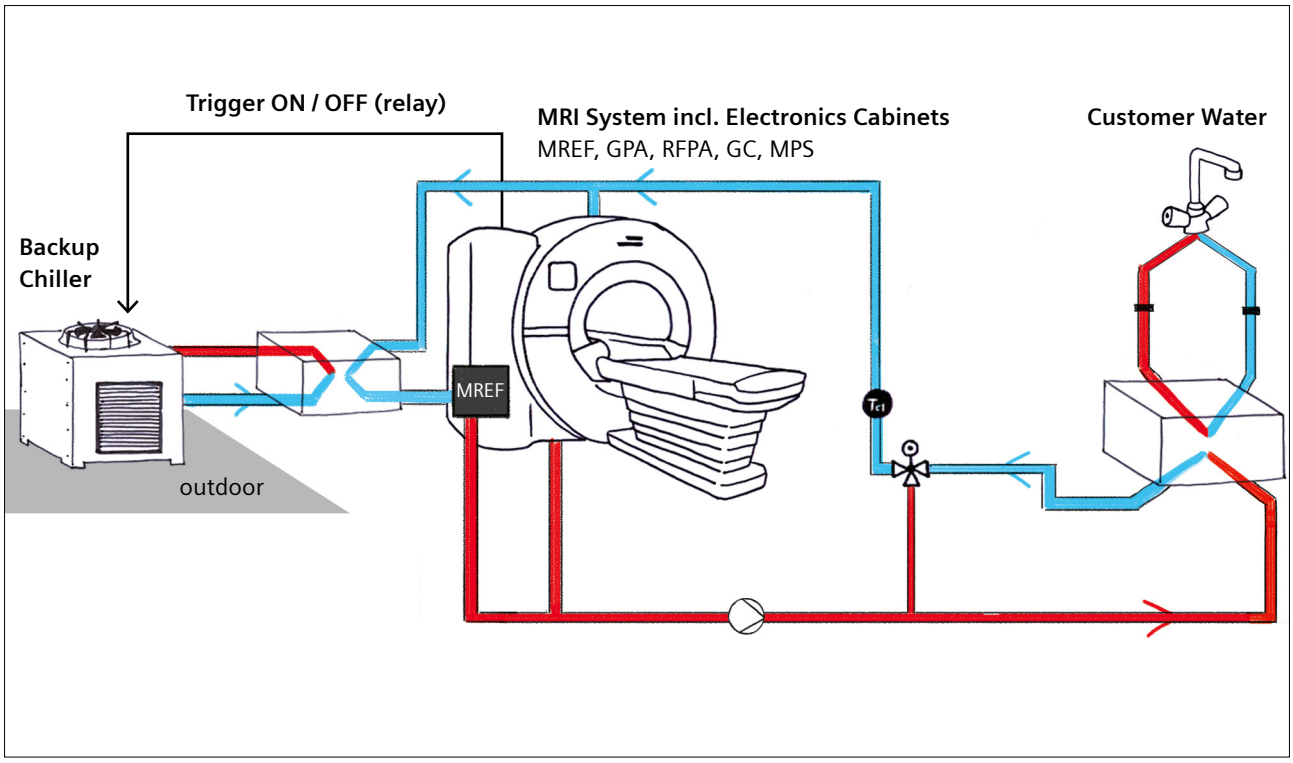

3B Passive cooling system with automatically triggered backup chiller.

Remote monitoring and service

Despite the best efforts to ensure high reliability, cooling systems with high water flow rates and pressure – such as those used in MRI systems – require regular service. With the MR cooling system running 24/7, most failures (leakage, clogging, corrosion, dirt on outdoor units) can be detected and solved by qualified service personnel before they cause the system to stop working. Furthermore, the built-in cooling system is connected to our online service and all parameters available via sensors are also transmitted and evaluated online to allow remote diagnostics and preventive maintenance. In particular, the magnet refrigerator (MREF) is equipped with sophisticated temperature and pressure sensors. Preventive maintenance makes it possible to detect problems by watching the trends of these parameters over time. As a result, many problems can be detected before they lead to a complete failure of a component.

Summary

The above overview shows how the system architecture, both for the cooling system and the system control, is tailored to deal with the new challenges of DryCool magnets and deliver maximum availability. Three different configurations are provided to achieve a high-reliability cooling system adapted to the individual needs and conditions of different sites. The basic principle is to provide redundancy for those parts that have an unacceptably high chance of failure. Combining this with remote monitoring, regular servicing, and automatic ramping guarantees extremely high availability for DryCool systems and independency of the scarce natural resource helium.

Reference

1 Calvert S. MAGNETOM Free.Max: from Concept to Product, a Brief History of the DryCool Magnet Development. MAGNETOM Flash. 2021; MAGNETOM Free.Max special issue: 44–48. Available from: https://www.magnetomworld.siemens-healthineers.com/hot-topics/lower-field-mri

Contact

Stephan Biber, Ph.D.
Siemens Healthineers
SHS DI MR R&D AEP
Postbox 32 60
91050 Erlangen
Germany
stephan.biber@siemens-healthineers.com

Meet Siemens Healthineers

Siemens Healthineers: Our brand name embodies the pioneering spirit and engineering expertise that is unique in the healthcare industry. The people working for Siemens Healthineers are totally committed to the company they work for, and are passionate about their technology. In this section we introduce you to colleagues from all over the world – people who put their hearts into what they do.

Zahra Hosseini, Ph.D.

Zahra Hosseini obtained a bachelor's degree in engineering from McMaster University in Hamilton, Ontario, Canada. She then completed an M.Sc. in biomedical engineering in the field of virtual reality and image-guided surgery. Zahra earned her Ph.D. at Western University, in London, Ontario, Canada, where she focused on ultrahigh-field MRI signal processing and developed multi-parametric imaging techniques for brain and cardiac applications. Following her Ph.D., she joined the MR Collaboration team at Siemens Healthineers in the United States, working with some of our leading collaboration partners in translational research and development. Zahra contributed to one of our latest Deep Resolve products: Deep Resolve Swift Brain. She moved to Germany in 2022 and became the global product marketing manager for one of our newest MRI platforms, the MAGNETOM Free. Platform. In this role, Zahra is helping bring a novel field strength into core and new imaging environments.

How did you first come into contact with MRI?
When I finished my master's in biomedical engineering, which involved creating a virtual reality system for image-guided therapy, I knew I wanted to pursue a doctorate degree, but it had to be in a field I knew little about. Magnetic resonance imaging was always a fascinating topic for me: as an engineer, I loved taking things apart and reverse engineering them to learn. I needed something that was visible to my eyes to learn about it. Physics and quantum mechanics were a whole new beast, though – and definitely worth spending four years of my life on for my Ph.D.!

What do you find most motivating about your job – and what are the biggest challenges?
From a scientific standpoint, I find it fascinating and exciting to be able to revisit low field and leverage the software and hardware innovations at Siemens Healthineers to deliver unmatched clinical performance. To work with a solution that also promises to simplify access for every patient globally in an innovative and unmatched way is icing on top of the cake for me. It feeds my ambition and drive to make a difference on a bigger scale.

What do you think are the most important developments in healthcare?
Providing timely diagnostic answers to our patients is of huge value and enables every patient to make better decisions – whether they're considering a course of treatment, healthier lifestyle habits, or simply their life plans. And of course, outside of diagnostics, tremendous work is being done on developing appropriate treatments, effective and efficient therapy delivery, and easier ways for each of us to make better and healthier life choices. Perhaps the most important development in healthcare is awareness and access to information.

What would you do if you could spend a month doing whatever you wanted?
I would teach science and engineering in a remote location where I'm unfamiliar with the culture and language. That way, I'll also learn something new as I teach.

Where do you think this field is headed?
When you add the open 80-cm bore of the MAGNETOM Free.Max to its unique field strength and the various features that enable its easy integration into an existing infrastructure, you cannot help but start thinking outside of the box – moving away from routine diagnostics to explore new possibilities with radiation therapy planning, which is now an available possibility after the MAGNETOM Free.Max RT Edition was launched at ASTRO this year, to MRI-based interventional procedures, an area which is already of great interest amongst our active research users. I'm really excited to be part of this movement in building the future of imaging and therapy with MRI.

Stephan Biber, Ph.D.

Stephan Biber was born in Eichstaett, Germany. From 1996 to 1999, he studied electrical engineering at Friedrich-Alexander-Universität Erlangen-Nürnberg (FAU) in Germany. After graduating, he moved to the University of Colorado Boulder in the U.S., where he earned an MS in electrical engineering with a focus on remote sensing and high-frequency technology. Stephan then returned to Germany and embarked on doctoral studies, earning his Ph.D. in engineering from FAU in 2005. The following year, he joined Siemens Corporate Technology in Erlangen as a developer of high-frequency electronics and a consultant for sensor systems. From 2006 to 2010, Stephan was a developer for local coil development in Magnetic Resonance Imaging at Siemens Healthcare in Erlangen, working in predevelopment, product development, and project management. Since 2012, he has been a system architect for MRI at Siemens Healthineers. In 2013, he was named Inventor of the Year by Siemens AG, and he was appointed Principle Key Expert for System Architecture at Siemens Healthineers in 2016. For his contributions to the MAGNETOM Free. platform he was nominated for the German Federal President's Award for Innovation and Technology in 2023.

How did you first come into contact with MRI?
After earning my Ph.D. in microwave technology, I started my career at Siemens within Corporate Technology, where my role was partly to work on radio frequency (RF) technology and partly on technology consulting. Half of the time, I was doing predevelopment for MR and this is how I found out that MRI is an extremely cool field to work in. I like the fact that the whole medtech industry is very multidisciplinary: It covers physics, engineering, and medicine, and everything is connected. Soon after starting with Corporate Technology, I became a developer at MR for local coils, leading the development of coils and receive system technology for MAGNETOM Aera and Skyra.

What do you find motivating about your job?
Working with people, seeing the outcome, improving patient care. My colleagues are the biggest asset I have: They are always open for new ideas, everyone shares their thoughts, and we are moving the technology forward together. Nothing can replace this. As an engineer, I just enjoy working with hardware, because I like to see and touch the things that I spend my time and my energy on. Although my actual work is more theoretical and focused on conceptual aspects, I see how it impacts the work of others and how I can influence the outcome of the complete system and improve clinical diagnostics. Also, MRI has so many different aspects: If one topic gets tedious, there are plenty of others to explore – probably too many to cover in a single lifetime.

What are the biggest challenges in your job?
During the early concept phases for new MRI scanners, it is very demanding to bring the different expectations from all stakeholders together and find one common solution which works for everyone. This requires a lot of communication about all aspects, including business, technology, medicine, and project management. It's often a painful process to go through, and it's different every time.

What do you think are the most important developments in healthcare?
Historically, I think anesthesia is a highly underestimated development and I always think about this when I am at the dentist. I've seen a few trends come and go, and in hindsight many of the things that were advertised as "gamechangers" turned out to be just buzzwords that didn't change the world very much. With AI today, this will be different: I believe this is really an innovation which will change the medtech industry dramatically. As well as leading to the creation of many new software products, it will also change the hardware as we know it today. The MAGNETOM Free. Platform is a very good and early example of this.

What would you do if you could spend a month doing whatever you wanted?
If you give me a month, I will be on a boat, scuba diving the tropical reefs with corals and sharks, and seeing the craziest creatures nature has created. Until then, I'll try to keep my fitness up with regular running. For more action, I have reserved a few weekends every year for white-water kayaking. Learning how to windsurf is still on my bucket list. And if you give me another month, I'd take a language course to refresh my poor Arabic.

Not for distribution in the U.S.

On account of certain regional limitations of sales rights and service availability, we cannot guarantee that all products included in this brochure are available through the Siemens Healthineers sales organization worldwide. Availability and packaging may vary by country and is subject to change without prior notice. Some/All of the features and products described herein may not be available in the United States.

The information in this document contains general technical descriptions of specifications and options as well as standard and optional features which do not always have to be present in individual cases, and which may not be commercially available in all countries. Due to regulatory reasons their future availability cannot be guaranteed. Please contact your local Siemens Healthineers organization for further details.

Siemens Healthineers reserves the right to modify the design, packaging, specifications, and options described herein without prior notice. Please contact your local Siemens Healthineers sales representative for the most current information.

Note: Any technical data contained in this document may vary within defined tolerances. Original images always lose a certain amount of detail when reproduced.

Siemens Healthineers Headquarters
Siemens Healthineers AG
Siemensstr. 3
91301 Forchheim, Germany
Phone: +49 9191 18-0
siemens-healthineers.com

Published by Siemens Healthineers AG · Order No. A91MR-9023-11-7600 · Printed in Germany · 14084 1123 ·